
UNIVERSITA' DEGLI STUDI DI MILANO

FACOLTÁ DI MEDICINA E CHIRURGIA

Dottorato di Ricerca in Fisiologia

Ciclo XXVII°

Tesi di Dottorato di Ricerca

# *Role of CLIC1 and L-type Calcium Channels in the pathophysiology of glioblastoma and ventricular arrhythmias*

Dottorando: **Dott. Marina Angelini**

Matricola R09669

Tutor e Coordinatore: **Prof. Michele Mazzanti**

Dept. of Biosciences, University of Milan

Co-tutor: **Prof. Riccardo Olcese**

Dept. of Anesthesiology, University of California Los Angeles

Anno accademico 2013-2014

# Index

# Abstract

Ion channels are transmembrane proteins that allow and control the flux of ions (sodium, potassium, calcium, and chloride) across the plasma membrane. They are present in all cell types and play critical roles in a variety of biological processes. Historically, ion channels have always been an attractive target for the treatment of different pathologies mainly because numerous drugs can specifically bind ion channels modifying their functional activity.

My PhD thesis addresses the role of two different ion channels in the two leading causes of death in the modern society: heart disease and cancer.

The first part of this PhD dissertation, developed at University of Milan under the mentorship of Prof. Michele Mazzanti, focuses on understanding the role of CLIC1 channels in glioblastoma cancer stem cells (CSCs). Glioblastoma is the most lethal among brain tumors. As other solid tumors, this cancer is composed of two cell types: a small population of cells able to self-renew and generate progeny (CSCs) and a larger population of differentiated cells (bulk cells). Glioblastomas are very aggressive tumors because of CSCs brain infiltration efficiency and resistance to chemotherapies. CLIC1 is a metamorphic protein mainly present as a soluble form in the cytoplasm that is able to translocate to the plasma membrane in response to oxidative stimuli where it acts as a $Cl^-$ channel. Several forms of glioblastomas show a high level of expression of CLIC1 compared to normal brains tissue. In electrophysiological experiments, overexpression of CLIC1 in murine CSCs were associated with a specific increase of the protein at the plasma membrane compared to normal stem cell (NSC). To study the relevance of CLIC1 we used CSCs isolated from human glioblastoma biopsies. By knocking down CLIC1 protein using siRNA viral infection (siCLIC1), we found that CLIC1-deficient cells proliferate less efficiently than control cells infected with siRNA for luciferase (siLUC). Since CLIC1 is a dimorphic protein we asked whether the reduction in proliferation was due to CLIC1 as ion channel. We performed perforated patches electrophysiological experiments for both siLUC and siCLIC1 cells. $Cl^-$ currents

mediated by CLIC1 were isolated using IAA94, a CLIC1 ion channel inhibitor. The results showed that siCLIC1 cells did not display IAA94-sensitive currents, while siLUC cells presented the CLIC1-mediated chloride current. These findings strongly suggest that CLIC1 ion channel activity is required in the proliferation activity of CSCs, and therefore represents a promising target direct in the reduction of CSC gliomagenesis. To target CLIC1 ion channel, the only effective drug so far identified is IAA94 which seems to be rather specific but toxic. For this reason we sought non-toxic drugs that could interact with CLIC1 ion channel. Epidemiological and preclinical studies propose that Metformin, a first-line drug for type-2 diabetes, exerts direct antitumor activity specifically on CSCs. Although several clinical trials are ongoing, the molecular mechanisms of this effect are unknown. To study Metformin's effect on CLIC1-mediated current (isolated with IAA94), we performed electrophysiological experiments from perforated patches using a glioblastoma U87 cell line. We constructed a dose response curve comparing Metformin effect on CLIC1 maximum current (isolated using IAA94) from which we calculated $EC_{50}$ 2.1 ± 0.4 mM. To validate the specificity of Metformin for CLIC1, we compared the extent of block of this drug to the one of IAA94 by sequentially adding the two inhibitors with either order. If the second drug perfusion did not show additional block, we can confirm that the two inhibitor share the same target. Interestingly, experimental data show that Metformin-mediated inhibition of CLIC1 is similar to IAA94 block, suggesting that they both act on CLIC1. Metformin displays antiproliferative activity mainly acting on CSC and not on the differentiated cells. Is this phenotype the result of different expression of CLIC1 in plasma membranes? Interestingly, the relative abundance of CLIC1-mediated current in CSCs was about three fold bigger than in differentiated cells, suggesting that CLIC1 inhibition is relevant in the antiproliferative activity of Metformin. We sought to understand how Metformin bind the channel. Taking advantage of computational modeling and the available CLIC1 crystal structure, our collaborator predicted that the arginin 29 (R29) in the CLIC1 transmembrane domain may be part of the Metfomin binding site. We test this hypothesis in perforated patch clamp experiment using CHO cells stably transfected with CLIC1 wild type or CLIC1 R29A. The substitution of Arg29 in the putative CLIC1 pore region impairs Metformin modulation of channel activity. These results demonstrate that CLIC1 is required for human glioblastoma cell

proliferation. Furthermore, we identified CLIC1 as direct target of Metformin antiproliferative activity in human glioblastoma cells. These findings are paving the way for novel and needed pharmacological approaches to glioblastoma treatment.

The second part of this PhD dissertation, focusing on cardiac arrhythmia, was developed at University of California, Los Angeles under the mentorship of Prof. Riccardo Olcese.

The electrical activity of the heart originates from the rhythmic activity in the sinoatrial node (SAN) and spreads across the heart as a wave of depolarization (the cardiac action potential). While the normal ventricular cardiac action potential (AP) repolarizes monotonically, returning to the diastolic membrane potential, under certain pathological conditions the repolarization can be interrupted by sudden depolarizations called early afterdepolarizations (EADs), occurring during phase 2 or phase 3 of the AP. These events, observable at the cellular and tissue level, are recognized triggers of cardiac arrhythmias. In fact, EADs can generate a new AP that propagates across the heart disrupting the propagation of normal AP wave leading to ventricular tachycardia (VT) and ventricular fibrillation (VF). Ventricular fibrillation is the most commonly identified arrhythmia in sudden cardiac death (SCD), one of the leading causes of death in the United States.

This project investigated the relevance of the voltage gated L-type calcium channel ($Ca_V1.2$) in the etiology of EADs of the cardiac action potential. EADs are largely induced by the reactivation of L-type $Ca^{2+}$ currents ($I_{Ca,L}$) that occurs at the range of membrane potential from –40 to 0 mV, called window current region. To study the dependence of EADs on the biophysical properties of L-type $Ca^{2+}$ current ($I_{Ca,L}$) we adopted a hybrid biological–computational approach: the dynamic clamp technique. Under dynamic clamp it was possible to replace the native $I_{Ca,L}$ of a ventricular myocyte with a computed $I_{Ca,L}$ defined by programmable parameters. We previously identified three L-type $Ca^{2+}$ channel (LTCC) biophysical parameters that effectively suppress EADs induced by oxidative stress or hypokalemia by preventing $I_{Ca,L}$ reactivation in the window current region. Specifically, EADs were potently suppressed by: i) a ~5 mV depolarizing shift of the steady-state activation curve, ii) a ~5 mV hyperpolarizing shift of the steady-state inactivation curve or iii) a reduction of the non-inactivating pedestal

component. Importantly, these changes did not significantly alter the peak $I_{Ca,L}$ or $Ca^{2+}$ transient amplitude during the action potential. Since LTCCs are multiprotein complexes in which Cavβ subunits modulate the gating properties and voltage dependence of the pore-forming Cav1.2 $\alpha_{1C}$ subunit, we explored whether modifying LTCC β subunit composition is a suitable therapeutic strategy to suppress EADs. Voltage clamp experiments, in which we expressed Cav1.2 α1c with different β subunits, showed that subunit subtypes $\beta_{2a}$ and $\beta_{2b}$, which are abundantly expressed in ventricular myocytes, give rise to LTCCs with voltage-dependent properties favoring EADs formation.

Accordingly, we tested an adenovirus-based shRNA delivery strategy to reduce $\beta_2$ expression in primary ventricular myocyte cultures; the rationale being that a LTCC population in a cell with a smaller proportion of $\beta_{2a}$- and $\beta_{2b}$-containing channels should generate $I_{Ca,L}$ with an overall voltage dependence disfavorable to EADs emergence. The simultaneous partial knock down of $\beta_{2a}$ and $\beta_{2b}$ shifted the whole-cell $I_{Ca,L}$ steady-state activation curve to more depolarized potentials by ~4 mV without significantly affecting peak $I_{Ca,L}$. A "narrower" $I_{Ca,L}$ window current could diminish the probability of EADs formation by preventing channel reopening. In congruence with the dynamic clamp results, EADs occurrence under oxidative stress ($H_2O_2$) was potently prevented in rabbit ventricular myocytes with $\beta_2$ knock-down (no EADs observed). Conversely, control myocytes from the same batches exhibited significant action potential prolongation and all cells developed EADs after $H_2O_2$ exposure. These findings demonstrate that manipulation of the subunit composition can be an effective strategy for modifying the steady-state properties of $I_{Ca,L}$. Thus, our results highlight the use of genetic engineering as a therapeutic avenue for the treatment of EADs-related cardiac arrhythmias.

# Chapter 1

## Functional Role of CLIC1 in the Pathophysiology of Human Glioblastoma

# 1.1. Introduction

## 1.1.1. Neuronal Stem Cells

Neural stem cells (NSCs) are a rare population of cells in the central nervous system. They are self-renewing and multipotent cells active in the development and repair of damaged components (Stiles and Rowitch, 2008). Thus, they have the capacity to differentiate into unipotent precursors which give rise to neurons, astrocytes and oligodendrocytes (Figure 1). Neogenesis of cells in the central nervous system (CNS) persists throughout life in certain brain regions such as the subventricular zone of the lateral ventricle and the dentate gyrus (Reynolds and Weiss, 1992). These regions have a network of microvasculature that provides the nutrients needed and factors for the maintenance of stem cells in a quiescent state (Gilbertson and Rich, 2007; Jones and Holland, 2010; Sanai et al., 2005). These special areas called vascular niches consist of endothelial cells, astrocytes, microglia and muscle cells that play a protective role for neural stem cells (Jones and Holland, 2010).

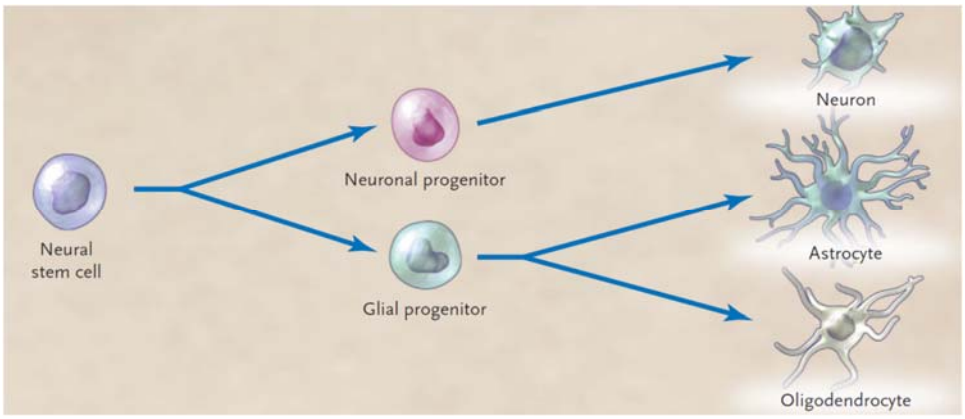


**Figure 1**. Neural stem-cell generates neuronal and glial progenitor cells, which subsequently generate the three differentiated cell types of the central nervous system: neurons, astrocytes, and oligodendrocytes (Sanai et al., 2005).

## 1.1.2. Cancer Stem Cells

Cancer stem cells (CSC) are defined, in analogy to NSC, as cells that possess ability of self-renew and differentiate into other, more specialized cancer cell types (multipotency) (Stiles and Rowitch, 2008; Huse and Holland, 2010; Baccelli and

Trumpp, 2012). Similar to neuronal stem cells, brain CSCs express stemness markers (such as nestin, CD133), are localized in perivascular niches and grow as neurospheres *in vitro* (Calabrese et al., 2007; Huse and Holland, 2010; Jones and Holland, 2010; Charles and Holland, 2010; Stiles and Rowitch, 2008). However unlike neuronal stem cell, they possess cancer properties, such as karyotypic anomalies or genetic mutation, unlimited proliferation and ability to reconstitute the original tumor upon transplantation (Huse and Holland, 2010).

In 1997 Bonnet and Dick showed for the first time the existence of a restricted population of cancer stem cells in human acute myeloid leukemia. In particular they identified for the first time that a subtype of cells, namely CSC were able to induce and recapitulate the heterogeneity of the original tumor through serial transplantations in mouse xenograft model (Bonnet and Dick, 1997). The existence of CSCs was then proved in many solid and liquid cancers including brain tumors (Singh et al., 2007; Singh et al., 2004; Galli et al., 2004).

During the last two decades a revolutionary hypothesis about the tumor composition has been theorized. "The cancer stem cell theory" in fact proposes that among all the tumors cells, only relatively small subset has stem cell-like properties. Therefore the tumor has hierarchical organization that consists of a rare tumor-initiating and propagating cancer stem cell (CSCs) and a larger population of differentiated cells without proliferative capacity (bulk) (Reya et al., 2001). The maintenance of the stem core can be achieved by two types of cell division: i) asymmetric division, by which the stem cell gives rise to a stem cell daughter, also capable of making self-renewal, and a cell that will encounter differentiation or ii) symmetric division, in which the stem cell divides give rise to two daughters or two stem progenitors mature identical to each other (Vescovi et al., 2006).

The origin of CSCs remains controversial. Cancer stem cell can arise from a series of mutations that occur in few or even single founder cells that confer unlimited and uncontrolled proliferation potential (Vescovi et al., 2006; Hanahan and Weinberg, 2000). Different studies demonstrate that cancer stem cells have a critical role in the formation, development and recurrence of the tumor (Baccelli and Trumpp, 2012). In addition, CSCs are predicted to be difficult targets for cancer therapeutics because: they cycle slowly, they highly express transport mechanisms that effectively extrude drugs,

they strongly activate anti-apoptotic pathways of DNA repair, and they may not express the oncoproteins targeted by the new generation of drugs. All these features make this cells resistant to conventional chemo and radio therapies currently in use (Stiles and Rowitch, 2008; Bao et al., 2006).

### 1.1.3. Glioblastoma

Gliomas are the most common primary tumor in the central nervous system in adults and represent 31% of all brain and central nervous system (CNS) tumors diagnosed in the United States, and 81% of malignant brain and CNS tumors (Cohen and Colman, 2015). They originate from the neoplastic degeneration of glia cells, including astrocytes, oligodendrocytes and ependymal cell (Sanai et al., 2005; Huse and Holland, 2010; Chen et al., 2012). These tumors are classified by World Health Organization (WHO) in four classes I to IV grade following histological criteria. The increase of degree reflects the increase of aggressiveness of the tumor and the duration of the prognosis (Denysenko et al., 2010; Huse and Holland, 2010; Maher et al., 2001). Although gliomas are typically malignant, not all types consistently behave in a malignant fashion. The heterogeneity of gliomas (in terms of histology, grade, clinical outcomes, and genomics) increases the complexity of risk factor research in this tumor type. The more aggressive tumor and, unfortunately, more common is the glioblastoma (grade IV) which shows uncontrolled proliferation, neovascularization, infiltration and necrosis.Glioblastoma (GBM) is the most aggressive and lethal among brain tumors in adults, and it still represents a tremendous clinical challenge. GBM has the poorest overall survival, with <5 % of patients surviving 5 years after diagnosis (Jones and Holland, 2010). Unfortunately, the occurrence of the GBM is more frequent than all the other glioma types, as reported in Figure 2. The life expectancy for patients diagnosed with GBM is between 12 and 15 month (Chamberlain, 2010; Maher et al., 2001). The reason for this poor prognosis mainly resides in the fact that GBMs are resistant to radiotherapy and chemotherapy. Moreover, due to its high invasiveness in the brain tissue, surgery is normally not successful and the tumor relapses within a few months.

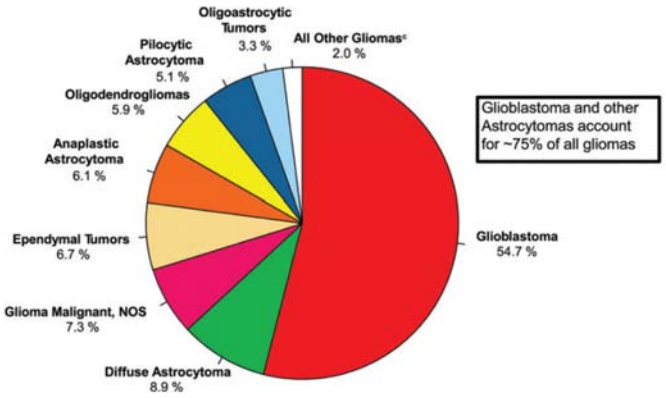


**Figure 2.** Distribution of primary brain tumor new primary gliomas in USA between 2007 and 2011. The glioblastoma account for more than 50% of all the gliomas (CBTRUS Statistical Report: NPCR and SEER, 2007–2011).

Treatment involves a three-pronged approach, which consists of maximal tolerable surgical resection followed by radiation and chemotherapy. (Lefranc et al., 2005; Furnari et al., 2007). Little is known about the molecular mechanisms underlying the genesis and the progression of GBM, which is characterized by the high propensity to infiltrate throughout the brain.

GBM is a highly heterogeneous tumor that contains multiple differentiated and undifferentiated cell types. In general, this elevated cellular and molecular heterogeneity makes even more difficult the development of a unique effective therapy (Huse and Holland, 2010). They are typically highly vascularized tumors often with extensive capillary beds that can provide a similar vascular niche for CSCs to reside in, similarly to neuronal stem cell (Calabrese et al., 2007). The new blood vessels favor tumor growth and infiltration by providing oxygen and nutrients to tumor cells (Denysenko et al., 2010; Sanai et al., 2005; Jones and Holland, 2010). Differently from other solid tumors, gliomas do not take advantage of the linfatic and blood streams to spread and form metastasis outside of the CNS (Maher et al., 2001). The heterogeneity of glioblastoma tumors and their tendency towards fast malignant progression, are coupled with the ability of glioma cells to migrate away from a tumor mass into normal brain tissue where they generate multiple new foci and recurrent growth (Denysenko et al., 2010; Huse and Holland, 2010; Sanai et al., 2005).

The origin of GBM has been an issue for discussion. Different studies suggest that GBM derive from the transformation of different cells, such as neural stem cells (NSCs) or glial progenitor (committed progenitors) or astrocytes. In general, cancer cells of origin are normal cells in which tumorigenic mutations first occur and accumulate to form a malignancy (Chen et al., 2012). In neuronal stem cells and progenitor cells, the oncogenic process can be viewed as a lack of regulatory mechanisms that control the ability of self-renewal and/or differentiation (Vescovi et al., 2006). Furthermore, it has been hypothesized that glioma originates from transformation of astrocytes, as the only known replication-competent population in the SNC. In this case the malignant transformation requires a ‘‘dedifferentiation’’ process in by which cells regain to immature glial and progenitor properties (Sanai et al., 2005; Stiles and Rowitch, 2008). To explain how GBMs initiate and develop, to date two alternative models are present (Figure 3). The stochastic model proposes that tumor cells are heterogeneous, and virtually all of them can function as a tumor-founding cell. On the other hand, the hierarchical model implies that only a small subpopulation of tumor stem cells can proliferate extensively and sustain the growth and progression of a neoplastic clone (Reya et al., 2001). The latter hypothesis fits with the cancer-stem-cell theory (Vescovi et al., 2006).

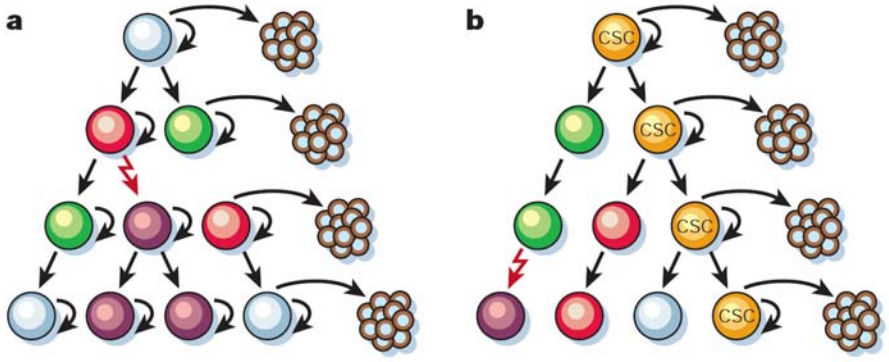


**Figure 3.** Tumor initiation model. A)Cancer cells of many different phenotypes have the potential to proliferate extensively, but any one cell would have a low probability of exhibiting this potential in an assay of clonogenicity or tumorigenicity. B) Most cancer cells have only limited proliferative potential, but a subset of cancer cells consistently proliferate extensively in clonogenic assays and ability to generate new tumors (Reya et al., 2001).

### 1.1.4. Chloride channels and glioblastoma

Ion channels are transmembrane proteins that allow and control the flux of ions (sodium, potassium, calcium, chloride and protons) across the plasma membrane. They are present in all cell types and play critical roles in a variety of biological processes, such as muscle contraction, cell excitability, hormone secretion, mechanosensitivity. In recent decades, growing scientific evidence supports the role of ion channels also in tumor development and growth (Fraser and Pardo, 2008). It has been shown that different types of ion channels play relevant roles in all six cancer hallmarks: 1) self-sufficiency in growth signals, 2) insensitivity to antigrowth signals, 3) avoidance of programmed cell death (apoptosis), 4) unlimited replicative potential, 5) angiogenesis and 6) tissue invasion and metastasis (Figure 4) (Prevarskaya et al., 2010; Fraser and Pardo, 2008).

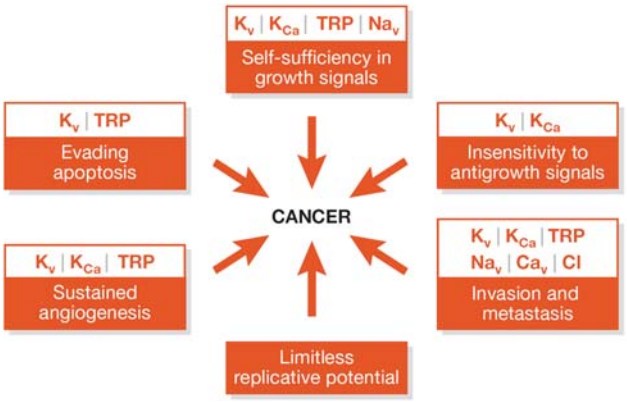


**Figure 4.** Different types of ion channels are involved in each of the six cancer hallmarks (Fraser and Pardo, 2008).

In particular, tumor invasiveness appears to be associated with $K^+$ and $Cl^-$ channels upregulations (Cuddapah et al., 2014) (Figure 5). These channels are required for efficient regulation of the cell volume by creating local osmotic gradients that facilitate the swelling or shrinking of cells (Cuddapah et al., 2014). The Chloride channel family is composed by four different classes: Voltage–dependent Chloride channel (ClC), Calcium-Activated Chloride Channels CLCA, Cystic Fibrosis Transmembrane conductance Regulator (CFTR), and Chloride Intracellular Channels (CLIC). Chloride channels are ubiquitously expressed and localized both in plasma membrane and in

intracellular organelles. The different families of chloride channels participate in the tumorigenesis process of different cancers.

Specifically in glioblastomas, mainly two types of $Cl^-$ channels have been reported to be relevant for glioma invasion and proliferation: ClC and CLIC.

Similar to immature neurons, glioblastoma cells maintain high intracellular $Cl^-$ (80–100 mM) (Habela et al., 2009; Sontheimer, 2008). Thus, even at a relatively depolarized resting potential (~ -40 mV), opening of $Cl^-$ channels causes $Cl^-$ efflux (Sontheimer, 2008), followed by water, in turn inducing cell shrinkage and likely tissue infiltration.

Indeed, three members of ClC class (ClC-2, -3 and 5) are expressed in glioma cell membranes and they are localized in the lamellipodia during migration process (Olsen et al., 2003).

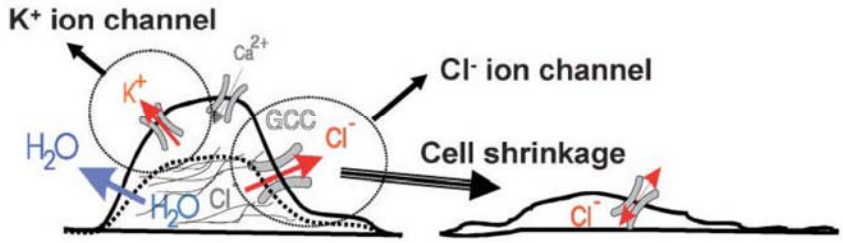


**Figure 5.** $K^+$ and $Cl^-$ efflux helps glioma-cell shrinkage. To reduce their cytosplasmic content, cells release $Cl^-$ and $K^+$ through ion channels, and water follows passively through water channels or aquaporins. For this mechanism to function, cells must accumulate $Cl^-$ and $K^+$ above their respective electrochemical gradients. This is accomplished by the combined activity of the NKCC $Cl^-$ transporter and the $Na^+$–$K^+$ ATPase for $K^+$ ions (McFerrin and Sontheimer, 2006).

ClCs participate in glioblastoma cells insomuch as now a generic blocker of ClC class of channel, chlorotoxin (CTX) is now in phase I/II clinical trial for gliomas treatment (Cheng et al., 2014).

Alike migration/invasion process, cell proliferation also requires considerable structural/volume changes that are mediated by activity of different channels that allow the progression and conclusion of the cell cycle (Lang et al., 2005). Correct progress through cell cycle is ensured by checkpoint controls that monitor DNA integrity and the

completion of each molecular events before allowing transition to the next phase (Becchetti, 2011) (Figure 6).

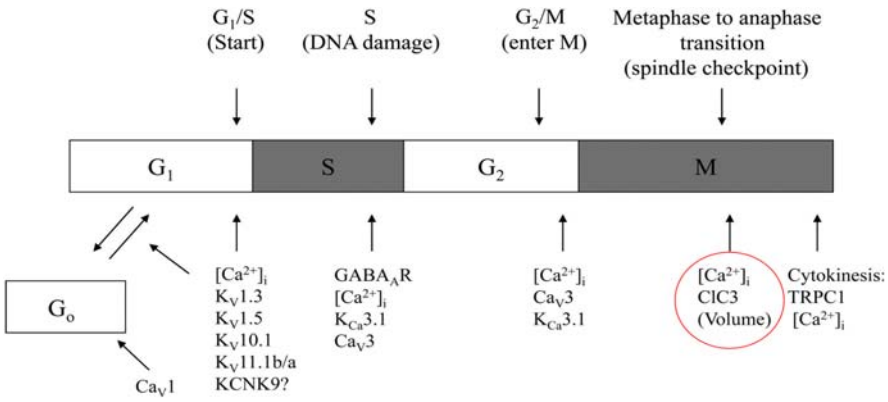


**Figure 6.** Schematic relation between ion channels and the main cell cycle checkpoints. Four main checkpoints have been identified in eukaryotic cells: at the $G_1$/S transition, in late S, at the $G_2$/M transition and at the metaphase to anaphase transition (Becchetti, 2011).

In eukaryotic cells, the main checkpoints are placed at the $G_1$/S transition, in late S (DNA synthesis) phase, at mitosis (M) entry and at the metaphase to anaphase transition are highly regulated by different channel (Figure 6). Little is known, however, about the involvement of chloride channel in cell cycle. Previously, Habela and colleagues found that ClC-3 channel activity is important for the regulation of glioma cell cycle (Habela et al., 2008). The activity of the channel is mainly upregulated during the M phase and during this phase the protein localizes both at the plasma membrane and at the mitotic spindles (Habela et al., 2008). In these cells, knocking down ClC-3 considerable delays mitosis impairing cell proliferation (Wang et al., 2002).

The role of CLIC1 in tumors will be discussed in the session "CLIC1 in tumors".

### 1.1.5. The chloride intracellular channel 1 (CLIC1)

The chloride intracellular channel (CLIC) protein family has been the last discovered and still largely underexplored. Until now seven members of the family have been identified: CLIC1 , CLIC2 , CLIC3 , CLIC4 , CLIC5a , CLIC5b and CLIC6 (Singh, 2010). They are highly conserved class of proteins expressed both in the

plasmamembrane and intracellular organelles. The CLIC family is defined by a conserved, approximately 230 amino acid core sequence which comprises the C-termini of all known CLICs. Sequences amino-terminal to the core region are divergent both in sequence and in size. Furthermore, they share structural homology with members of the superfamily of omega glutathione S-transferase (ΩGST) also with regard to the highly conserved active site binding to glutathione (GSH) in the N-terminal domain ( in CLIC1 is the Cysteine 24 ) (Littler et al., 2010). Recently, it has been demonstrated that CLICs soluble form have glutaredoxin-like glutathione-dependent oxidoreductase enzymatic activity that may be important for protecting the intracellular environment against oxidation in physiological (Al Khamici et al., 2015). A unique feature of CLIC proteins is their ability to exist in two different forms: a soluble globular form in the cytoplasm and an integral membrane protein, suggested forming functional ion channels.

In 1989, Landry and Al Awqati isolated the first protein of this family called p64 (or CLIC5b). It was isolated from bovine tracheal apical epithelium and kidney cortex microsomal membrane fractions showed chloride-selective channel function in lipid bilayers (Landry et al., 1993). The localization of these proteins is mainly intracellular, some are identified for example in the mitochondrial membrane (CLIC4), in the nuclear (CLIC1), in the endoplasmic reticulum (CLIC4), in the Golgi (CLIC4) and secretary vesicles (CLIC5b) (Harrop et al., 2001).

The cloning of p64 facilitated the identification of homologous proteins in mammalian tissues and lately in the ‘90s NCC27 (or CLIC1) was cloned in human monocytic cell line (Valenzuela et al., 1997). CLIC1 is a small protein composed by 241 aminoacids, with a molecular weight of 27 KDa (Valenzuela et al., 1997). The crystal structure of the soluble form of the protein has been resolved few years ago by Harrop and colleagues (Harrop et al., 2001). The N-terminus and the C- terminus domains are connected by a proline-rich region, in which proline 91 has been suggested to have a main role in the changes from the soluble to the membrane-inserted form of the protein, due to its change from cis to trans configuration (Harrop et al., 2001) (Figure 7). Furthermore, CLIC1 has a reduced glutathione (GSH)-binding site in its N-terminal domain, which render this protein sensitive to the oxidative state of the cell.

In fact, it has been shown that changes in the cellular redox state determine a reversible transition of CLIC1 protein between a reduced, soluble monomeric state and an oxidized, soluble dimeric state (Littler et al., 2004). However, a different study suggests that the dimerization process during oxidation is not necessary for the insertion of the protein into membranes (Goodchild et al., 2009). In this model, CLIC1 monomer interact by itself with the membrane and only successively the oxidation promotes the structural changes that allow the protein to cross the membrane.

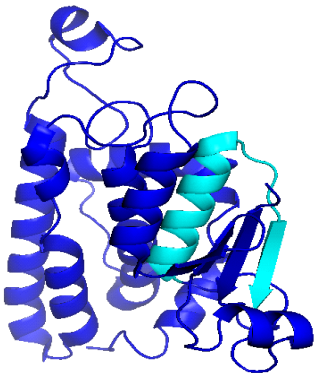

**Figure 7.** CLIC1 is a small protein of 241 amino acids. In light blue is highlighted the hypothetical transmembrane domain (image created with PyMol )

Studies on the localization of CLIC1 showed that this protein is found mainly in the nuclear membrane and in the nucleoplasm even though fractions of this protein are also present in the cytoplasm and in the plasma membrane (Tonini et al., 2000; Valenzuela et al., 1997; Valenzuela et al., 1997). To understand the characteristics of the ion channel, biophysical experiments were carried out on CLIC1 transfected CHO-K1 cells through cell and nuclear patch clamp (Tonini et al., 2000).

By transfecting these cells with CLIC1 tagged with FLAG epitope tag either a N- or C-terminal they demonstrate with the antibody anti-FLAG, that CLIC1 spans the plasma membrane with the C terminus (Tonini et al., 2000). It has also been proven that CLIC1 purified protein can form a chloride channel in artificial bilayer with characteristics very similar to those observed in CHO cells transfected in inside-out configuration (Warton et al., 2002; Singh et al., 2007; Tulk et al., 2002). The insertion of the channel in the membrane appears to be facilitated by the oxidation but also by other factors, for

example pH acidification. In experiments of artificial bilayer, using solutions with acid pH, it has been shown that CLIC1 has a higher probability of entering into the lipid bilayer (Warton et al., 2002). Recently, it has been demonstrated the relevance of Glu85 and Glu228 as a "pH-sensor residues" that contribute to the pH-response (Cross et al., 2015). CLIC1 single channel conductance in 140 mM KCl symmetric solution is approximately 30 pS (Tulk et al., 2002; Warton et al., 2002). To further support the ion channel nature of CLIC1, it has been reported that a single point mutations (C24A, R29A, K37A) in CLIC1 putative transmembrane region results in alterations of the electrophysiological characteristics of the channel (Singh and Ashley, 2006; Averaimo et al., 2013).The only effective channel blocker so far identified is the Indanyloxyacetic acid 94 (IAA94), with an EC50 of 8.6 μM (Tulk et al., 2000) whereas DIDS (4'-2,2'-disulfonic Diisothiocyanatostilbene-acid disodium salt hydrate), another chloride channel blocker, has no effect on the conductance of this channel (Valenzuela et al., 2000).

CLIC1 is expressed in different epithelial and non-epithelial cell types where it shows tissue- and cell-specific patterns of subcellular localization (Ulmasov et al., 2007). Although CLIC1 clearly can function as a channel in vitro, the role of CLIC1 in normal physiology remains uncertain. In 2010, Qiu and collegues generated a Clic1 KO mouse that does not show any embryonic lethality but only a mild bleeding disorder and decreased platelet activation (Qiu et al., 2010). Moreover, in a mouse model of Alzheimer disease, CLIC1 is mainly localized in the plasma membrane of activated microglia (Figure 8). Our laboratory has previously shown that blockade of CLIC1 functional expression with specific inhibitors or its downregulation by small interference RNA, impairs the production of reactive oxygen species (ROS), limiting the detrimental effects of microglia over activation (Milton et al., 2008). Therefore the reduction of CLIC1 activity, may limit neurodegeneration without affecting the phagocytic ability of microglia (Paradisi et al., 2008). Furthermore, it has been demonstrated that CLIC1 ion channel is required for maintaining the morphology and elongation of neurite in retinal ganglion cell (RGCs) (Averaimo et al., 2014).

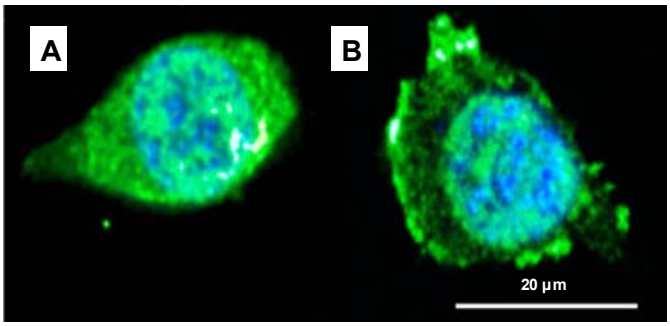


**Figure 8.** Immunolocalization of CLIC1 (green, antibody directed against the N-terminus of the protein) in BV2 cells (nuclei are stained in blue, DAPI). Following β-Amyloid (Aβ) stimulation, which induces oxidative stress, CLIC1 translocates into the plasma membrane (Milton et al., 2008).

### 1.1.6. CLIC1 in tumors

CLIC1 protein levels are reportedly increased in different cancers, such as: human breast ductal carcinoma (Wulfkuhle et al., 2002), gastric cancer (Chen et al., 2007), gallbladder metastasis (Wang et al., 2009), colorectal cancer (Petrova et al., 2008), nasopharyngeal carcinoma (Chang et al., 2009), ovarian cancer (Tang et al., 2012), hepatocellular carcinoma (Wei et al., 2015), and high-grade gliomas (Wang et al., 2012). All these analyses propose CLIC1 as a tumor marker, sometimes detectable even in the plasma of patients and so very useful in the clinic.

CLIC1 is overexpressed in brain tumors compared with normal brains and the expression at both mRNA and protein levels increasing along with WHO tumor grades and reaching the highest expression level in glioblastoma (Wang et al., 2012).

CLIC1 is a dimorphic protein and under oxidative stress is mainly localized at the plasma membrane (Milton et al., 2008). Thus, CLIC1 appears to have a main role in all the diseases that involve oxidative stress, including tumors (Averaimo et al., 2010). Furthermore, in CHO-K1 cell line CLIC1 chloride current varies according to the stage of the cell cycle and it is mainly expressed in the plasma membrane of cells in G2/M phase (Valenzuela et al., 2000). Since oxidative fluctuations drive the cells through the cell cycle phases (Menon and Goswami, 2007), it is not surprising that CLIC1 may be

very active as an ion channel in cancer cells, which are cells in a highly proliferative state.

### 1.1.7. Metformin

Metformin (1,1-dimethylbiguanide), a biguanide derivate, was originally described in 1921 (Werner and Bell, 1921). It is a small-molecule weight (129.2 KDa), water-soluble, which at physiological pH-values exists as an organic cation. Although the molecular weight and protein binding of Metformin are low, it poorly diffuses passively through membranes (Detaille et al., 2002). OCT1 and OCT2 are the main active transporters, which facilitate the transport of Metformin across the liver, intestine and kidney tissues (Shu et al., 2007; Graham et al., 2011). Metformin is the most widely used drug for treating patients with type 2 diabetes (prescribed to approx. 120 million patients with type 2 diabetes/year) (Pollak, 2012). Although Metformin has been widely used as a very effective anti-diabetic drug for many decades, the exact molecular mechanism(s) of Metformin action against diabete is not completely understood (Bao et al., 2014).

Metformin alleviates hyperglycemia by reducing hepatic glucose production (gluconeogenesis) and increasing glucose utilization (glucogenolysis). Thus Metformin is antihyperglycemic (not hypoglycemic) as it does not stimulate insulin release from the pancreas and generally does not cause hypoglycemia, even in large doses (Inzucchi, 2002). Metformin metabolic effects mainly rely on mitochondrial activity: it decreases ATP production and activates AMP-activated protein kinase (AMPK), thus regulating gluconeogenesis and fatty acid synthesis (Hardie et al., 2012). Due to its very cost-effective and safe properties, Metformin has been widely prescribed as the first line of medication as an anti-diabetic drug (Bao et al., 2014). Importantly, the long-term use of Metformin in diabetic patients is associated with minor adverse effects (Bolen et al., 2007). Metformin is absorbed mainly from the small intestine and its oral bioavailability is 50-60%. The peak plasma concentration is reached within 1-3 hours after oral intake of immediate release tablets and within 4-5 hours after oral intake of extended release tablets (Tucker et al., 1981). The half-life of elimination is about 6.5 hours. Metformin

is not metabolized, and 90% is excreted unchanged into the urine by tubular secretion. It is also able to cross the blood-brain barrier (Sato et al., 2012; Labuzek et al., 2010).

### 1.1.8. Metformin and Glioblastoma

Epidemiological studies reported that Metformin is associated with reduced cancer incidence (Evans et al., 2005) and mortality (Bowker et al., 2006) and increases the number of breast carcinoma patients obtaining complete response to neo-adjuvant therapy (Jiralerspong et al., 2009).

Metformin controls cell proliferation and tumor growth, but the molecular mechanism by which this compound reduces tumor development is not clear (Viollet et al. 2012). Metformin antitumorigenic effects are thought to be independent of its hypoglycemic actions (Kourelis and Siegel, 2012). The anticarcinogenic effects of this drug have been attributed to several mechanisms: (1) activation of LKB1/AMPK pathway, (2) induction of cell cycle arrest and/or apoptosis, (3) inhibition of protein synthesis, (4) reduction in circulating insulin levels, (5) inhibition of the unfolded protein response (UPR), (6) activation of the immune system, and (7) eradication of cancer stem cells (Kourelis and Siegel, 2012).

Isakovic and collegues demonstrated antiproliferative effect of Metfromin using rat and human glioma cell line. They establish that Metformin causes cell cycle arrest and apoptosis of glioma cells through unique AMPK-dependent mechanisms (Isakovic et al., 2007). Furthermore, Würth and colleagues using glioblastoma cancer stem cell (CSC) isolated from patients demonstrated that Metformin exerts antiproliferative activity on glioblastoma cells, showing a higher specificity toward normal stem cell (umbilical cord-derived mesenchymal stem cells) and differentiated cells (Wurth et al., 2013; Wurth et al., 2014). Metformin also decreases spherogenesis of CSCs mainly acting on the inhibition of Akt pathway. Furthermore Sato and colleagues identified Metformin as a therapeutic activator of the transcription factor forkhead box O3 (FOXO3) (Sato et al., 2012). This activation of FOXO3 by Metformin promotes the differentiation of glioblastoma CSCs into non-tumorigenic cells. The heterogeneity of the reported mechanisms of action of Metformin can imply that is a promiscuous drug

acting on multiple pathways. Furthermore there are several on going and upcoming clinical trials, including glioma, on the use of Metformin for cancer treatment and prevention (Kourelis and Siegel, 2012).

This thesis focuses on the pivotal role of CLIC1 ion channel as a molecular target for anti-proliferation activity of human glioblastoma cancer stem cell, highlighting the relevance of this protein in the antiproliferative activity exerted by Metformin on glioblastoma CSCs.

## 1.2. Methods

### 1.2.1. Human glioblastoma cancer stem cell

Tumor biopsies classified as glioblastoma grade IV (GBM IV) were collected from consenting patients at the Istituto Neurologico Carlo Besta, Department of Neurosurgery, Milan (Italy) and at Azienda Ospedaliera Universitaria "San Martino", Department of Neurosurgery, Genoa (Italy). The tissues were enzymatically digested with papain (2mg/ml) (Worthington Biochemical, Lakewood, NJ) at 37°C and mechanically dissociated until a single cell suspension was achieved, as previously described by Vescovi and colleagues (Vescovi et al., 2006) (Figure 9).

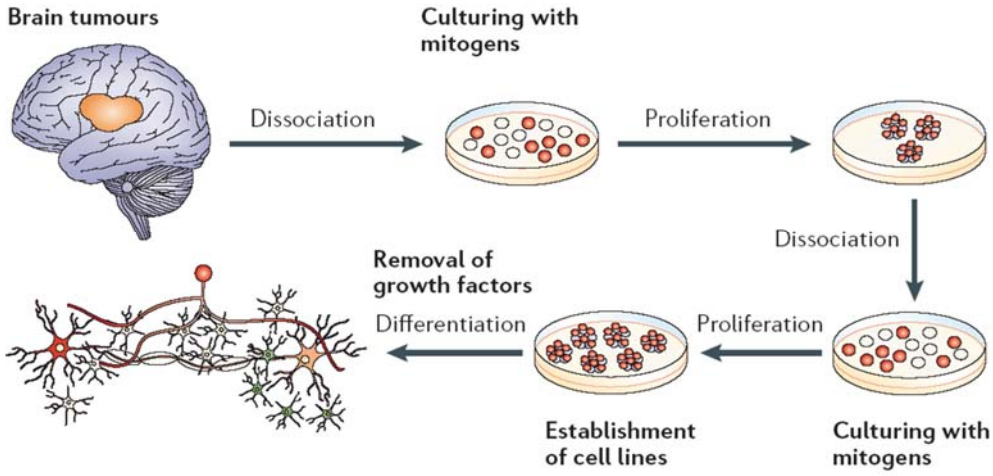


**Figure 9.** Human brain tumor biopsys were dissociated and cultured in a specific medium that allows only CSCs to grow (no serum, plus EGF and FGF) (Vescovi et al., 2006).

Glioblastoma cancer stem cell: human and murine GBM cancer stem cell (CSC) and normal stem cell (NSC) were grown in stem cell permissive medium composed by NeuroCult medium (StemCell Technologies, Vancouver, BC, Canada) supplemented with 20 ng/ml epidermal growth factor (EGF), 10 ng/ml basic fibroblast growth factor (bFGF) (PeproTech, Rocky Hill, NJ), and 0.0002% heparin (Sigma-Aldrich, St. Louis, MO) (Ortensi et al., 2012). The CSCs were grown in suspension were they form a spheroid aggregates (neurospheres), each deriving from a single cancer stem cell. Neurospheres can be further mechanically dissociated into a single-cell suspension and

then re-plated in fresh medium to produce secondary neurospheres every 5-10 days. This process can be repeated several times (Figure 9). The absence of serum in the neurosphere medium allows the isolation and propagation of cancer stem cell only. To induce the differentiation of GBM CSC cell, the single CSC were cultured in growth factor-deprived medium (no EGF, bFGF) containing 10% fetal bovine serum (FBS, Lonza) for at least 2 weeks.

### 1.2.2. Other cell cultures

U-87MG (human primary glioblastoma) and CHO (Chinese hamster ovary) cell line were grown under standard condition with DMEM+10%FBS. CLIC1 wild type (CLIC1 wt) and R29A (CLIC1 R29A) mutant were stably transfected in CHO cells using FuGENE Reagent (Roche). N-terminal FLAG-tagged human CLIC1 (WT) or its R29A mutant cloned in pIRES2-EGFP vector (Clontech Laboratories Inc., San Jose, CA). The pIRES2-EGFP plasmid used for these experiments contains the internal ribosome entry site (IRES), which permits both the gene of interest and the gene reporter (EGFP) to be translated as separate proteins.

### 1.2.3. Clonogenic Assay

To measure the clonogenicity, cells were resuspended in Dulbecco's modified Eagle medium/F12 medium containing methylcellulose (StemCell Technologies, Vancouver, BC, Canada) and seeded on 35-mm culture plates (3000 cells per dish). A minimum of three plates per condition was used. Two weeks after plating, the number of clones was counted.

### 1.2.4. Quantitative Real Time Polymerase Chain Reaction (qRT-PCR)

Total RNAs from glioblastoma cell were isolated by RNAeasy Mini kit (Quiagen, Valencia, CA). RNAs from each sample (1μg) were retrotranscribed using ImProm-II

Reverse 2 Transcriptase (Promega, Madison, WI) at the following temperature steps: 25°C for 5', 42°C for 60', 70°C for 10'. Quantitative real time PCR (qRT-PCR) analysis was then performed by 7,500 Fast Real-Time PCR System (Applied Biosystems, Foster City, CA) with Syber Green PCR Master Mix (Applied Biosystems, Foster City, CA). The sequence of primers was the following:

CLIC1 fw: 5'-GTTGACACCAAAAGGCGG-3', rev: 5'-TCTCCAGATTGTCATTGAGTGC-3';

TBP fw:5'-TGCACAGGAGCCAAGAGTGAA-3', rev: 5'-CACATCACAGCTCCCCACCA-3';

HPRT1 fw:5'-TGACCTTGATTTATTTTGCATACC-3', rev: 5'-CGAGCAAGACGTTCAGTCCT-3'.

### 1.2.5. Lentiviral infection

RNA interference (RNAi) is a biological process in which small RNA molecules, called siRNAs, inhibit the expression of a gene of interest, by causing the destruction of the specific mRNA. Experimentally, this process can be induced by introduction of synthetic small interfece (siRNAs) into the cells or by intracellular generation of siRNA from vector driven expression of the precursor small hairpin (sh) RNAs. shRNA has been shown to be more effective and potent in silencing genes. In these "method", a double-stranded oligonucleotide containing the siRNA sequence linked by a ~9 nucleotide loop is cloned in plasmid or viral vectors to endogenously express shRNA which is subsequently processed in the cytoplasm to siRNA. To delivery the plasmid into the cell we used a Lentiviruses. This type of virus is suited for long-term shRNA expression and gene silencing since the viral DNA gets incorporated in the host genome.

The short hairpins specific to human CLIC1 (5'-GATGATGAGGAGATCGAGCTC-3') and to firefly luciferase (5'-CGTACGCGGAATACTTCGA-3') mRNAs were cloned into the PLentiLox 3.7 lentiviral vector using the XhoI/HpaI sites. The PLentiLox 3.7 lentiviral vector also includes the puromycine gene to select infected cells and the Green Fluorescent Protein (GFP) gene to evaluate transduction efficiency. Lentiviral and packaging plasmids (vpMDLg/pRRE, pRSV-REV and pMD2G) were amplified in the E.Coli-strain Top10 and purified using a QUIAGEN MAXI KIT. HEK

293T cells were used to amplify the viral particles and they were grown in IMDM (Iscove's Modified Dulbecco's Medium, plus Glutamax, Invitrogen) with 10% FBS and 25 U/ml Penicillin/Streptomycin. HEK 293T cells were co-trasfected with all the plasmids using the calcium phosphate method according to established procedures (TronoLab). The viral particles were collected and concentrated using PEG-it. The transducing unit (TU) concentration was then determined by GFP expression. The viral suspension was used to infect dissociated CSCs from human GBM (104 TU/µl). 72 hours after infection, cells were positively selected with 1.5 mg/ml puromycine.

### 1.2.6. Western Blot

Cell samples were collected by centrifugation and pellets were lysated on ice in 50-100 µl of lysis buffer (50 mM Tris–Cl buffer, 10 mM CaCl2, 5mM EGTA, 250 mM NaCl , 10% Glycerol, 1% triton-x 100, pH 8) containing a cocktail of proteinase inhibitors (50 mM NAF, 10 mM NAPP, 10mM NaOrtoV, 0.1mg/ml PMSF, Leupeptin , Apoprotinin ). Concentration of protein lysates was assessed by Bradford assay (Biorad). Membrane/cytoplasm fractions were obtained using the "Membrane protein extraction kit" (Thermo Scientific), following the manufacturer's instructions. Each lysate (10 µg) was loaded onto a SDS-polyacrylamide gel electrophoresis (PAGE) under reducing conditions, and resolved proteins were transferred onto Nitrocellulose membranes (Protran ®) of 0.2 µm pore size. Membranes were incubated overnight at 4°C with anti-CLIC1 mouse monoclonal antibody, anti-Vinculin, anti-GFAP, anti-tubulin diluted in Tris-Buffered Saline and Tween 20 (TBS-T [50mM Tris, 150mM NaCl, 0.05% Tween 20]) supplemented with 5% Milk Powder. Antibody binding was assessed by horseradish peroxidase (HRP)-conjugated secondary antibody (Sigma Aldrich, 1:10000 dilution). Immunoreactive bands were detected with enhanced chemiluminescence reagents (GE Healthcare Bio-Sciences).

### 1.2.7. Patch clamp

The patch clamp technique was developed by Neher and Sakmann in the late '70s. This technique revolutionized the field of physiology and biophysics by allowing the direct study of ion channel function. In this technique a small heat-polished glass pipette is pressed against the cell membrane where the ion channels are embedded and forms an

electrical seal with a resistance of ~1-2 GΩ that allow the measurement of ionic current (Hamill et al., 1981). An electrode (a silver wire coated with AgCl), located inside the glass pipette and connected to the circuitry, converts the ionic current into electrical current. This configuration is defined as cell-attached (Figure 10 A). After achieving a gigaseal there are several configurations that can be used. Whole cell configuration, in which the membrane patch is disrupted and the the pipette solution is continuous with the cytoplasmic mileu allowing for recordings from the ion channels present in the whole cell membrane (Figure 10 B).

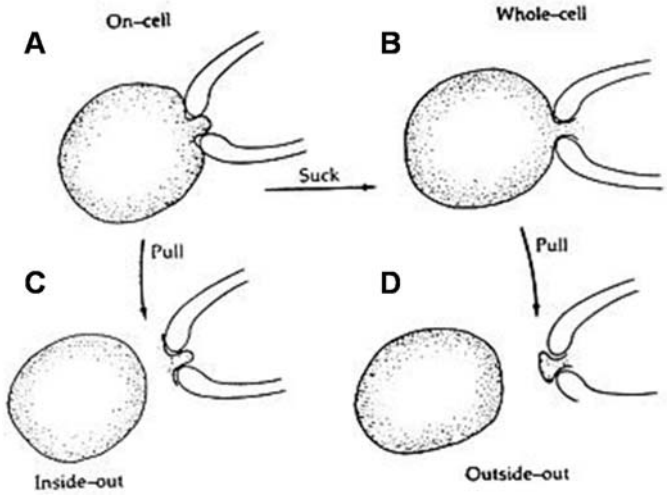


**Figura 10. Patch clamp configurations.** A high resistance seal called a "gigaseal" is formed when negative pressure is applied after the pipette is in contact with the cell membrane (A). B) In whole-cell mode, the cell membrane is ruptured by applying additional negative pressure thereby allowing one access to the interior of the cell and record a sum of all currents crossing the entire cell membrane. From cell-attached mode, one can retract the pipette to detach a portion of the membrane from the rest of the cell to enter the "inside-out" excised patch mode (C). D) Alternatively, from whole-cell mode, one can retract the pipette to form a vesicle at the tip of the pipette, called the "outside-out" excised patch. (www.bphys.uni-linz.ac.at/bioph/res/icg/patch.html).

Alternatively, it is possible to rapidly withdrawed the pipette from cell-attached configuration to achieve the inside-out configuration in which one has access to the cytoplasmic face of the channels and allowing then current recordings in known intracellular solutions (Figure 10 C). If this maneuver is made in whole cell mode, the

cell membrane will reseal upon itself to form a small vesicle at the pipette tip, called outside-out excised patch, in which the extracellular side of the channels can be manipulated (Figure 10 D). Another configuration is perforated patch, where the pipette contains specific antibiotics (such as gramicidin, anphotericin B or nystatin) that can inserted in the membraneof the cell in order to provide electrical access to the cell interior preserving the cytoplasm content (Figure 11).

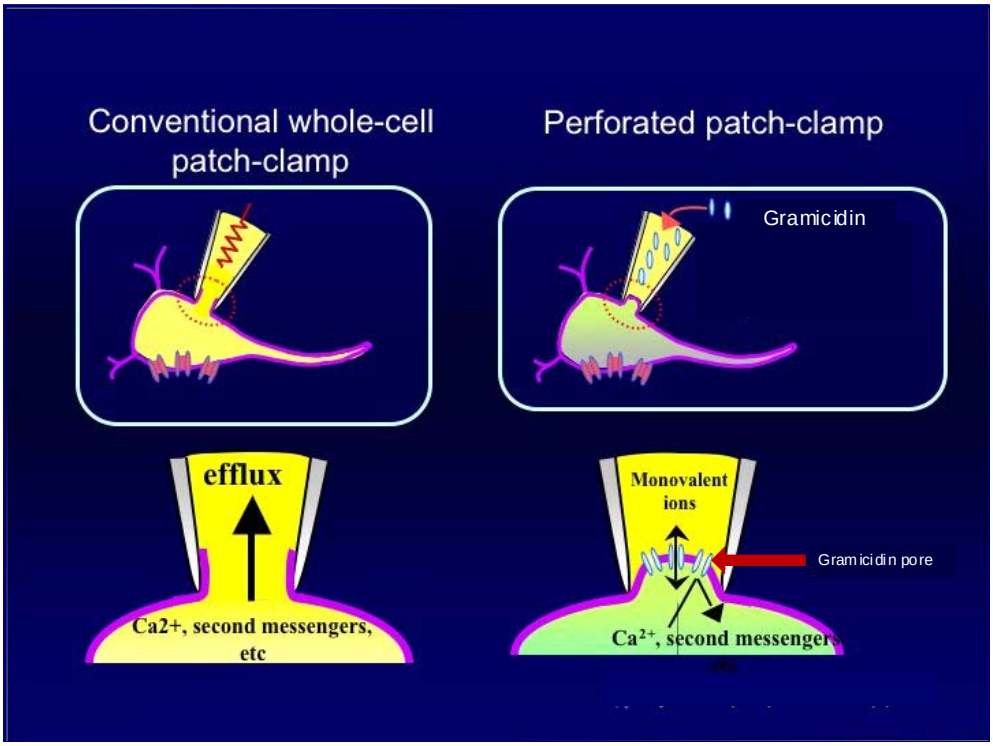


**Figure 11.** Comparing the conventional whole cell patch-clamp configuration (left) and the perforated patch technique (right). In perforated patch, the electrical access to the cell is achieved taking advantage of the pore forming ability of certain antibiotics (such as gramicidin), the main advantage of this configuration is the preservation of the intracellular content.

Patch clamp experiments: The patch electrodes (GB150F-8P with filament, Science Products) were pulled from hard borosilicate glass on a Brown-Flaming P-87 puller (Sutter Instruments, Novato, CA.) and fire polished to a tip diameter of 1-1.5 µm and an electrical resistance of 4-5 MΩ. The cells were voltage-clamped using an Axopatch 200 B amplifier (Molecular Devices) in the perforated patch configuration or whole cell configuration. Ionic currents were digitized at 5 kHz and filtered at 1 kHz. Patch-clamp electrophysiology in perforated-patch experiments, the bath solution contained (in mM):

130 NMDG-Cl; 1.8 $CaCl_2$; 2 $MgCl_2$; 10 HEPES; 10 Glucose; 5 TEACl; pH 7.4 and the electrode solution contained (in mM): 145 KCl; 10 HEPES; 1 $MgCl_2$; pH 7.25. The antibiotic Gramicidin (Sigma-Aldrich) was added to the pipette solution (2.5 µg/ml). Gramicidin is capable to insert into plasma membranes and form pores permeable only to monovalent cations, allowing to gain electrical access to the cell as well as preserve the $[Cl^-]_i$ and the cytoplasm content. For whole cell experiments, the bath solution contained (in mM): 130 NaCl; 1.8 $CaCl_2$; 2 $MgCl_2$; 10 HEPES; 10 Glucose; 1 $BaCl_2$; pH 7.4, while the pipette solution contained (in mM): 135 KCl; 5 TEACl; 10 HEPES; 0.5 $MgCl_2$; 0.1 $CaCl_2$; 1 EGTA; pH 7.2. The voltage protocol consisted of 800 ms pulses from -100/-60 mV to +80/+60 mV (20 mV voltage steps); the holding potential was set according to the resting potential of the cell (between -40 and -80 mV). Cell capacitances were measured in whole cell configuration using a two-step protocol (from 0 mV to -5 mV and from 0 mV to -10 mV), and resulting capacitances were used to calculate current densities. For time-course experiments, we held the voltage at -20 mV, measuring the current at the end of 800 ms voltage step from -40 to +60 mV membrane potential every 5 seconds.

CLIC1-mediated Cl- currents were isolated from the other ionic currents in the cells by perfusing a specific inhibitor (Indanyloxyacetic acid 94, IAA94 100 µM) dissolved in the bath solution. Other $Cl^-$ currents were isolated using the aspecific inhibitor DIDS 200 µM (Disodium 4,4′-diisothiocyanatostilbene-2,2′-disulfonate). In the experiment with metformin we isolate the metformin sensistive current ($I_{metformin}$) by perfusing 10mM.

Analysis: Offline analysis was performed using Clampfit 9.0 (Molecular Devices), OriginPro 8.5. IAA94-sensitive ($I_{IAA94}$), DIDS-sensitive ($I_{DIDS}$) and metformin-sensitive ($I_{metformin}$) currents were estimated by analytical subtraction of ionic currents after addition of either inhibitor from the total current ($I_{TOT}$) of the cell at each membrane potential tested. Current/Voltage relationships (or I/V curves) were constructed by plotting the averaged ionic current data points in the last 100 ms of the pulse against the corresponding membrane potential. IAA94-sensitive/DIDS-sensitive/Metformin-sensitive currents were normalized to the total ionic current of the cell ($I_{IAA94}/I_{TOT}$ and $I_{DIDS}/I_{TOT}$, $I_{Metformin}/I_{TOT}$ respectively); $I_{IAA94}/I_{TOT}$%, $I_{DIDS}/I_{TOT}$% $I_{Metformin}/I_{TOT}$% and

from the same cell types were averaged and plotted against the membrane potential. For the dose response Metformin-sensitive currents were normalized to maximum CLIC1 current isolated using IAA94 ($I_{IAA94\ max}$) of the cell. Error bars are the standard error of the mean in all plots.

## 1.3. Results

My thesis is part of a larger study aimed at understand the role of CLIC1 protein in cancer stem cells (CSC) from human glioblastoma. The goal is to comprehend the functional role of CLIC1 ion channel in the proliferation of the CSCs in order to possibly develop new therapeutic strategies.

This project has been developed in collaboration with Dr. Pelicci laboratory at the European Institute of Oncology of Milan (IEO) and in Dr. Florio laboratory at the Center of Excellence for Biomedical Research of the University of Genoa (CEBR).

### 1.3.1. CLIC1 is overexpressed in glioblastoma cancer stem cell and it mainly localizes at the plasmamembrane

In order to assess the role of CLIC1 in glioblastoma, our collaborators in Dr Pelicci laboratory established primary cultures of cancer stem cell (CSC) isolated from different human glioblastomas (hGBM). The cells isolated from the tumor, were grown in a stem-cell-permissive medium as describe previously by Vescovi and colleagues (Vescovi et al., 2006).

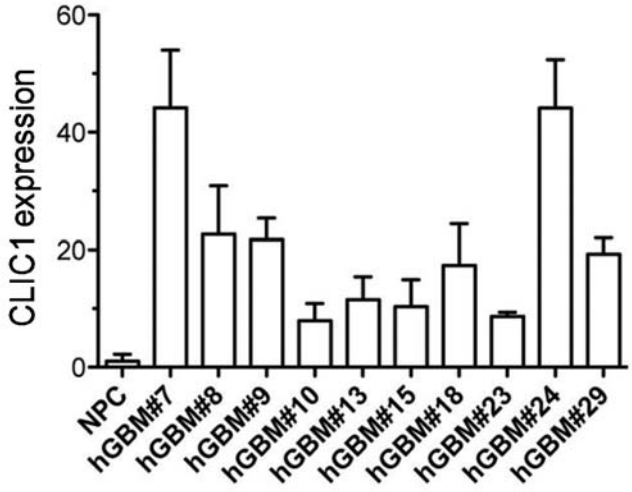


**Figure 12. CLIC1 is overexpressed in human glioblastoma (hGBM) CSCs.** CLIC1 expression level validates by quantitative reverse-transcription polymerase chain (qRT-PCR) in normal brain and in different patient-derived GBM neurospheres. (n=3 each, error bars represent 95% confidence interval).

Using RT-PCR they compared CLIC1 mRNA expression in different patient derived-glioblastoma neurospheres (Figure 12). CLIC1 expression was clearly more abundant in cancer stem cell by ~15-20 fold increase as compared to human normal progenitor cells (NPC).

Since CLIC1 is a metamorphic protein able to fold in at least two conformations (one as a soluble protein in the cytoplasm, the other as a membrane protein to form ion channels), we sought to understand whether the increase in CLIC1 mRNA was related to an increase in CLIC1 mediated current. To address this question, we took advantage of the patch clamp, a very powerful technique used to measure ionic conductances in single cells. Specifically, we used the variant of whole-cell patch-clamp recording, called perforated patch clamp that was developed to overcome the dialysis of cytoplasmic constituents that occurs with traditional whole cell.

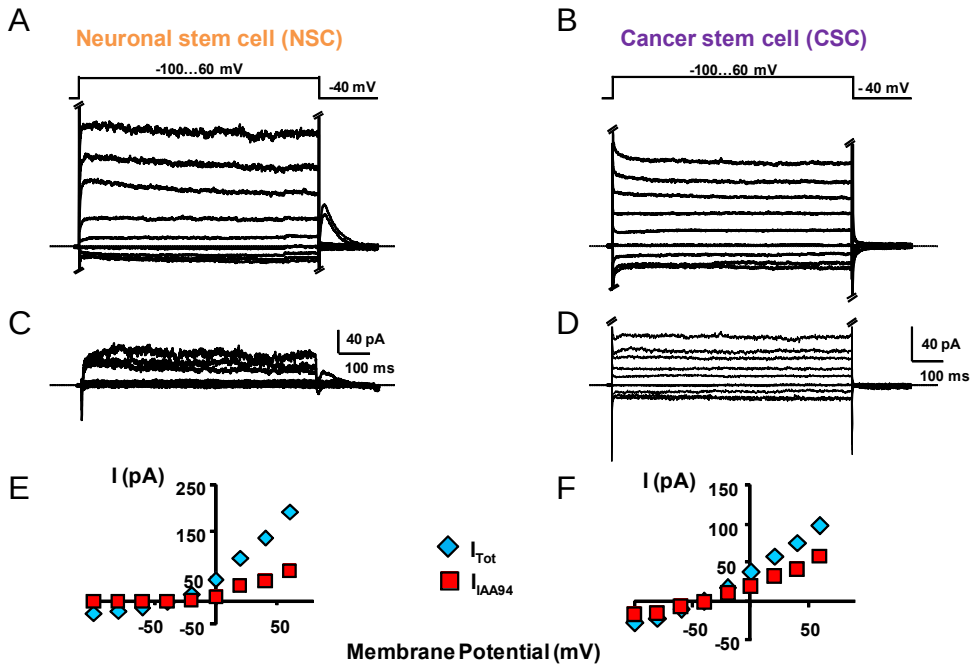


**Figure 13. CLIC1-mediated current is more represented in CSCs.** Rapresentative ionic current traces from perforated patches of neuronal stem cells (NSCs) (A) and glioblastoma cancer stem cells (CSCs) (B). The voltage protocol is shown above the traces. By analytical subtraction of the ionic current after 100 µM IAA94 addition from the total current of the cell, we obtained the IAA94-sensitive current (C,D). E-F) show I-V relationships for the corresponding experiments in NSC and CSC, respectively.

The electrode solution contains antibiotics which diffuse and form small pores in the membrane, providing electrical access to the cell cytoplasm. In the experiments presented here, we used gramicidin, which forms pores permeable only to monovalent cations. After gigaseal formation, the gramicidin inserted into the plasmamembrane within few minutes and this was ascertained by monitoring the capacitive current increase and the resting potential stabilization. The resting potential could vary between -30 mV and -80 mV and the holding potential of each experiment was set according to the resting potential of that specific cell. During the experiment we sequentially perfused bath solution and 100 μM IAA94 (CLIC1 inhibitor) on the cell and ionic currents were recorded at different imposed membrane potentials. By analytical subtraction, IAA94-sensitive currents were isolated from the total current of the cell ($I_{tot}$). Since the absolute values of these currents were different from cell to cell, they were normalized to $I_{tot}$ obtaining the percentage of IAA94-sensitve current (% $I_{IAA94}$) (also see methods for more details).

In Figure 13, representative experiments are shown for murine neuronal stem cell (NSC) (Figure 13 A) and CSC (Figure 13 B). The Current/Voltage relationships showed the total current and IAA94-sensitive current relative to the experiments presented in A and B (Figure 13 E and F). Averaging all the experiments performed at each membrane potential, we found that CLIC1-mediated current was more represented in tumoral cells. For example at 20 mV % $I_{IAA94}$ was 32.38% ± 7.7% (n = 5) in CSC and 13.09% ± 4.39% (n = 5) in NSC (Figure 14 A).

In addition, to quantify the protein content we performed western blot analysis using neurospheres lysate fractions obtained from CSC and NSC. By probing the lysate fractions with antibodies anti-CLIC1, we found that CLIC1 protein expression was increased in the plasma membrane of CSC compare to normal counterpart (Figure 14 B).

Taken together, these results suggest that the increase in CLIC1 mRNA level in CSC was correlated with an enhancement in CLIC1 as ion channel at the plasma membrane.

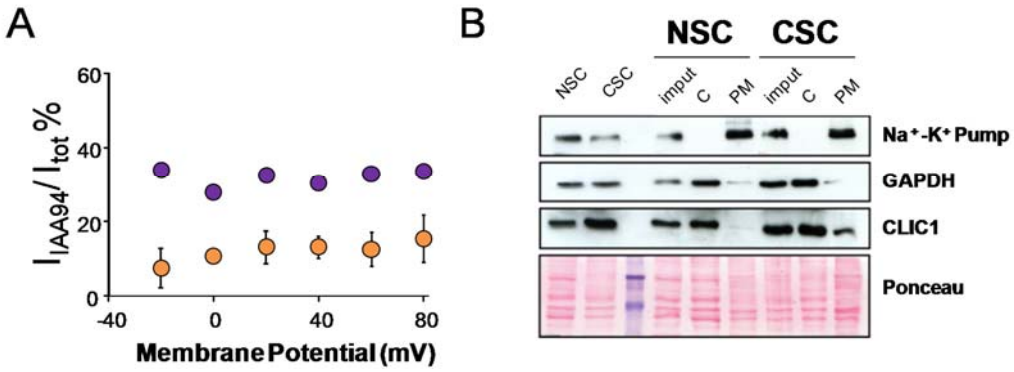


**Figure 14. Enrichment in the plasma membrane fraction of CLIC1 protein in glioblastoma CSCs.** A) Averaged ratio of IAA94-sensitive currents over the total current of the same cell are plotted against membrane potential. Note that IAA94-sensitive currents are more represented in CSCs (purple) compared to NSCs (orange). Error bars are SEM B) Western blotting analysis of CLIC1 expression level in the plasma membrane (PM) and cytoplasm-containing fractions from murine NSC and CSC neurospheres.

### 1.3.2. CLIC1 silencing impairs cell proliferation in glioblastoma neurospheres

In order to study the functional role of CLIC1 in glioblastoma CSCs, the strategy was to reduce the expression of the total protein using RNA interference (RNAi) technique. A lentiviral vector encoding for the shRNA (short hairpin RNA) against human CLIC1 (siCLIC1) or against the firefly luciferase (siLUC) for control, were engineered and trasduced into CSCs. To verify the extent of CLIC1 silencing in CSCs isolated from a patient (hGBMR#), a western blot was performed on both the infected cells and the control cells (no infection). By probing the blot with antibodies anti-CLIC1 and anti-Vinculin, we found that CLIC1 protein expression was reduced by ~50 % in siCLIC1 infected CSCs (Figure 15 A).

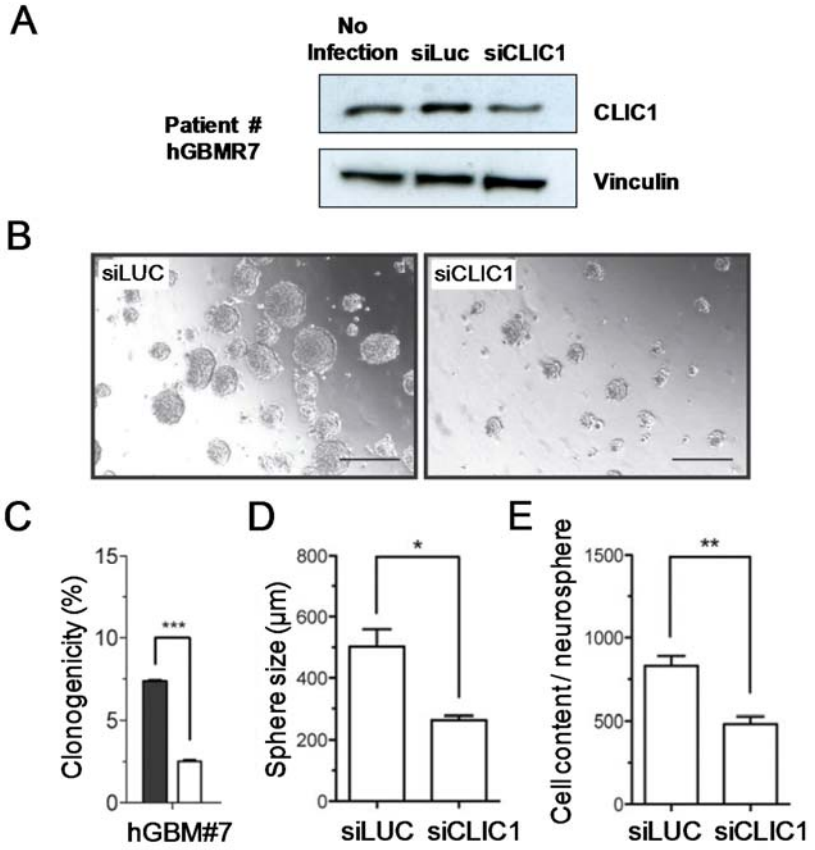


**Figure 15. CLIC1 silencing reduces clonogenicity and proliferation of glioblastoma (GBM) stem/progenitor cells.** A) Western blot analysis was performed on whole lysates from siLUC, siCLIC1 and not-infected cells and probed with anti-CLIC1 and anti-Vinculin antibodies. B) Representative microphotographs of control (siLUC) and CLIC1-silenced (siCLIC1) neurospheres formed in methilcellulosecontaining medium after 15 days in culture. Scale bar = 300 µm. C) Neurosphere formation assay. The clonogenic capacity of control (siLUC) and CLIC1-silenced (siCLIC1) cells was evaluated by plating cells in methylcellulose-containing medium. After 15 days, each plate was examined under a light microscope, and the total number of neurospheres was determined. D) Quantification of the maximal diameters of control (siLUC) and CLIC1-silenced (siCLIC1) neurospheres from GBM patient 7 (hGBM#7). Ten neurospheres for each sample were analyzed. E) Quantification of hGBM#7 neurosphere cell number. Ten neurospheres for each sample were picked and dissociated, and the cell number was determined.

The self renew ability of CLIC1-silenced and control cell was assessed in vitro, using the methylcellulose assay. This technique consists in plating single cell in a semisolid medium and count the colonies after 15 days in culture. The clonogenicity was calculated as the percentage of the total number of seeded cells. The first observation

was that the silencing of CLIC1 caused an evident decrease in the ability of generating colonies as shown by microphotographs in Figure 15 B. Accordingly, the clonogenicity for CLIC1-silenced CSC (white bar) was 3.83 ± 1.75% and 11.63 ± 5.23 % for the control (black bar) (Figure 15 C). This observation reflected a decrease in the sphere size (siCLIC1 264.0 ± 13.50 μm and 502.5 ±56.85 μm for siLUC) and a lower neurosphere cellular content (siCLIC1 483.33 ± 85.68 cells and to 830 ± 119.22 cells in siLUC) for CLIC1-silenced CSCs (Figure 15 D and E).

Taken together, these data show that CLIC1 is required for proliferation of CSCs, therefore in the cell propagation in GBM neurospheres.

### 1.3.3. siRNA completely abolishes CLIC1-mediated currents in glioblastoma cancer stem cells

Since glioblastomas are highly proliferating tumors and CLIC1 is involved in the proliferation, we asked whether the reduction in CLIC1 protein level obtain with shRNA was associated with the modification in the CLIC1 mediated current.

To address this question we carried out perforated patch clamp experiments in CLIC1-silenced human CSCs (siCLIC1) and control CSCs (siLUC). During the experiments I perfused bath solution, 100 μM IAA94 (CLIC1 inhibitor) and 100 μM IAA94 + 200 μM DIDS ($Cl^-$ channels inhibitor that does not affect CLIC1 current) and the ionic currents were recorded at different imposed membrane potentials in each condition. By analytical subtraction IAA94- and DIDS-sensitive currents were isolated from the total current of the cell ($I_{tot}$) and they were normalized to $I_{tot}$ obtaining the percentage of IAA94-sensitve current (% $I_{IAA94}$) and DIDS-sensitive current (% $I_{DIDS}$).

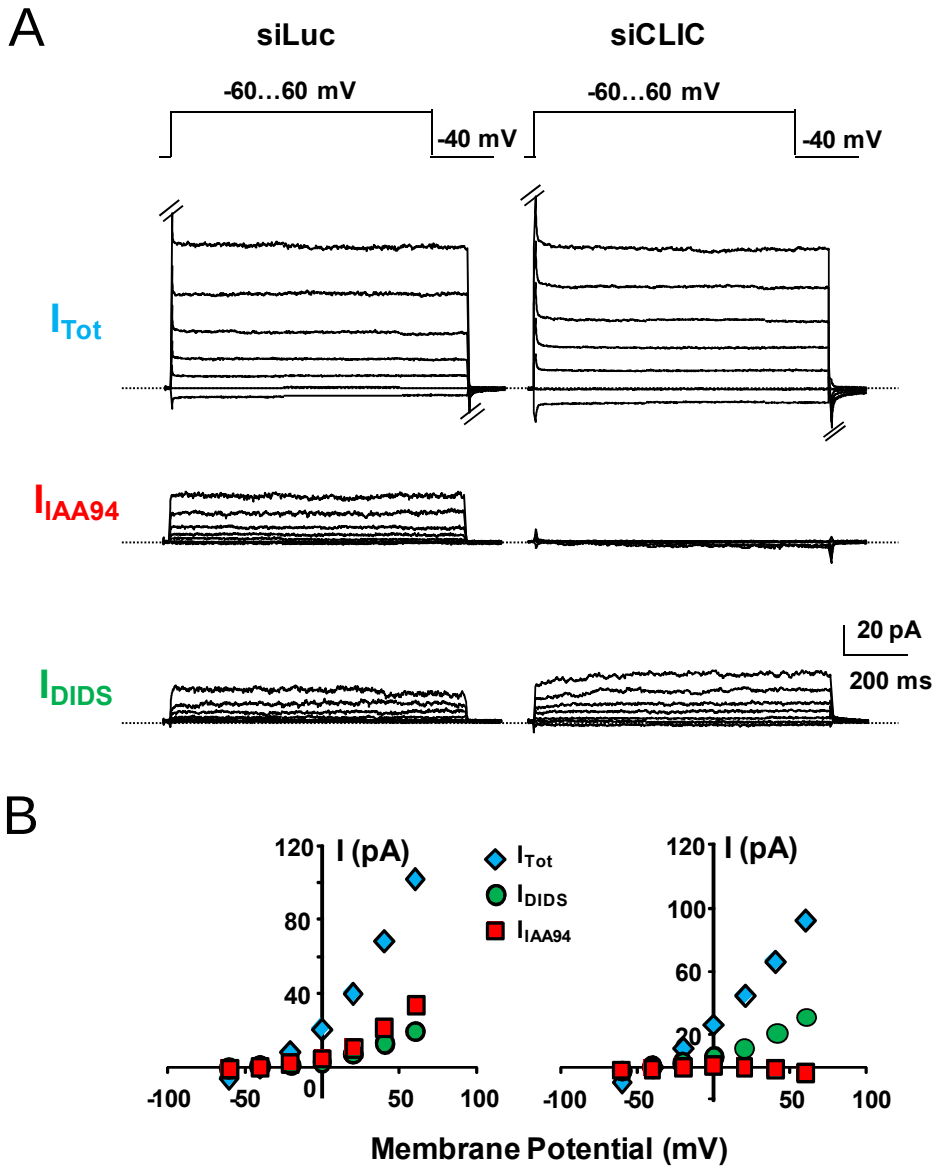


**Figure 16. siRNA abolishes CLIC1 currents in CSCs.** A) Rapresentative ionic current traces from perforated patches of CSCs from hGBM#7 tumors siLuc and siCLIC1 cells. The voltage protocol is shown above the traces. By analytical subtraction of the ionic current after 100 µM IAA94 addition from the total current of the cell, we obtained the IAA94-sensitive current ($I_{IAA94}$); the DIDS-sensitive current ($I_{DIDS}$) is calculated by subtracting the current after 200 µM DIDS addition from the current after IAA94 effect. B) shows I/V relationships for the corresponding experiments in A. CLIC1-silenced cells display a complete abolishment of the CLIC1-mediated current, while the DIDS-sensitive current is unaltered.

The IAA94-sensitive current was absent in the siCLIC1 cells (Figure 16 A, right pannel) unlike DIDS-sensitive currents, which were recorded from all cell groups. The Current/Voltage relationships showed the total current, IAA94-sensitive current and DIDS-sensitive current relative to the experiments presented in Figure 16 A. Averaging all the experiments performed at each membrane potential, I found that, for example, at 20 mV % $I_{IAA94}$ 28.05% ± 3.97% (n = 7) and 2.38% ± 0.91% (n = 5) in siLUC and siCLIC1 cells respectively; while $I_{DIDS}$ was 21.09% ± 5.65% (n = 4) in siLUC cells and 28.45% ± 13.05% (n = 3) in siCLIC1 cells (Figure 17 A and B).

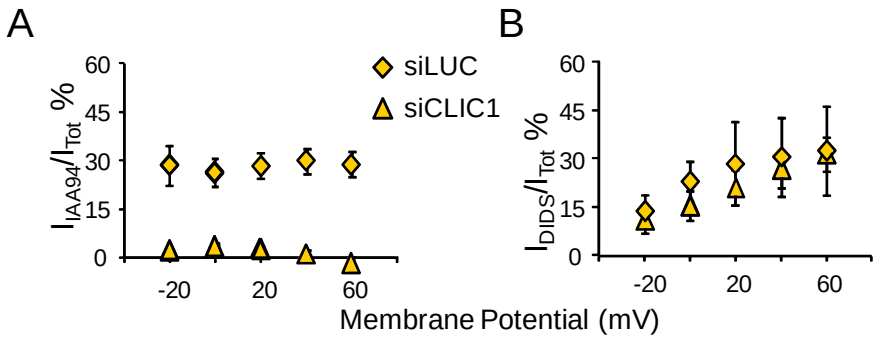


**Figure 17. siRNA abolishes CLIC1 currents in CSCs**. These plots report the averages of the ratio of IAA94-sensitive currents (A) and DIDS-sensitive currents (B) over the total current of the same cell, for experiments performed in hGBM#7 glioblastomas CSCs. IAA94-sensitive currents, but not DIDS-sensitive currents, are abolished in siCLIC cells underlying the specificity of siRNA effect.

These results demonstrate that siRNA against CLIC1 completely abolished CLIC1 ion channel activity, while the DIDS-sensitive current were unaltered, indicating that the viral infection did not produce off target effect on other chloride conductances. These findings support the view that CLIC1 ion channel activity is relevant in the proliferation activity of CSCs.

### 1.3.4. IAA94 and Metformin exert similar effects on CLIC1 mediated current

To target CLIC1 ion channel, the only effective drug so far identified is IAA94 which seems to be rather specific, but toxic. For this reason we sought non-toxic drugs that could interact with CLIC1 ion channel. Different epidemiological studies reported that Metformin, the most widely used antidiabetic drug in the world, is associated with reduced recurrence and favorable prognosis in several cancers (Kourelis and Siegel, 2012; Ning et al., 2013). Furthermore Metformin directly inhibits cancer proliferation, preferentially acting on CSC (Sato et al., 2012; Wurth et al., 2013; Ning et al., 2013).

Since CLIC1 is overexpressed in human glioblastoma and it is involved in proliferation of CSCs, we wanted to test whether Metformin exerted its antiproliferative role acting on CLIC1 ion channel.

We assessed a dose-response curve for Metformin in perforated patch experiment using a human glioblastoma cell line U87-MG (Ponten and Macintyre, 1968) (Figure 18). The cells were perfused with a single dose of Metformin, in order to isolate the Metformin sensitive current. The ratio between the Metformin sensitive current and total CLIC1 maximum current (isolated using 100 μM IAA94) was then calculated for each cell and plotted against [Metformin] (Figure 18). The dose-response data points followed a sigmoidal trend that was fitted using Hill function with Metformin $EC_{50}$ = 2.1 ± 0.4 mM.

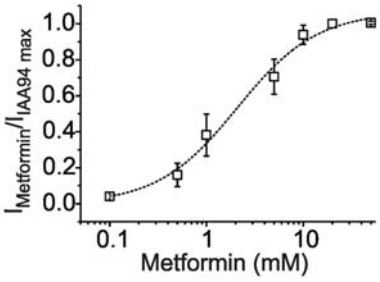


**Figure 18. Metformin dose response curve**. The ratio between Metformin and IAA94 sensitive currents (+60 mV, 750 ms test potential) was used to calculate a Metformin $EC_{50}$ of 2.1 ± 0.4 mM (mean ± s.e.m.) from a dose/response plot (n=4 independent experiments for each concentration).

To test the specificity of Metformin (10 mM) for CLIC1, we compared the extent of block of this drug to the one of IAA94 (100 μM) by sequentially adding the two inhibitors with either this order or the opposite (Figure 19). In panel A of Figure 19, I perfused IAA94 and subsequently IAA94 + Metformin, whereas in B the order was: Metformin and Metformin + IAA94. By analytical subtraction, IAA94- and Metformi-sensitive currents were isolated from the total current of the cell ($I_{tot}$). These currents were normalized to $I_{tot}$ obtaining the percentage of IAA94-sensitive current (% $I_{IAA94}$) and Metformin-sensitive current (% $I_{Metformin}$). In both cases the first compound (IAA94 in A or Metformin in B) decreased the whole cell current, but most importantly the addition of the second inhibitor (Metformin in A or IAA94 in B) did not produce further sensitive current in both cases (Figure 19). Averaging all the experiments performed at each membrane potential, we confirmed that % of inhibition due to the first inhibitor were similar: at 40 mV the % of current blocked by the first inhibitor IAA94 is 34.33% ± 6.69 % (n=5) and with Metformin is 33.23 ± 4.52% (n=5, Figure 14 A and B). Furthermore the addition of the second inhibitor resulted in % of sensitive current essentially null (For example 20mV %$I_{IAA94}$ was 0.77 % ± 1.27% and $I_{Metformin}$ 0.60% ± 0.78% (n = 5, Figure 20 A and B). Interestingly, experimental data show that Metformin-mediated inhibition of CLIC1 is similar to IAA94 block, suggesting that they both act on blocking CLIC1 current.

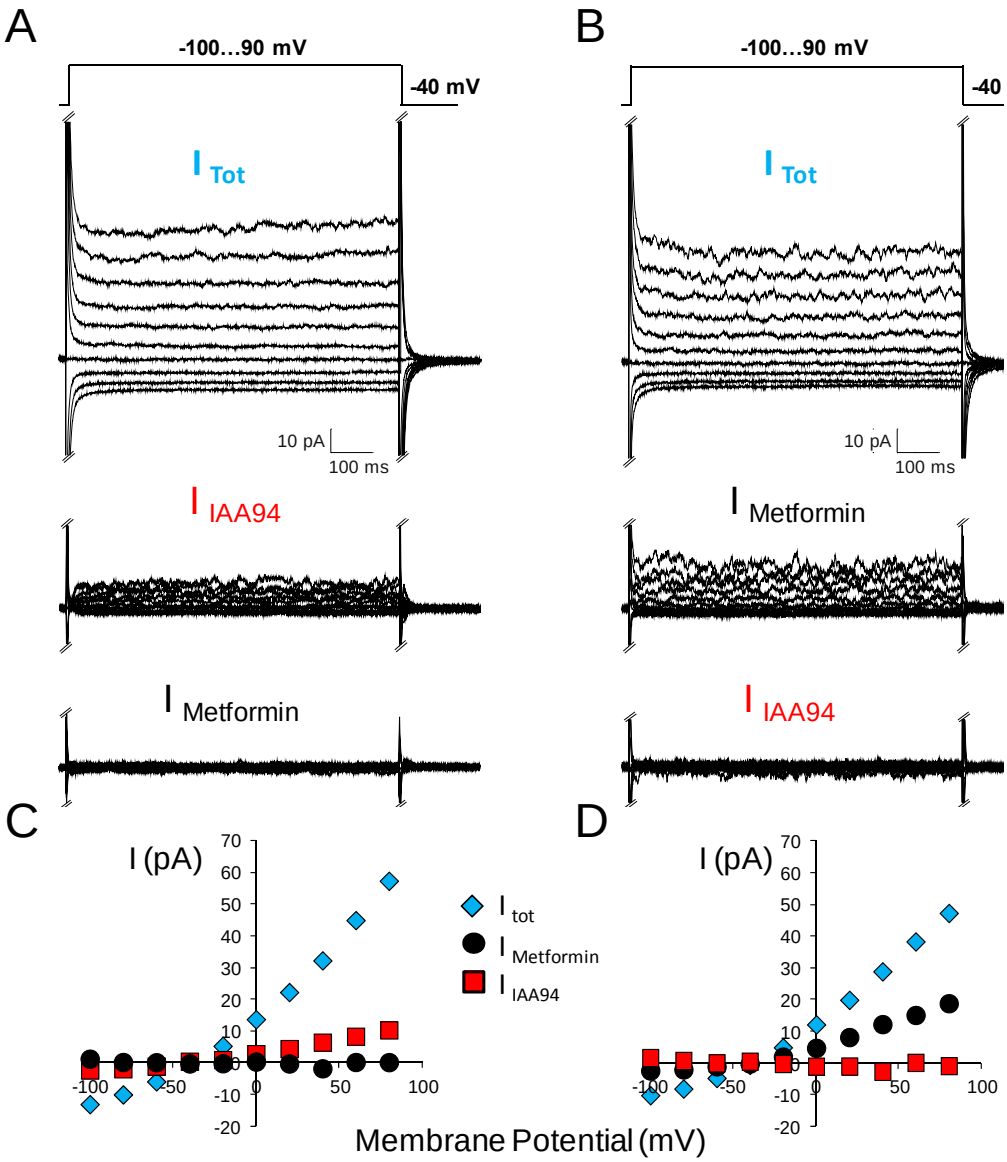


**Figure 19. Inhibition of CLIC1 current by Metformin or IAA94.** Representative traces of Metformin- and IAA94-sensitive currents recorded in perforated patch configuration elicited by different 800ms voltage step (from -80 to 80mV). IAA94 (100 µM) and Metformin (10mM) were perfused on the same cell in this (A) or in the reverse order (B). (C, D) show I/V relationships for the corresponding experiments in A and B, respectively.

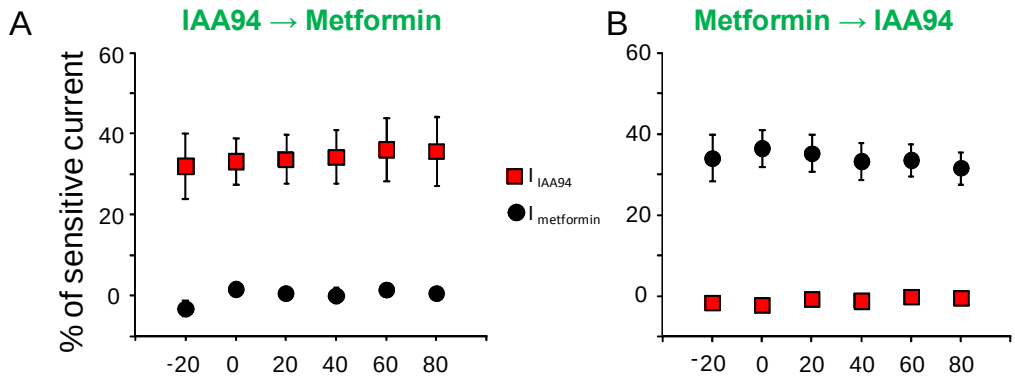


**Figure 20. CLIC1 mediated current is equally sensitive to Metformin and IAA94.** These plots report the averages of experiments performed in U87-MG in which we perfused IAA94 and later Metformin in this (panel A) or in reverted order (B). It is reported the ratio of IAA94-sensitive current (red square) or Metformin-sensitive current (black circle) over the total current of the same cell.

### 1.3.5. CLIC1 involvement in Metformin antiproliferative effect in human glioblastoma

Considering that metformin displays antiproliferative activity mainly acting on CSC (not in differentiated cells) (Wurth et al., 2013) and that CLIC1 it has been demonstrated important for CSC proliferation, we asked whether the Metformin antiproliferative activity is in part mediated by CLIC1.

The CSCs were grown as floating neurospheres in stem cell-permissive medium (No FBS) or in FBS-medium (without growth factors) to induce the differentiation (Figure 21 A). Using western blot analysis, we verified the extent of the differentiation process, by assessing the expression level of an astrocytic marker, the glial fibrillary acidic protein (GFAP), in differentiated cells and CSCs (Figure 21 B). This analysis revealed that the differentiated cells are enriched in GFAP content compared to CSCs, as expected for glial cells (Figure 21 B). By probing the blot with antibodies anti-CLIC1 and α-tubulin, we found that CLIC1 expression was significantly reduced in differentiated cells (Figure 21 B) suggesting that CLIC1 was highly expressed in CSCs but their protein level dropped down after differentiation. Has the differentiation process changed CLIC1 ion channel expression? To address this question, we

performed perforated patch experiments measuring Metformin-sensitive current in CSCs and differentiated cells using Metformin (Figure 22 A). During the experiments we noticed that the differentiation process considerably changed the morphology of the cells, from spherical (CSCs) to fully spread (differentiated cells) (Figure 21 A). How is this affecting current density?

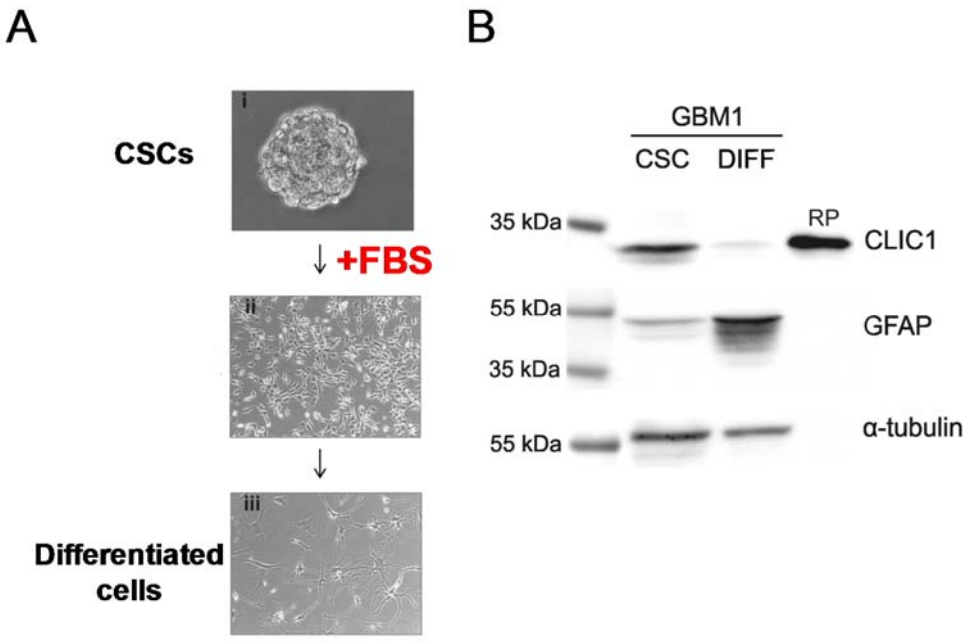


**Figure 21. CLIC1 expression is reduced in differentiated cells.** A) Representation of the differentiation process. By shifting CSCs from growth factor-supplemented (top) to growth factor-free and FBS-containing medium (medium/bottom) we obtained a stable culture of differentiated cells. B) Representative expression of CLIC1 and GFAP in GBM1 CSC-enriched and differentiated cell cultures. CLIC1 expression is reduced in differentiated cells, which conversely show increased GFAP expression.

One disadvantage of perforated patch is that the evaluation of cell capacitance remains uncertain, because of the low accessibility to the cytoplasm when the antibiotic perforates the membrane. To overcome this issue, we measured the membrane capacitance in the two groups of cells using the whole-cell configuration. The averaged membrane capacitance was statistically different between two groups of cells: 6.52 ± 0.92 pF in CSCs and 69.56 ± 6.46 pF in differentiated cells (Figure 22 B). We used these measurements to normalize the Metformin-sensitive CLIC1 current, I observed

that for example at +20mV the current density was 1.57 ± 0.51 pA/pF for CSCs (n=6) and 0.51 ± 0.15 pA/pF for differentiated cells (n = 5) (Figure 22 C). Interestingly, the relative abundance of CLIC1-mediated current in CSCs was about three-fold bigger than in differentiated cells.

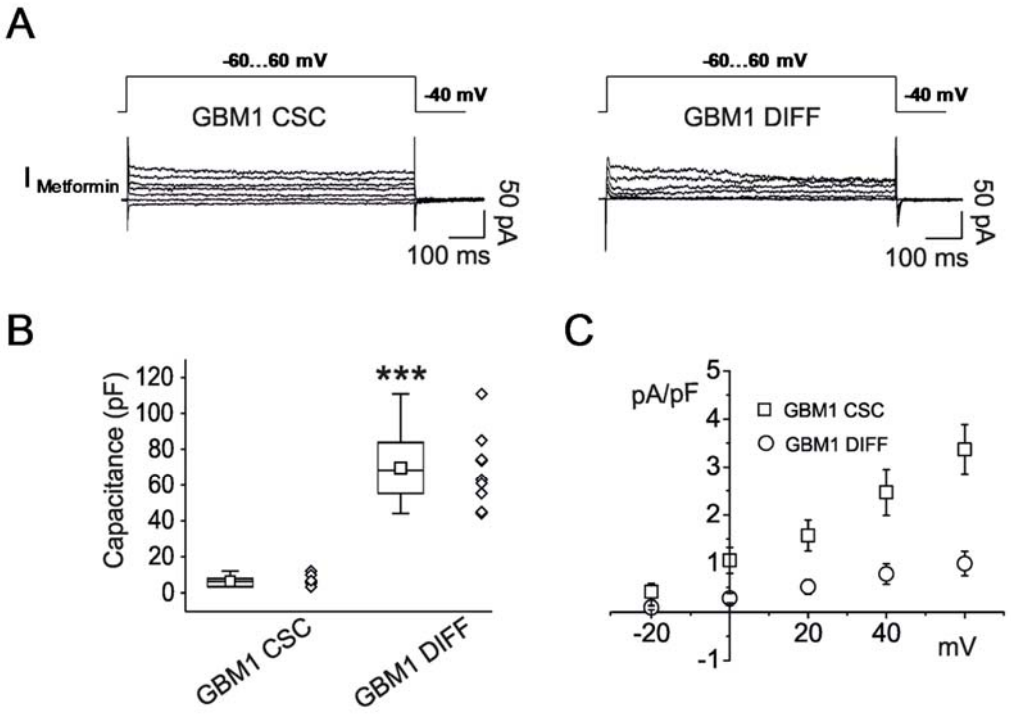


**Figure 22. Differentated cells have less Metformin-sensitive current compared to CSCs.** A) Comparison of Metformin-sensitive membrane current recorded in perforated patch experiments, in CSC (left) and differentiated (right) from GBM1. B-C) Cell capacitance measurements (***p<0.001, t-test) (B), were used to obtain membrane current densities in CSC (square) and differentiated cells (circle) (C) (n=5, mean ± s.e.m. from 5 independent experiments)

### 1.3.6. Point mutation in CLIC1 Arginine 29, impairs the Metformin inhibition

Since Metformin blocks CLIC1 mediated current, we asked in which portion of CLIC1 ion channel Metformin can effectively bind. CLIC1 has a single putative transmembrane domain composed by 22 amino acids, including two charged residues: arginine 29 (Arg29) and lysine 37 (Lys37). In particular the arginine 29 is likely to be near the mouth of the pore and it has been recently demonstrated to be important for the

channel open probability (Averaimo et al., 2013). Taking advantage of computational modeling and the available CLIC1 crystal structure, our collaborator predicted that the arginine 29 may form part of the Metfomin binding site.

To test this hypothesis we used CHO cells stably transfected with two constructs: CLIC1 WT and CLIC1 R29A, where Arg29 was substituted with an alanine.

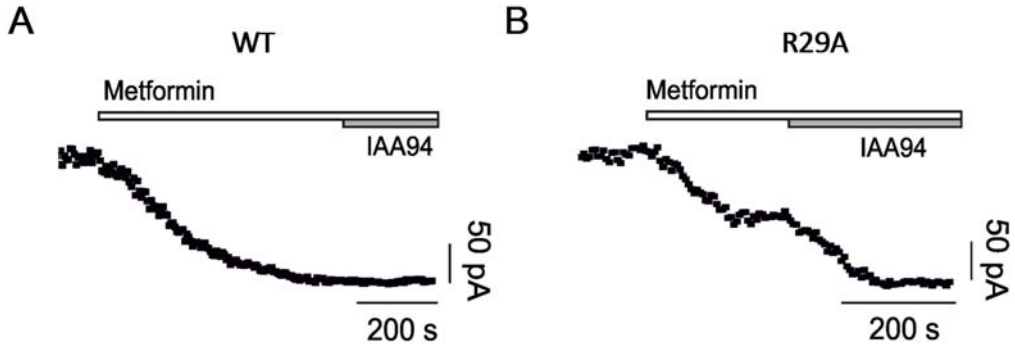


**Figure 23. Arginin 29 is important in the CLIC1 block mediated by Metformin.** A) Whole-cell current time-course of CHO cells transfected with CLIC1-wt. Metformin (10mM) inhibited membrane current, which was not further decreased by IAA94 (100μM). B) Time-course using CHO cells transfected with CLIC1 R29A. This representative experiment showed that Metformin achieved only a partial block of CLIC1 mediated current, in fact the addition of IAA94 further reduced the total current.

We performed time course experiments in perforated patch configuration, pulsing the cells to +60 mV every 5 sec. After reaching the stability of the recording we subsequently perfused Metformin (10 mM) and IAA94 (100 μM) (Figure 23 A and B). In CHO transfected with CLIC1 WT the perfusion of Metformin completely blocked CLIC1-mediated current and therefore IAA94 did not further decrease the membrane current (Figure 23 A). This result confirmed again that Metformin and IAA94 have CLIC1 as a common target. In CHO cells transfected with CLIC1 R29A, Metformin indeed partially blocked the membrane current and the addition of IAA94 was necessary for a complete block of CLIC1-mediated current. Quantifying the Metformin-sensitive current compared to the CLIC1 total current ($I_{Metformin}/I_{IAA94max}$) we estimated the effect of Metformin in CHO transfected with WT, R29A or native cells (not transfected) (Figure 24). The ratio in native and CLIC1 WT cells were similar (0.83 ±

0.06 and 0.83 ± 0.03 respectively) underlying again the specificity of Metformin on CLIC1.

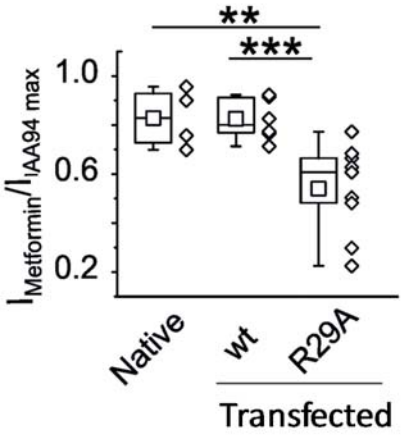


**Figure 24. Arginin 29 is important in the CLIC1 block mediated by Metformin.** Box-plot quantifying metformin insensitive portion of IAA94-sensitive current. Ratio between metformin (10mM) and IAA94 (100μM) is reported for native CHO cells, cells transfected with CLIC1-wt (n=8) and CLIC1-R29A (n=9).Only the trials with CLIC1-R29A produced a value significantly different from the others (**p <0.01 vs native CHO, ***p <0.001 vs CLIC1 wt).

Furthermore $I_{Metformin}/I_{IAA94max}$ in R29A was 0.54 ± 0.06. These results suggested that the arginine 29 is a critical amino acid that mediates the action of Metformin.

## 1.4. Discussion

This thesis points out the pivotal role of the transmembrane fraction of CLIC1 chloride channel in the proliferation of human glioblastoma cancer stem cells (CSCs), the pool of cells that appears to be associated to invasiveness and recurrence of the tumor after initial treatment (Stiles and Rowitch, 2008; Bao et al., 2006). Thus, more effective interventions to contain or eradicate this disease can be achieved by pharmacologically targeting CLIC1 using an antidiabetic drug, Metfomin.

Glioblastomas are the most common and aggressive primary brain tumors. Despite different treatment modalities, overall results have remained unchanged over the last years suggesting that standard therapies are actually ineffective in the eradication of the glioblastoma cancer stem cells. Recently it has been demonstrated the overexpression of CLIC1 in several tumors (Petrova et al., 2008; Chen et al., 2007; Tang et al., 2012; Wei et al., 2015), including high grade glioblastoma (Wang et al., 2012). Not only CLIC1 is overexpressed in glioblastoma, but most importantly the expression of this protein greatly correlates with the glioblastoma prognosis, as previously shown by Wang and collegues and in our recent paper (Wang et al., 2012; Setti et al., 2013). These discoveries suggest that CLIC1 is an actor in the cancer progression and most importantly that this protein could actually be a potential prognostic marker in monitoring glioblastoma progression.

What is the role of CLIC1 in favoring tumor progression?

By silencing CLIC1 in CSCs from human glioblastoma biopsies, we established that CLIC1 is extremely important for *in vitro* CSC proliferation (Figure 15). This interesting observation was corroborated by *in vivo* experiments in which by orthotopic injection of CLIC1 silenced CSC (siCLIC1) in the brain of immunocompromised mice, we demonstrate the impairment of tumorigenic potential of these cells as reported in our recent paper (Setti et al., 2013). Being CLIC1 a dimorphic protein, we ask whether the proliferation impairment is mediated by the cytoplasmic protein fraction or by the transmembrane one. Interestingly, electrophysiological recordings from siCLIC1 cells show that the CLIC1-mediated current is completely abolished (Figures 16 and 17). Furthermore, the CLIC1 ion channel, and not the cytoplasmic one, is the discriminating

factor between CSC vs normal stem cell or differentiated cell (Figures 13, 14 and 22). Thus, it is reasonable to think that the overexpression of CLIC1 and the localization at the plasma membrane confer a proliferative advantage to CSCs and therefore to the tumor mass development. This is actually in line with previous studies reporting the involvements of CLIC1 in cell proliferation (Valenzuela et al., 2000; Tung and Kitajewski, 2010). We know that the soluble form of CLIC1 has glutaredoxin-like enzymatic activity that may be important for protecting the intracellular environment against oxidation in physiological condition (Al Khamici et al., 2015). It is also likely that this activity regulates CLIC1 ion channel function, favoring the insertion of CLIC1 in the membrane under oxidative cytoplasmic potential. Furthermore, in our recent paper (Gritti et al., 2014) we demonstrated that CLIC1 is relevant in the GBM cell cycle only when the protein translocates to the plasma-membrane to allow the G1-S transition of the cells. Since the progression of the cell cycle is due to rhythmic oxidative fluctuations (Menon et al., 2003; Menon and Goswami, 2007; Havens et al., 2006), it is reasonable to hypothesize that CLIC1 following the cytoplasmic oxidative oscillations relocates to the plasma membrane where it acts as chloride channel. We might hypothesize that the translocation of CLIC1: i) determines a flux of $Cl^-$ ions out of the cell, necessary in the volume rearrangements during the proliferation or migration (Mao et al., 2008; Pani et al., 2010) or ii) may support the function of NADPH-oxidase, an enzyme actives during oxidative conditions and thus in CSC, by balancing the excess of positive charges supporting the production of superoxide anions by the enzyme (Averaimo et al., 2010; Milton et al., 2008; Menon et al., 2003). We do not have a full explanation about the mechanism yet, and further experiments need to be done focusing on the difference of the role of CLIC1 in physiological condition in order to better understand what happen in the pathological condition.

Overall these findings suggest CLIC1 as a novel pharmacological target in glioblastoma treatment due to its accessibility from outside the cell and transient appearance in the membrane relevant for CSCs proliferation. So far, the only effective CLIC1 channel blocker identified is IAA94 (Valenzuela et al., 2000). This compound acts as a pore blocker, interrupting the ion flux through the channel. IAA94 seems rather specific but highly toxic. Important in these context is to find and test other compounds that block CLIC1 current more specifically and that can be administer to patients. Recently,

several studies reported the in vitro and in vivo efficacy of metformin, the most widely used antidiabetic drug in the world, as antitumoral agent for several human tumors, including GBM (Wurth et al., 2013; Sato et al., 2012) showing its efficacy in reducing proliferation, survival, clonogenicity and in vivo tumorigenicity of CSCs subpopulation. These studies are really important because they contribute and accellerate the ongoing clinical trial (Kourelis and Siegel, 2012; Pernicova and Korbonits, 2014), but in most of the cases they did not unravel the mechanism by which metformin reduces tumor and why this compound is selective for CSCs. We propose CLIC1 to be the molecular target of metformin activity.

Interestingly, we found that Metformin and IAA94 share the same target acting on CLIC1 ionic current in very similar manner (Figures 19 and 20). As reported in our recent paper (Gritti et al., 2014), Metformin exerts antiproliferative activity similar to IAA94 showing a higher specificity toward CSC in human glioblastoma compared to differentiated cells. To further validate these findings, we have compared the expression of CLIC1 ion channel in these two groups of cells.

The differentiation process decreases CLIC1 protein expression (as verified by western blot) and the related current (Figures 21 and 22). Thus, the different activity and availability of CLIC1 as active chloride channel in CSCs and differentiated cells dictates the strict selectivity of metformin towards CSCs. In addition the selectivity of metformin for cancer cells is a rather unique characteristic for antitumoral drugs and it is also demonstrated by the absence of significant toxicity of metformin when chronically used in diabetic patients.

Where does Metformin bind CLIC1? We demonstrate that Metformin interacts with CLIC1 from the external side of the membrane at the amino terminus of the channel, presumably near the side chain of Arg29 (Figures 23 and 24), which it has recently describe as responsible for destabilizing the closed state of the channel (Averaimo et al., 2013). These data allowed us to build a theoretical model for Metformin action. Arg29 is likely to be near the anion path proximal to the extracellular surface. As it destabilizes the closed state of the channel, it could interact with a polar portion of the channel *via* its guanidinium moiety (Figure 25A).

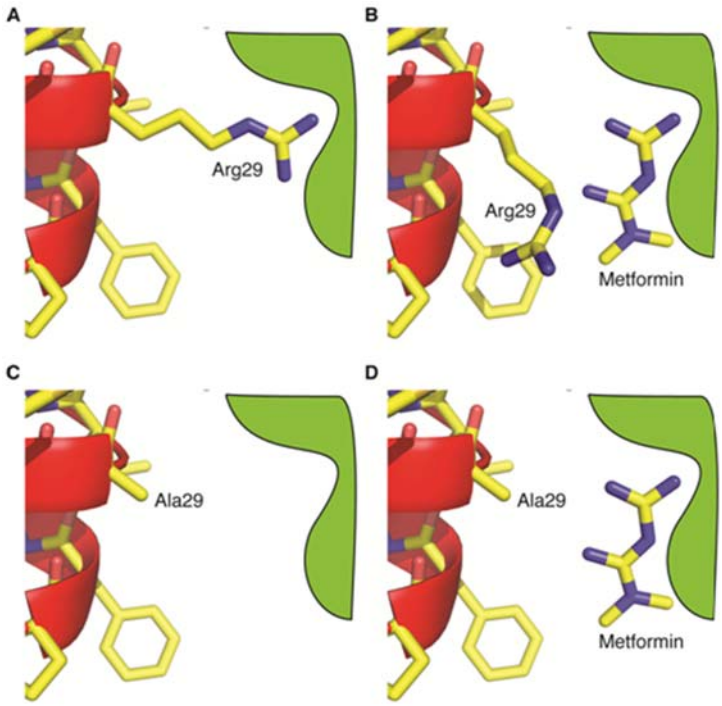


**Figure 25. Modelling of Metformin-CLIC1 interaction.** Schematic representation showing a possible mechanism of Metformin's inhibition of CLIC1 wt, while it has no effect on R29A mutant. A) In the closed state of CLIC1 wt, the side chain of Arg29 makes an interaction that destabilizes the closed state. This facilitates the opening of the channel near the chloride reversal potential. B) Metformin displaces the guanidinium moiety of Arg29, stabilizing the closed state. In addition, the displaced Arg29 side chain may obstruct the channel pore. C) In the R29A mutant, the closed state is stable near the chloride reversal potential, as there is no Arg29 side chain to make the destabilizing interaction as it is replaced by Ala29. D) Metformin is free to bind to the guanidinium site in R29A, as it is unoccupied. It has no effect on channel opening at high membrane potentials.

Using its double guanidinium group, Metformin may displace the side chain of Arg29 from this polar pocket, stabilizing the closed state and possibly obstructing the channel pore displacing the large arginine side chain (Figure 25 B). Metformin can only access this polar site from the outside of the cell, as the binding site is near to the cell surface, given the position of Arg29 in the putative TM segment. In contrast, CLIC1- R29A, lacking Arg29 side chain, displays a more stable closed state, only opening at high membrane potential (Figure 25 C). The polar binding pocket (normally occupied by the guanidinium moiety of Arg29) is exposed and free to bind Metformin (Figure 25 D). However, Metformin binding has no effect on the electrophysiological properties of the

Arg29-lacking mutant, as there is no arginine side chain to displace to cause channel inhibition.

In conclusion, the ability of Metformin to block CLIC1-mediated current suggests that its anti-proliferative activity in GBM CSCs is, at least partially, independent from other intracellular pathways. However, comparing the effects of Metformin and IAA94 (CLIC1 inhibitor) some differences in efficacy and cell sensitivity are apparent in GBM cells. In our and other reports, Metformin antitumor effects occur at concentration in the millimolar range (1-50mM) (Gritti et al., 2014; Cufi et al., 2012; Hirsch et al., 2009; Martin-Castillo et al., 2010; Chen et al., 2012). We are aware of the fact that Metformin is not the ideal CLIC1 blocker due to the low affinity ($EC_{50}$=2.1 ± 0.4 mM) (Figure 18), but on the other hand Metformin treatment has been demonstrated to have negligible side-effects in patient and it is not toxic to normal stem cells and differentiated cells (Kusne et al., 2014; Lee et al., 2014; Wurth et al., 2014; Wurth et al., 2013). Furthermore a recent study demonstrates that Metformin is able to cross the blood-brain barrier (Sato et al., 2012; Labuzek et al., 2010) and therefore represents a valuable therapeutic tool that can be considered in glioblastoma drug design. Based on the proposed Metformin binding site of CLIC1 ion channel, the future effort will be directed towards designing new pharmacological compounds inspired on IAA94 and Metformin in order to reach high specificity, efficacy and non toxicity.

# Chapter 2

## Genetic modification of the L-type Calcium Channels subunit composition as a therapeutic strategy to suppress triggers of cardiac arrhythmia

## 2.1. Introduction

### 2.1.1. Electro-Mechanical activity of the heart

The heart is an electromechanical pump that requires to be electrically activated in order to contract. In the normal heart, action potentials are spontaneously generated by the pacemaker cells in the sinus node (SAN), propagate to the atria and via a specialized conduction system to the ventricles (Figure 1). A tight regulation of this electrical conducting system is critical for the synchronous contraction of both atria and ventricles in order for blood to be pumped efficiently to the lungs for oxygenation and to the body for delivery of oxygen and nutrients. At the cellular level, the depolarization of a cardiac cell (myocyte) activates an influx of calcium that triggers the contraction after an electromechanical delay of a few milliseconds (Bers, 2002; Ashikaga et al., 2007). In fact, during AP the plateau phase (Figure 2) is critical for the proper functioning of the cardiac tissue since allows sufficient time for $Ca^{2+}$ to enter the cell, induces $Ca^{2+}$ release from the sarcoplasmic reticulum (SR) (Figure 3). This massive increase in $[Ca^{2+}]$ engages the contraction machinery (actin and myosin filaments), and initiates contraction of the cardiac muscle, an event which ultimately pumps blood to the tissues in the body. Following the contraction (systole) the muscle fibers must relax (diastole) to allow refilling of the blood of the heart for the next beat. The intracellular $Ca^{2+}$ must be recycled back into the SR through the sarco-endoplasmic reticulum $Ca^{2+}$-ATPase pump (SERCA) pump or extruded back into the extracellular medium via Na/Ca-exchanger (NCX) (Figure 3). The tissue must repolarize before the next oncoming AP, when the process begins again (Bers, 2002). This cycle of excitation, contraction and relaxation occurs billions of times in an average human lifespan.

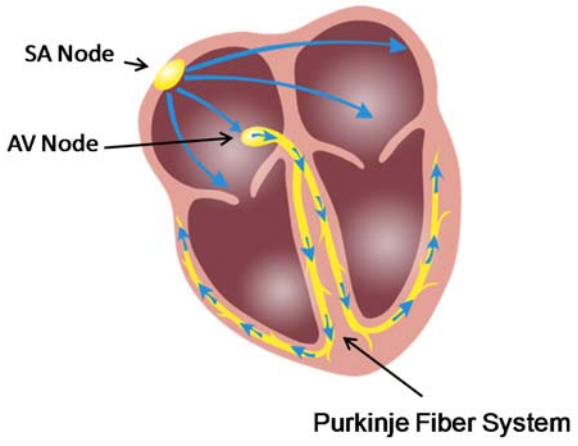


**Figure 1.** The Conduction System of the Heart. The natural rhythm of the heart is dictated by the pacemaker cells within the Sinoatrial (SA) node. The electrical impulse travels from the SA node, through the atrial tissue to the atrio-ventricular (AV) node, and via the His-Purkinje fibers to the ventricular tissue.

### 2.1.2. The Ventricular action potential

The cardiac action potential (AP) is a rapid rising and falling of the electrical potential across a membrane of a myocyte. The shape of the AP is dependent on the overall interactions between the various inward and outward ionic conductances over the course of the AP (Figure 2) (Ravens and Cerbai, 2008). The action potential shape and duration differs in various parts of the heart mainly because of different type and density of ion channels and transporters expressed. In a ventricular myocyte the AP typically displays 5 phases ("**phase 0**" to "**phase 4**"). During **phase "0"**, a massive flux of $Na^+$ ions (generated by the activation of voltage-gated $Na^+$ channels, VGSC) drives the membrane potential (Vm) from its resting level (~-80 mV) towards $Na^+$ electro-chemical equilibrium potential ($E_{Na}$) forming the upstroke of the AP (~40 mV, **phase 0**) (Figure 2). Following this rapid membrane depolarization, sodium channels begin to inactivate, causing a reduction of $Na^+$ conductance. The positive Vm activates a transient outward $K^+$ current ($I_{to}$) that produces a partial repolarization (**phase 1**) interrupted by a plateau phase (**phase 2**) where a substantial $Ca^{2+}$ influx produced by the activation of L-type $Ca^{2+}$ current ($I_{Ca,L}$) is counterbalanced by a $K^+$ efflux through

voltage gated delayed rectifier channels ($I_{Kr}$ and $I_{Ks}$). This plateau phase (~300 ms) is essential for the prevention of electrical re-excitation and tetanic contraction in the heart, which could inhibit relaxation needed for the filling of blood prior to ejection (Bers, 2002). The influx of $Ca^{2+}$ through L-type $Ca^{2+}$ channels (LTCC) during this plateau phase has implications. First, the $Ca^{2+}$ entry induces $Ca^{2+}$ release from the SR by activating ryanodine receptors (RyRs), a phenomenon known as Calcium-Induced Calcium-Release (CICR) (Figure 3) (Bers, 2002; Bers and Guo, 2005). This massive increase in $Ca^{2+}$ concentration in the myocyte (from 0.1 μM up to 1μM), engages the contraction machinery as the actin and myosin filaments transduce chemical energy into mechanical force (Bers, 2002). Moreover, $Ca^{2+}$ entry binds to calmodulin (CaM) which is directly associated with the L-type $Ca^{2+}$ channel, and initiates $Ca^{2+}$-dependent inactivation (CDI) (Peterson et al., 1999). Eventually, a decay in the $Ca^{2+}$ current due to CDI and voltage-dependent inactivation (VDI) of the LTCCs allows $K^+$ conductances to dominate, and hence repolarize the Vm towards the equilibrium potential for $K^+$ (**phase 3**).

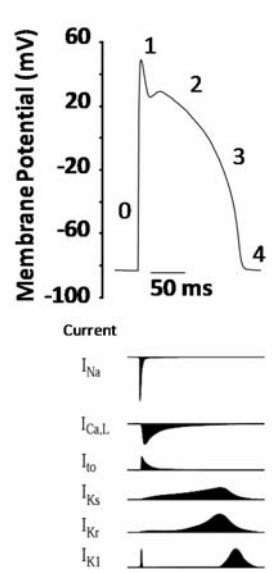


**Figure 2.** Inward and outward currents that shape the ventricular action potential. The top panel shows a ventricular action potential (AP) and the different phases that characterize the AP. Inward currents are mainly conducted by $Na^{2+}$ and $Ca^{2+}$ channels; outward currents are mainly conducted by various potassium channels. Phase 0 shows a rapid depolarization; phase 1 shows a rapid early repolarization; phase 2 shows a slow 'plateau' of repolarization; phase 3 shows a rapid late repolarization; and phase 4 shows resting potential. Adapted from (Boukens et al., 2009)

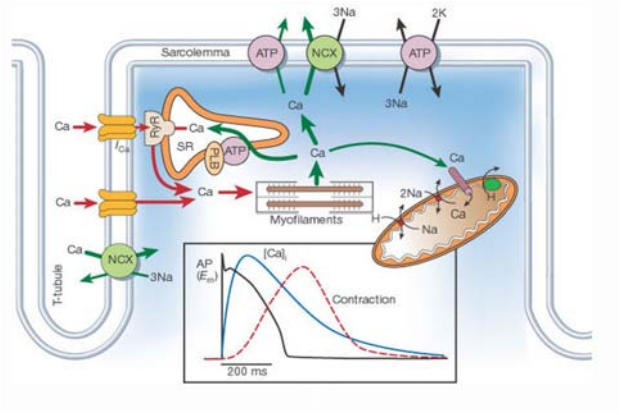


**Figure 3.** Scheme of calcium cycle in a ventricular myocyte. $Ca^{2+}$ enters via $I_{Ca}$ (L-type calcium channel) and Na/Ca-exchanger (NCX). The influx of $Ca^{2+}$ controls the sarcoplasmic (SR) $Ca^{2+}$ release via ryanodine receptor (RyR). The massive increase of $[Ca^{2+}]$ controls engages the contraction machinery (actin-myosin) that determines the contraction. The main entryway of $Ca^{2+}$ from the extracellular medium is the L-type $Ca^{2+}$ channels shown in orange. $Ca^{2+}$ is then mainly removed from the cytoplasm by SR Ca-ATPase (SERCA) (modulated by phospholamban, PLB) and by the Na/Ca-exchanger (NCX) and mitochondrial uniporter. ATP is Na/K ATPase, PLB is phospholamban, SR, sarcoplasmic reticulum. The graphs in the box show, in black, a ventricular myocyte's AP; in blue the intracellular $[Ca^{2+}]$ during the course of the AP; in red, the contraction of the cardiac muscle (Bers, 2002).

During this phase, the surplus intracellular $Ca^{2+}$ is pumped back to either the extracellular medium or the sarcoplasmic reticulum (SR) via the Na/Ca-exchanger (NCX) or the sarco-endoplasmic reticulum $Ca^{2+}$-ATPase (SERCA), respectively (Figure 3). This resets the cell to a diastolic state (**phase 4**), during which the myocyte relaxes and is ready for the next heartbeat.

### 2.1.3. Triggers of ventricular arrhythmias

Sudden cardiac death (SCD) is one of the major leading causes of death in the United States, accounting for about more than 300,000 deaths every year. SCD is often caused by cardiac arrhythmias that lead to the heart being unable to pump blood efficiently to the body. The most dangerous cardiac arrhythmias arise in ventricular tissue and include ventricular tachycardia (VT) and ventricular fibrillation (VF) (John et al., 2012). Ventricular tachycardia can often be diagnosed and treated but ventricular fibrillation

almost always results in cardiac arrest and death if not terminated quickly. The cardiac excitation that occurs for every single beat can be viewed as a electrical wave that emerge focally in the SAN and spreads out through the whole heart (the cardiac action potential). If this wave of depolarization during the propagation brakes at one point originates two new broken end that become the locus of potential reentrant waves (spiral waves) (Weiss et al., 2000; Qu and Weiss, 2015). Thus, if this reentrant waves propagate in the heart tissue and collide with some anatomical obstacle, they create an reentrant circuit which represent an ectopic focus that rapidly and repetitively activate the ventricles. This produces an activity that contrasts the sinus rhythm and determined an abnormal rapid heartbeat. This situation is called ventricular fibrillation (VT). Sometimes the heart can reset this condition but in a more dangerous situation the VT can degenerate in a condition called ventricular fibrillation (VF).

In fact sometime the reentrant wave presents in VT collides and develop wavebreaks that generate multiple reentrant waves characterized by multiple wavelets.

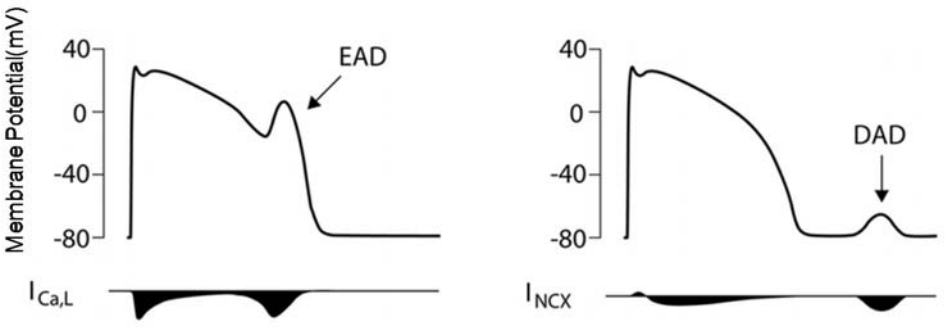


**Figure 4.** Early Afterdepolarizations and Delayed Afterdepolarizations. Early afterdepolarzation (EAD) are single or multiple reversal of repolarization occurring in phase 2-3 of the cardiac action potential. A delayed afterdepolarization (DAD) occurs after repolarization of the AP is complete. Since $Ca^{2+}$ channels cannot be activated at hyperpolarized membrane potentials during diastole, the cellular mechanisms for DADs involve $I_{NCX}$ (Adapted from (Hoekstra et al., 2012).

In VF the ventricle are activated in a rapid and asynchronous way (The ventricles "fibrillate" rather than beat) that results in a disordered activity in which the heart cannot pump blood, causing cardiac arrest (Weiss et al., 2000; John et al., 2012). Cellular triggers of VT and VF are abnormal depolarization of the AP, called early afterdepolarizations (EADs) if they occur during systole or delayed afterdepolarizations

(DADs) if they occur during diastole (Cranefield, 1977; Qu and Weiss, 2015) (Figure 4). Although both EADs and DADs are considered highly arrhythmogenic, the underlying mechanism for each is still an open area of investigation.

### 2.1.4. Early afterdepolarizations

Early afterdepolarizations (EADs) are secondary voltage depolarizations occurring during the repolarization of the cardiac AP (phase 2 or 3) that tend to emerge at low pacing rate and hence are associated with bradycardic arrhythmias (Damiano and Rosen, 1984; January et al., 1988).

EADs were first described by Cranefield and his colleagues in 1972 as they observed them in a Purkinje fibers of an intact cardiac tissue in canine (Cranefield et al., 1972). EADs were subsequently described as a form of "triggered activity" in myocardium caused by the transition from a normal to a rapid and asynchronous electrical activity of the heart that can cause VT and VF (Cranefield and Aronson, 1974; Cranefield, 1977) (Figure 5).

Formation of EADs is largely dependent upon the net ionic conductance governing the phase 2 and 3 of the action potential. In fact they are mainly due to either abnormally decreased outward currents, increased inward currents, or both, classically defined as reduced repolarization reserve (Qu et al., 2013). Therefore, it could be due to an increase in the inward $I_{Ca,L}$ and/or a reduction in the outward $K^+$ current that could alter the repolarization phase such that the net increase in inward current eventually reverses the repolarization of the membrane potential (Weiss et al., 2010). Marban and colleagues demonstrated that an increase in extracellular $Ca^{2+}$ augmented EADs occurrence, while blocking SR $Ca^{2+}$ release with ryanodine or chelating intracellular $Ca^{2+}$ maintained EADs in ferret ventricular tissue (Marban et al., 1986). Furthermore, they also showed that EADs were directly connected with the increase in the opening of $Ca^{2+}$ channels by applying Bay K8644, a $Ca^{2+}$ channel agonist and that EADs were subsequently eliminated using a $Ca^{2+}$ channel blocker, Nitrendipine.

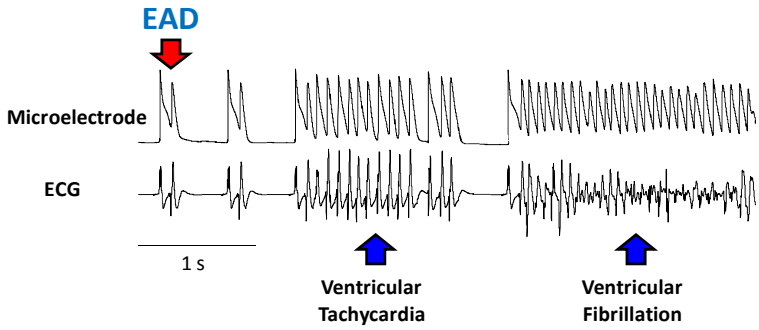


**Figure 5**. Early Afterdepolarizations trigger Ventricular Tachycardia and Ventricular Fibrillation in a perfused rat heart, exposed to $H_2O_2$ (Courtesy of A. Karaguezian laboratory UCLA).

The relevance of L-type calcium channel (LTCC) in the EADs formation was further studied by January and colleagues. Their findings suggested that EADs induction was dependent on both time and voltage-dependent mechanisms. In fact they observed that the voltages where EADs were induced, overlapped with the voltages where recovery from inactivation of the LTCCs occured (January and Riddle, 1989). January and Riddle subsequently tested their hypothesis that reactivation of LTCCs contributes to EAD formation by demonstrating that the voltage dependence of EADs mirrors the voltage-dependence and time-dependent recovery of LTCCs (January and Riddle, 1989). Their experiments provided the first indication that L-type $Ca^{2+}$ channel reopening during steady-state may allow the flux of an inward current due to the overlap of the activation and inactivation curves of LTCCs (Shorofsky and January, 1992). Most EADs are initiated between -40 and 0 mV, corresponding to the range of membrane potentials where the steady-state activation and inactivation curves of $I_{Ca,L}$ overlap, often referred to as the 'window current' region (shaded area in Figure 6) (January and Riddle, 1989; Antoons et al., 2007). Steady state curves of $I_{Ca,L}$ show the voltage dependency of LTCC activation and inactivation over a range of membrane potentials. As the AP repolarizes into this voltage range of potential, a fraction of the L-type $Ca^{2+}$ channels not inactivated may be available for reactivation thus conducting inward $Ca^{2+}$ current that induces the upstroke of the EADs. Another direct confirmation that EADs are related to $I_{Ca,L}$ "window current" was assessed in our laboratory. In fact Madhvani and colleagues, established that EADs formation is highly dependent on the $I_{Ca,L}$ biophysical properties and therefore on the "window current" region (Madhvani et

al., 2011). Using the dynamic clamp technique they identified two parameters of the L-type $Ca^{2+}$ channel (LTCC) biophysical properties that potently suppress EADs occurrence. In particular subtle changes in the steady-state activation or inactivation properties of $I_{Ca,L}$ (~5mV depolarizing shift of the $V_{1/2}$ steady-state activation curve and ~5mV hyperpolarizing shift of $V_{1/2}$ the steady-state inactivation curve) potently suppress EADs formation. These results point out that a reduction of the $I_{Ca,L}$ "window current" represents an effective maneuver to suppress EADs without blocking the early peak $I_{Ca,L}$ required to maintain normal excitation-contraction coupling (Madhvani et al., 2011).

EADs can be classified based on AP phase where they occur: during the plateau (called phase 2 EADs) or during repolarization (called phase 3 EADs). Depending on this classification, the proposed mechanism for EADs occurrence is different. Since phase 3 EADs tend to arise at more hyperpolarized membrane potentials (below -40 mV) compared to phase 2 EADs, which occur at the plateau potential (between -10 mV and +20 mV), a number of laboratories have proposed that either the $Na^{2+}$ "window current" or reverse-mode action of the Na-Ca exchanger could play a major role in phase 3 EADs (Qu et al., 2013). The main reason is due to the fact that $Ca^{2+}$ channels are not active below -40mV, and therefore unlikely to contribute to EAD formation. Modeling studies also corroborated the possibility of Na-Ca exchange current contributing to phase 3 EADs ($I_{Na-Ca}$) (Luo and Rudy, 1991; Luo and Rudy, 1994).

In isolated myocytes there are several modalities to induce EADs. Different studies EADs were induced either by the presence of $Cs^{+}$ to block $K^{+}$ currents and delay repolarization or by directly altering the gating properties of LTCCs using an agonist such as Bay K8644.

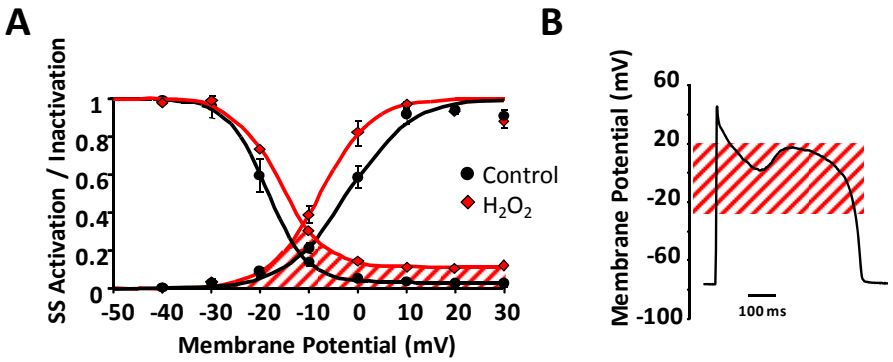


**Figure 6.** EAD formation occurs within the voltage range of "window current" region. A) the black curves show the steady-state activation and inactivation curves of $I_{Ca,L}$ measured in rabbit ventricular myocytes in normal physiological Tyrode's buffer solution. The red curves show the steady-state activation and inactivation curves of $I_{Ca,L}$ after being exposed to 0.6 mM $H_2O_2$. The shaded areas are known as the "window current" region, which is the region where steady state activation and inactivation curves overlap. B) A rabbit ventricular cardiac AP with EADs recorded in 0.6 mM $H_2O_2$. The red shaded area reflect the "window current" regions of (A). This is showing that EADs often occurs within the "window current" region, between approximately -30 mV and +10 mV and that $H_2O_2$ increases the height of the "window current". Adapted from (Madhvani et al., 2011).

Alternative methods being used are hypokalaemia, by lowering extracellular [$K^+$] (from 5.4 to 2.0-2.7 mM) to block $I_{K1}$ and other potassium conductances (Sato et al., 2009) or oxidative stress, by exposure to 600 μM $H_2O_2$ (Xie et al., 2009). Several groups have demonstrated the EAD-genic effects of ROS. Hydrogen peroxide ($H_2O_2$), a potent biologically reactive ROS which can easily cross the plasma membrane, is directly produced in cardiac tissue upon reperfusion following ischemic injury (Slezak et al., 1995; Brown et al., 1988a; Brown et al., 1988b). Furthermore many laboratories have provided evidence which suggests that $H_2O_2$ promote EADs by activating $Ca^{2+}$–calmodulin-dependent protein kinase II (CaMKII) (Xie et al., 2009), which alters late component of $I_{Na}$ (Wagner et al., 2011; Wagner et al., 2006). In addition it has been reported the effect in other conductanced involved in shaping the AP included $I_{Kr}$, $I_{NCX}$ and RyRs (Beresewicz and Horackova, 1991; Liu and Gutterman, 2002; Liu and O'Rourke, 2013). Madhvani and colleagues reported that $H_2O_2$ modified the $I_{Ca,L}$, slowing down the inactivation and shifting the peak of the current–voltage (I–V) relationship by −5 mV. Furthermore $H_2O_2$ changes the voltage dependence of the channel producing ∼−5 mV shift of the steady state half-activation potential ($V_{1/2}$ act)

and ~+5 mV shift in the steady state half-inactivation potential ($V_{1/2}$ inact). Effectively, $H_2O_2$ increased the height of the $I_{Ca,L}$ "window current" region, changes which are expected to promote EAD formation increasing the number of $I_{Ca,L}$ channel available to activate during the AP repolarization (Madhvani et al., 2011) as in Figure 6.

### 2.1.5. Voltage-gated calcium channel

Voltage-gated calcium channels are integral cell membrane proteins that mediate $Ca^{2+}$ influx into the cell in response to membrane depolarization. The entered $Ca^{2+}$ serves as an essential intracellular messenger that regulates a variety of cellular processes including muscle contraction, hormone secretion, neuronal transmission, and gene expression (Yang and Berggren, 2006; Flavell and Greenberg, 2008; Catterall, 2011; Catterall and Few, 2008).

There are several $Ca^{2+}$ currents that have been classified by their electrophysiological properties in L-, N-, P-, Q-, R-, and T-type (Catterall, 2011).

### 2.1.6. L-type calcium channel (LTCC)

In the ventricular myocytes, the predominant $Ca^{2+}$ channel present is L-type channel ($Ca_V1.2$) and it is primarily localized in the T-tubules of skeletal and cardiac muscle cells (Wibo et al., 1991). LTCCs activate at depolarized voltage (-40mV) and have slower voltage-dependent inactivation that contributes to their long lasting conducting property (Tsien et al., 1988; Ono and Iijima, 2010). LTCCs are crucial in maintaining the time course of a cardiac AP, in providing the passageway of $Ca^{2+}$ entry into the cell, and ultimately in excitation-contraction coupling of a cardiac myocyte. $Ca^{2+}$ entering the cell during an AP triggers SR release of $Ca^{2+}$ via $Ca^{2+}$-induced $Ca^{2+}$-release phenomenon (Bers, 2002). Although the inward current carried by LTCCs was characterized in the 1960s (Orkand and Niedergerke, 1964), the molecular identity of the cardiac L-type $Ca^{2+}$ channel was established by Mikami and colleagues from rabbit hearts in the late 1980s (Mikami et al., 1989). The heteromultimeric LTCCs were first

cloned from rabbit skeletal muscle by Tanabe and colleagues in 1987 (Tanabe et al., 1987).

**Topology**

LTCCs were first known as dihydropyridines receptors attributing to their sensitivity to dihydropyridines (DHP). They are multimeric protein complexes form by ion-conducting pore $\alpha_1$ subunit and auxiliary subunits $\alpha_2\delta$, β, and γ that involved in anchorage, trafficking, and regulatory functions (Figure 7).

**$\alpha_1$ subunit**

The LTCC $\alpha_1$ is encoded by a single gene (CACNA1) and has multiple splice variants, in the heart $\alpha_1$c ($Ca_V1.2$). The $\alpha_1$ subunit contains four homologous domains (I–IV), each comprising of six membrane-spanning segments (S1–S6) connected by intracellular loops. The S1–S4 segments from each domain form a voltage-sensing domain (VSD), whereas segments S5 and S6 contribute to the channel pore and contain the selectivity filter (Catterall, 2011). VSDs are structurally and functionally conserved modules capable of transducing a change in the cell membrane electrical potential. Recently it has been demonstrate that each of $Ca_V1.2$ VSDs possesses unique properties in the channel activation (Pantazis et al., 2014). The four domains are linked by intracellular loops which have residues that interact with β subunits via the α-interaction domain (AID) in the linker between I-II domain, while the intracellular C-terminal tail contains critical structural elements (pre-IQ, and IQ regions) necessary for $Ca^{2+}$/calmodulin (CaM) binding site (Halling et al., 2006). In fact $Ca^{2+}$/Calmodulin acts as an intrinsic calcium sensor modulating calcium-dependent inactivation (CDI) and calcium-dependent facilitation (CDF), both important for regulating the level of $Ca^{2+}$ during cardiac AP (Catterall, 2011). Alseikhan *et al.* demonstrated the physiological importance of CaM as a $Ca^{2+}$-sensor mediating CDI in LTCCs of cardiac myocytes using engineerined CaM (Alseikhan et al., 2002). This approach, in which the CaM was mutated at all four $Ca^{2+}$-binding sites to abolish its $Ca^{2+}$-sensitivity and heterogously expressed in adult rat cardiomyocytes, allowed the investigators to probe the physiological role of $Ca^{2+}$-dependent regulation of LTCCs associated with CaM. Their

intriguing results show that in cells expressing the recombinant CaM, CDI was eliminated and only a monotonic decay remained resulting in very long APDs.
In addition to CDI a slower, a purely voltage-dependent inactivation (VDI) process is present in Cav1.2. This control of the inactivation process is relevant for myocytes activity as it serves to limit the level of $Ca^{2+}$ influx during prolonged depolarization and as a result, it regulates the toxic downstream effects of elevated intracellular $Ca^{2+}$.

Different mutation in Cav1.2 $\alpha_{1c}$ subunit has been associated with the Timothy syndrome, the Brugada syndrome, and early repolarization syndrome, all diseases connected with an abnormal heart rhytm (Napolitano and Antzelevitch, 2011).

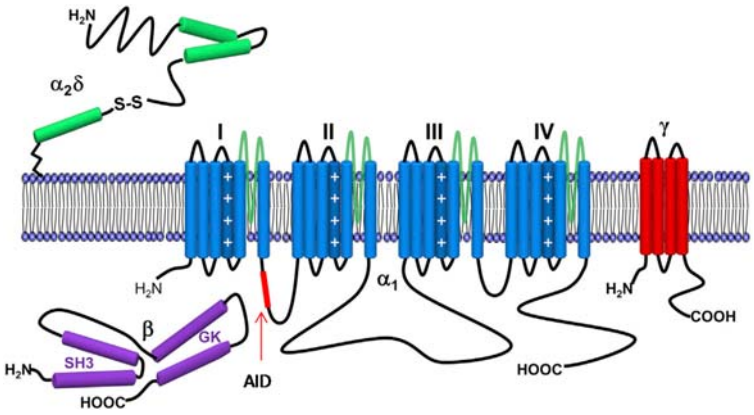


**Figure 7.** The L-type calcium channel (Cav1.2) is a multi-protein complex composed of $\alpha_{1C}$ (pore-forming subunit) and distinct auxiliary subunits: $\alpha_2\delta$, β and γ. The L-type $Ca^{2+}$ channel polypeptide consists of four tandem domain (I-IV), each crossing the membrane six times (S1-S6). Helix S4 contains positively charged residues, which together with S1-S3, make up the voltage-sensing domain (VSD), whereas the loop between S5-S6 from each repeat contribute to the ion-selective pore. The intracellular loop between domains I and II contains the α-interaction domain (AID) which binds β subunits, while the C-terminal tail contains the calmodulin (CaM) binding IQ-motif. Adapted from (Simms and Zamponi, 2014).

### Auxiliary subunits

Three different auxiliary subunits, $\alpha_2\delta$, β and γ, are known to modulate the activity of the $\alpha_1$ pore-forming subunit. $\alpha_1$ subunits normally interact with at least the $\alpha_2\delta$ and β subunits (Hosey et al., 1996). Singer and colleagues showed that expression of $\alpha_1$ subunit alone contributes to functional LTCCs (Singer et al., 1991), while coexpression

with $\alpha_2\delta$ and β subunits increases the current conductance by promoting trafficking of $\alpha_1$ subunit to the plasma membrane (Dolphin, 2012).

**$\alpha_2\delta$** There are four $\alpha_2\delta$ subunit isoforms ($\alpha_2\delta$-1–$\alpha_2\delta$-4). These proteins are the product of a single gene that is post-translationally cleaved into separate $\alpha_2$ and δ peptides held together by disulphide bonds (Dolphin, 2012). Most of $\alpha_2\delta$ subunit is extracellular, infact the large $\alpha_2$ protein is entirely extracellular and tethered to the plasma membrane via the δ subunit which has a short hydrophobic region that traverses the membrane (Davies et al., 2010; Catterall, 2011).

**β** There are four distinct $Ca_V\beta$ subunits (β1–β4) encoded by four different genes, each subunit with multiple splice variants (Buraei and Yang, 2013). β subunits are cytosolic protein located near the plasma membrane. $Ca_V\beta$ was first purified as part of the complex of skeletal muscle voltage-gated $Ca^{2+}$ channels and was cloned in 1989 (Curtis and Catterall, 1984; Ruth et al., 1989). All $Ca_V\beta$s contain a conserved core comprised of *src* homology 3 (SH3) and guanylate-kinase like (GK) domains and three variable unstructured regions—N-terminus, C-terminus, and a HOOK domain that separates SH3 and GK (Buraei and Yang, 2013). Different biochemical and electrophysiological have been demonstrated that in GK domain of $Ca_V\beta$s there is a conserve $\alpha_1$-binding pocket (ABP) region that binds with high (nM) affinity to a conserved 18-residue $\alpha_1$ interaction domain (AID) located in the intracellular loop between domain I–II of pore-forming $\alpha_1$

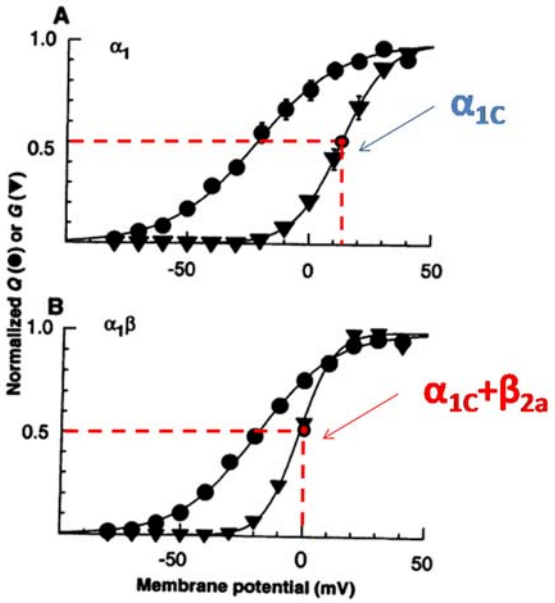


**Figure 8.** $Ca_V\beta$s modulate the biophysical properties of cardiac cardiac LTCC causing a shift in the steady-state activation curve to more hyperpolarized membrane potential. Adapted from (Neely et al., 1993).

subunits (Pragnell et al., 1994). In 2004, three independent research groups reported the crystal structures of the $Ca_V\beta$ core region of $\beta_{2a}$, $\beta_3$ and $\beta_4$, alone or in complex with the AID (Chen et al., 2004; Opatowsky et al., 2004; Van et al., 2004).

$Ca_V\beta$s play a role as traffic regulators of the pore-forming α subunit to the plasma membrane and in modulation of biophysical properties of LTCC by associating with α1 subunit (Dolphin, 2012).

Characterization of the effects of β subunit interaction on the gating properties of LTCCs demonstrated a significant shift of the conductance-voltage (G-V) relationship toward more negative potentials in the presence of $\beta_{2a}$ in heterologously expressed channels, while the voltage dependence of the charge movements (gating currents) remained unchanged (Figure 8) (Neely et al., 1993). Furthermore, in addition to the steady-state voltage-dependence, it is well established that both the activation and inactivation kinetics are significantly altered in the presence of β subunits (Varadi et al., 1991; Singer et al., 1991). $Ca_V\beta$ subunits increase the open probability (Po) in a single channel measurements causing a hyperpolarizing shift in the voltage-dependence of activation, and imparting unique profiles of voltage-dependent inactivation (Wakamori et al., 1999; Colecraft et al., 2002) , with $\beta_{2a}$ producing the most dramatic increase in channel open probability (Dzhura and Neely, 2003). Thus, $Ca_V\beta$s regulate biophysical properties of LTCC: increasing channel open probability ($P_o$), causing a hyperpolarizing shift in the voltage-dependence of activation, and imparting unique profiles of voltage-dependent inactivation. Furthermore, different β subunits confer a specific signature to LTCC voltage dependent properties. Different isoforms, when coexpressed with human $\alpha_{1E}$, have been shown to modulate inactivation of VGCCs expressed in *Xenopus* oocytes (Olcese et al., 1994). A study done in rat ventricular myocytes has demonstrated that four isoforms of $Ca_V\beta$ subunits, namely $\beta_1$, $\beta_2$, $\beta_3$, and $\beta_4$, contribute to an increase in the open probability of LTCC to different degrees (Colecraft et al., 2002). Among the different $Ca_V\beta$ subunits, $Ca_V\beta_{2a}$ subunit seemed to produce the greatest enhancement in the current density compared to all other β isoforms (Alseikhan et al., 2002). The difference in the modulation confers by β subunit is present even between splice variance. In fact five different splice variants ($\beta_{2a}$–$\beta_{2e}$) that differ only in their N-termini where expressed in heterologous cells and each splice variance impart unique inactivation and single-channel-gating signatures (Takahashi et al., 2005).

In the heart $\beta_2$ and $\beta_3$ are the most abundant subunit expressed ($\beta_2 > \beta_3$), in particular it is reported that $\beta_{2b}$ is the most abundant transcript in ventricular myocytes compare to $\beta_{2a}$ and $\beta_3$ (Hullin et al., 1992). The functional significance of having diverse Cav$\beta$ isoforms and splice variants in the heart is unknown. Knockout of $\beta_2$ in mice is embryonic lethal due to impaired cardiac development that is secondary to a decreased L-type $Ca^{2+}$ current ($I_{Ca,L}$) (Weissgerber et al., 2006). On the contrary, in a recent study it is reported that a cardiac-specific excision of $\beta_2$ in adult mice substantially knocked-down $\beta_2$ protein (by 96%), but only moderately decreased $I_{Ca,L}$ suggesting that Cav$\beta_2$ may not be critical for $\alpha_{1C}$ trafficking in adult ventricular myocytes (Meissner et al., 2011). Additionally, increased expression of $\beta_{2a}$ has been seen in failing human hearts, which are prone to arrhythmias, and it has also been shown to play a role in pathological membrane excitability leading to cell death in adult cardiomyocytes (Hullin et al., 2007).

**γ** There are eight distinct γ isoforms (γ1–γ8). γ subunits are membrane proteins with a predicted four membrane-spanning segments and intracellular N- and C-termini. The cDNA of four γ subunit isoforms (γ4, γ6, γ7, and γ8) has been detected in human heart, although only γ6 expression has been confirmed at the protein level in rat heart (Shaw and Colecraft, 2013).

### 2.1.7. Using Dynamic clamp to study the biophysical properties of LTCC

The patch clamp technique was developed by Neher and Sakmann in the late ‘70s. This technique revolutionized the field of physiology and biophysics by allowing electrophysiologists to directly study the ion channel function. Therefore, the patch clamp technique can generate important information about the behavior of ion channels, transporters and pumps in various physiological setting allowing to understand the behavior of excitable cells in vitro and in vivo. Furthermore, it has facilitated the development of mathematical models of complex electrophysiological phenomena.

A powerful evolution of the patch clamp is the dynamic clamp technique that combines electrophysiological recordings and mathematical modeling in real-time. This allows for

the introduction of a virtual (computer-simulated) ionic current into a cell to test its impact on the cell electrical properties and excitability. The concept of dynamic clamp was first demonstrated in the '90s by Tan and Joyner. They studied the artificial electrical coupling between isolated rabbit ventricular myocytes in a whole-cell clamp (Tan and Joyner, 1990). They did a simulation of two cells with a variable coupling resistance without physically coupling them to observe changes in the properties of each cell individually as a result of artificially providing electrical coupling between them (Tan and Joyner, 1990).

Dynamic clamp has been used by several groups to studythe behavior of different excitable cells, mainly in the neuroscience field (Tan and Joyner, 1990; Sharp et al., 1993; Wilders, 2006; Berecki et al., 2005; Berecki et al., 2007; Madhvani et al., 2011). We took advantage of this hybrid experimental-computation system to explore with great precision the different biophysical properties of $I_{Ca,L}$ that could potentially serve as a therapeutic target for EADs suppression.

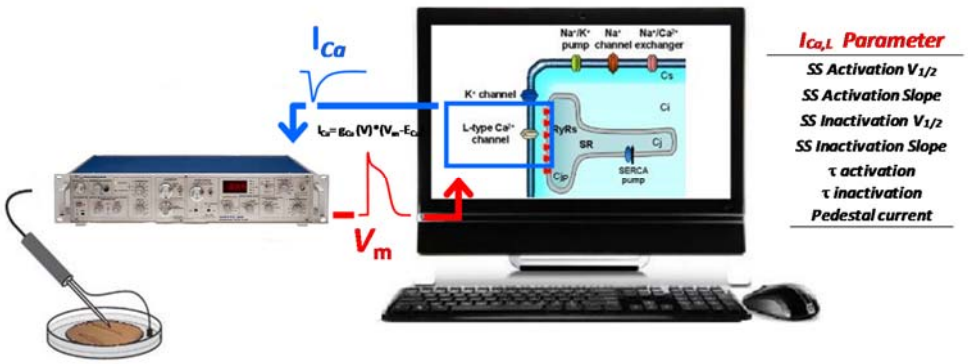


**Figure 9.** A diagram of our Dynamic Clamp set-up. The dynamic clamp is a powerfull technique that allow to manipulate in real time the ionic conductance of a cell.

In our experiments, we use the cardiac action potential model-UCLA model (Mahajan et al., 2008) containing five macroscopic conductances ($I_{Ca,L}$; the fast Na channel $I_{Na}$; the Na/K pump $I_{NaK}$; the Na/Ca exchanger $I_{NCX}$; and the $Ca^{2+}$-dependent K rectifier $I_{Ks}$). Specifically, the formulation of $I_{Ca,L}$ is an Hodgkin-Huxley-type formulation to allow us to modify specific parameters of $I_{Ca,L}$ in a discrete manner, rather than changing the gating behavior of the channel, which can be more difficult to interpret.

A ventricular myocyte is whole-cell patch-clamped with an amplifier in current-clamp mode (Figure 9). The myocyte's membrane potential (Vm) signal (red arrow) is digitized and input to a computer running the AP model. The computer calculates the ionic conductances that can be output in any combination to produce $I_{Command}$. In our case case, $I_{Command}$ is $I_{Ca,L}$ (blue arrow). $I_{Command}$ is combined with a pacing AP stimulus and converted to analog before being input to the amplifier to be injected into the clamped myocyte. This alters the myocyte Vm, which is in turn sampled for the next computation. Thus, there is a dynamic, bidirectional relationship between Vm and model conductance output, at a sampling/computation frequency of 10 kHz. In our experiment a virtual $I_{Ca,L}$ with programmable properties is injected into a cell in real time to study its effects on action potential characteristics without altering other existing ionic conductance in the cell. Using this technique, our laboratory was able to previously show that a ~5 mV leftward shift in half-inactivation potential and a ~5 mV rightward shift in half-activation potential, both of which lower the area encompassing the "window current" region, potently abolished EADs in rabbit ventricular myocytes (Madhvani et al., 2011). These studies strongly supported the relevance of $I_{Ca,L}$ in EADs formation and showed that by manipulating only the $I_{Ca,L}$ biophysical properties, EADs could be abolished, even though there may be many other ionic currents involved in the initial EADs genesis (Madhvani et al., 2011).

This thesis investigated the relevance of the non-inactivating $I_{Ca,L}$ (pedestal current) in the etiology of EADs using dynamic clamp technique. Furthermore, we tested the hypothesis that a decrease in the expression of $Ca_v\beta_2$ subunits in ventricular myocytes can reduce the EADs susceptibility.

## 2.2. Methods

### 2.2.1. Ethical Approval

All animal handling protocols were approved by the UCLA Institutional Animal Care and Use Committee and conformed to the Guide for the Care and Use of Laboratory Animals published by the US National Institutes of Health.

### 2.2.2. Myocytes isolation

Ventricular myocytes were isolated from three- or four-month-old male New Zealand white rabbits as previously described (Madhvani et al., 2011). The rabbits were first injected with heparin sulfate (1000 U) and sodium pentobarbital (100 mg/kg) intravenously. Adequacy of the anesthesia was confirmed by the lack of pedal withdrawal reflex, corneal reflex, and motor response to pain stimuli. Following excision, the heart was submerged in Tyrode's buffer solution containing (in mmol/L): 136 NaCl, 5.4 KCl, 1 $MgCl_2$, 0.33 $NaH_2PO_4$, 0.2 $CaCl_2$, 10 Glucose, and 10 HEPES adjusted to pH 7.4. Using a retrograde Langendorff perfusion system, the rabbit's excised heart was first perfused with Tyrode's solution until all blood was washed out thoroughly; then, Tyrode's solution containing 0.8mg/mL bovine serum albumin and 1.65mg/mL collagenase was constantly perfused for about 30 to 40 minutes to ensure sufficient digestion time. The enzyme-containing solution was washed out after the digestion time and the heart was submerged and mechanically torn apart with forceps in Tyrode's solution containing 0.2 mmol/L $Ca^{2+}$. The pieces of the tissue were swirled in the solution to aid cell dissociation. The dissociated myocytes were then washed several times in 1.8 mM $Ca^{2+}$-containing Tyrode's buffer solution using centrifugation to remove as much dead cells as possible following the isolation. The myocytes were either used directly for electrophysiological experiments or for culturing.

### 2.2.3. Adenoviral construct

RNA interference (RNAi) is mechanism of specific gene-silencing at the post-transcriptional level in which small RNAs molecules, called siRNAs, inhibit the expression of a gene of interest, by causing the destruction of the specific mRNA. Esperimentally, this process can be induced by introduction of synthetic small interfece (siRNAs) into the cells or by intracellular generation of siRNA from vector driven expression of the precursor small hairpin (sh) RNAs. shRNA has been shown to be more effective and potent in silencing genes. In these "method", a double-stranded oligonucleotide containing the siRNA sequence linked by a ~9 nucleotide loop is cloned in plasmid or viral vectors to endogenously express shRNA which is subsequently processed in the cytoplasm to siRNA. To delivery the plasmid into the cell we use adenoviruses. This type of virus is suited for short-term shRNA expression and gene silencing since the viral DNA is not incorporated in the host genome. To delivery the plasmid into the cell we use adenovirus. This type of virus is suited for short-term shRNA expression and gene silencing since the viral DNA is not incorporated in the host genome.

We design a short hairpins specific for Cav$\beta_2$ mRNA transcripts. The shRNA sequence is: 5'-AAAAAAACATGAGGCTACAGCATGAATTGGATCCAATTCAGCTGTAG CCTCATGTTTTTTT- 3'. This shRNA was subcloned into adenovirus plasmids under the human U6 promoter, which have been widely used to induce RNAi in mammalian cells. Within the same plasmid is a CMV promoter driving the expression of GFP. The adenovirus production was done following a protocol previously designed (Luo et al., 2007). The control virus is an another adenovirus which containing just GFP (without the shRNA). The viruses were first propagated in transfected HEK 293 cells and maintained at 5% CO2, 37 °C in Minimum Essential Media (MEM) (Life Technologies) with Earle's salts and L-glutamine, supplemented with 5% fetal bovine serum (FBS), and 1% Penicillin-Streptomycin (pen/strep) antibiotic solution. The viruses were then purified from the HEK 293 cells once enough fluorescence of GFP was observed under fluorescence microscopy.

### 2.2.4. Myocytes culture and infection

Ventricular myocytes dissociated in 1.8 mM $Ca^{2+}$-containing Tyrode's buffer solution were subsequently washed in sodium bicarbonate buffered Medium 199 with Earl's salts, L-glutamine, 1% penicillin/streptomycin and 5% bovine serum (Cellgro) at pH of 7.3 to 7.4 that has been incubated at atmosphere of 5% CO2 for at least an hour. The myocytes were then plated on Geltrex coated glass coverslip at densities of about $10^4$ cells/cm2 for 3 to 4 hours to allow them to attach to coverslips prior to adenovirus infection. Before the infection, the media in the dish containing attached myocytes was replaced with Medium 199 supplemented with 1X insulin-transferrin-selenium (ITS) and 15 μM Blebbistatin, for nutrients and reduced contraction. One dish that served as a control was prepared for GFP-only virus infection, while another dish was prepared for β2 shRNA-GFP virus infection.

### 2.2.5. Electrophysiology

For dynamic clamp experiments, freshly dissociated ventricular myocytes bathed in Tyrode's buffer solution were then patched under whole-cell current clamp. The myocytes were first patched in Tyrode's solution before 600 μM $H_2O_2$ was perfused to induce EADs. Once EADs were seen in consecutive APs, Tyrode's solution containing a specific L-type calcium channel blocker, nifedipine (20 μM) and 0.6 mM $H_2O_2$ was perfused. Once the nifedipine effect showed, the dynamic clamp was turned ON. The charges (q) on the membrane was measured by taking the integral of the capacitative current with a 5 mV pulse. The membrane capacitance was calculated using the equation C = q/V. The capacitance value is then inputted into the parameters shaping the virtual $I_{Ca,L}$ on real time experimental interface (RTXI) for each cell. Cells were paced at 6 s pacing cycle length.

Cultured myocytes: Whole-cell current clamp was conducted between 36-48 hr after the myocytes were infected with the viruses. All recordings were measured using AxoPatch 200B (Axon Instruments). Whole-cell patch-clamp recordings were performed using electrodes with tip resistance of 1-3 MΩ borosilicate pipettes. The pipette solution contained (in mmol/L): 110 K-Aspartate, 30 KCl, 5 NaCl, 10 Hepes, 0.1 EGTA, 5 MgATP, 5 creatine phosphate, 0.5 cAMP, adjusted to pH 7.2. All electrophysiological

experiments were performed at 34-36°C. 600 μM $H_2O_2$ was used as an oxidative stress to induce EAD in the myocytes. $I_{Ca,L}$ recordings were done using the Tyrode's buffer and pipette solutions described above, with the following changes: 10 μM Tetradotoxin (TTX) was added to the extracellular solution to eliminate $Na^+$ conductance, and $K^+$ was replaced with $Cs^+$ to block $K^+$ conductance. $I_{Ca,L}$ was calculated by subtracting the current recorded after addition of 20 μM Nifedipine from the total current. The steady state activation and inactivation curves were constructed as previously described (Madhvani et al., 2011). The steady state activation curves: divide the peak I–V curve by the driving force to calculate conductance (G) and divide G by Gmax. The steady state inactivation curves were constructed by graphing the normalized peak current during a test pulse at +10 mV after a 300 ms inactivating pulse at different voltages. Boltzmann distribution fitting was used to estimate the half-activation/inactivation potential of the steady state activation/inactivation curves. The Boltzmann distribution fitting for steady state activation is given by the following equation: (Imax)/(1+EXP((Vhalf-Vm)/slope)); while the steady state inactivation is given by the following equation: (Imax-Imin)/(1+EXP((Vm-Vhalf)/slope))+Imin.

Oocytes: *Xenopus* oocytes of stages V-VI were prepared and injected with 0.05 μl of cRNA containing 0.1 to 1 mg/mL of $\alpha_{1c}/\alpha_2\delta$, $\alpha_{1c}/\alpha_2\delta/\beta_3$, and $\alpha_{1c}/\alpha_2\delta/\beta_{2a}$ in equal molarity. The oocytes were then incubated for 4-7 days prior to electrophysiological experiments at 18°C in an amphibian saline solution containing 50 μg/mL gentamycin (Invitrogen). Immediately preceding each experiment, each oocyte was injected with 0.1 μl of 50 mmol/L BAPTA, which is 1,2-Bis(2-aminophenoxy)ethane-N,N,N′,N′-tetraacetic acid tetrakis (acetoxymethyl ester) (Sigma). Cut-open oocyte voltage clamp technique was used to obtain electrophysiological recording of the injected oocytes. The oocytes were bathed in a solution containing (in mmol/L): 105 NaMES, 10 HEPES, 10 CaMES, and 0.1 Ouabain, adjusted to pH 7.0. The internal solution contained 110 mmol/L K-Glutamate and 10 mmol/L HEPES, also adjusted to pH 7.0. Steady state activation curves were fit to a Boltzmann given by the following: $(I_{max})$ / (1+EXP(z(Vm-$V_{half}$)/(RT/F))). Steady-state inactivation curves were fit with a Bolztmann distribution given by the following equation: $(I_{max}-I_{min})/(1+EXP(z(Vm-V_{half})/(RT/F))) + I_{min}$.

### 2.2.6. Quantitative Real Time Polymerase Chain Reaction (qRT-PCR)

RNA was isolated from myocytes infected with GFP only and myocytes infected with $\beta_2$ shRNA-GFP following 24-48 hr of culturing. The isolation was done using Trizol (Invitrogen) and the RNAs were subsequently reverse-transcribed with gene specific primers using the Omniscript RT kit (Qiagen). The primer sequences used were as follows: $\beta_{2a}$ forward primer (5'-GTA CGC GCG AGT CCT GGG C-3'), reverse primer (5'-GTC GCT CAG CTT CTC TGC GC-3'); $\beta_{2b}$ forward primer (5'-GCA GCT CGC TCG TGC CTG C-3'), reverse primer (5'-CAG GAG CGA CGA GAG CTG AG-3'); $\beta_3$ forward primer (5'-AGA CTA TGC GGA CGC CTA CCA-3'), reverse primer (5'-GCT AGG GTG GGA ACA TCA GGA-3'); GADPH forward primer (5'-CCT GCA CCA CCA ACT GCT TAG-3'), reverse primer (5'-ATG ACC TTG CCC ACG GCC TT-3'). GAPDH transcript levels were used as a baseline for normalization of the relative fluorescence obtained from RT-PCR.

### 2.2.7. Dynamic Clamp

This technique combines mathematical model and biological systems for electrophysiological allows for a computer-simulated ionic conductance to be injected into a live cell in real-time using a real-time experimental interface (RTXI). We use a UCLA ventricular myocytes model. The virtual $I_{Ca,L}$, with the properties of the native $I_{Ca,L}$ is injected into the myocytes. To predict $I_{Ca,L}$ and its $Ca^{2+}$-dependent inactivation, our ventricular myocyte model also computes intracellular $Ca^{2+}$ cycling. To predict the spatiotemporal distribution of intracellular calcium, average $[Ca^{2+}]$ was computed in four different cellular compartments, namely the "submembrane space" in proximity of the sarcolemma ($C_s$) and the "bulk myoplasm", the "junctional SR" (JSR) and "network SR" (NSR) (as previously, (Shiferaw et al., 2003); (Mahajan et al., 2008); (Madhvani et al., 2011). The main $Ca^{2+}$-regulated ionic conductance were also included in the model (*i.e.* the fast sodium current ($I_{Na}$), the $Na^+/K^+$ pump current ($I_{NaK}$) the $Na^+/Ca^{2+}$ exchange current ($I_{NCX}$) and the $Ca^{2+}$-dependent slow component of the delayed rectifier

potassium channel ($I_{Ks}$). Calcium modulated currents sense the [$Ca^{2+}$] at submembrane space ($C_s$) which is higher than the global [$Ca^{2+}$] ($C_i$) (Weber et al., 2002). The average $C_s$ is used to calculate $Ca^{2+}$-dependent inactivation (CDI) in the $I_{Ca,L}$ formulation, while $C_i$ was acquired during the course of the experiments to predict the amplitude and shape of the $Ca_i$ transient.(Mahajan et al., 2008) (Madhvani et al., 2011). Briefly, the $Ca^{2+}$ flux into the cell due to $I_{Ca,L}$ is given by:

$$J_{ca} = g_{ca} P_o i_{ca} \quad ; \qquad i_{ca} = \frac{4 P_{ca} V_m F^2}{RT} \frac{Cse^{2a} - 0.341[Ca^{2+}]_o}{e^{2a} - 1}$$

where *Cs* is the submembrane concentration in units of mmol/L. $P_{Ca}$ is the permeability of Ca (0.0054 m/s), V is the voltage, F is the Faraday's constant, T is temperature. $P_o$ was formulated as:

$$P_o = d \cdot f \cdot q$$

where *d* is the voltage-dependent activation gate, *f* is the voltage-dependent inactivation gate and *q* is the $Ca^{2+}$-dependent inactivation gate.

Data Analysis. All data acquired on G-Patch were analyzed on Analysis, both of which are custom-made. APD at 90% repolarization ($APD_{90}$) was measured by using a custom-made software, AP analyzer. EAD amplitude was calculated by taking the difference in Vm from the inflection point where dV/dt is 0 to the peak of the EAD where dV/dt is also 0. Only the EAD having the largest voltage excursion was included in the analysis for cells displaying APs with multiple EADs. % EAD is reported as the percentage of APs that displayed at least one EAD. Error bars show the standard error of the mean (SEM). The control parameters in the $I_{Ca,L}$ formulation were determined by fitting formulated current to experimental nifedipine-sensitive $I_{Ca,L}$ records (Madhvani et al., 2011) using Berkeley Madonna and then implemented for dynamic clamp in Real-Time eXperiment Interface RTXI (www.rtxi.org) (Lin et al., 2010). The sampling/computation frequency was 10 kHz.

## 2.3. Results

This project has been developed in collaboration with Dr. Weiss, Dr. Qu, Dr. Garfinkel and Dr. Karaguezian at University of California-Los Angeles (USA).

### 2.3.1. Reducing the non-inactivating component of $I_{Ca,L}$ potently abolished EADs

Using dynamic clamp technique (Dorval et al., 2001) in isolated rabbit ventricular myocytes under hypokalemia or oxidative stress conditions, our laboratory previously identified two interventions of the L-type $Ca^{2+}$ channel (LTCC) biophysical properties that could potently suppress EADs occurrence: i) a ~5mV depolarizing shift of the steady-state activation curve and ii) a ~5mV hyperpolarizing shift of the steady-state inactivation curve. These results point out that a reduction of the $I_{Ca,L}$ "window current" may represent an effective maneuver to suppress EADs without blocking the early peak $I_{Ca,L}$ required to maintain normal excitation-contraction coupling (Madhvani et al., 2011). Furthermore other parameters can also affect the $I_{Ca,L}$ "window current" and in this study, taking advantage of the dynamic clamp technique we systematically evaluated the sensitivity of EADs to the non-inactivating (late component) of $I_{Ca,L,}$. Thus, we tested the hypothesis that EADs can be suppressed by selectively targeting the $I_{Ca,L}$ non-inactivating component.

The inactivation of L-type $Ca^{2+}$ channels (LTCC), due to Voltage-dependent inactivation (VDI) and $Ca^{2+}$-dependent inactivation (CDI) mechanisms (Catterall, 2011) is incomplete during the time course of an action potential (AP). The residual, non-inactivating component known as $I_{Ca,L}$ pedestal (Rose et al., 1992);(Qu and Chung, 2012) has a large impact on the voltage level and duration of the AP plateau. The early afterdepolarizations (EADs) are largely induced by the reactivation of L-type $Ca^{2+}$ currents ($I_{Ca,L}$) that occurs at the range of membrane potential from –40 to 0 mV, called "window current" region (January and Riddle, 1989; Antoons et al., 2007). Therefore the generation of EADs is related on the fraction of LTCC that may be available when the AP repolarizes into this voltage "window" range. In our laboratory we have previously reported that one of the effects of $H_2O_2$ in producing EADs is to enhance the non-inactivating component of $I_{Ca,L}$ pedestal from ~3% to ~10% of the peak current

(Madhvani et al., 2011). To determine the relevance of the non-inactivating pedestal $I_{Ca,L}$ on EAD genesis, we used dynamic clamp to alter the pedestal current parameter while keeping all other biophysical parameter of $I_{Ca,L}$ unchanged. In our experimental protocol utilizing the dynamic clamp technique, we first paced every 6s a rabbit ventricular myocyte to record the AP in the current clamp mode in control condition. The myocyte was then exposed to 600 μmol/L $H_2O_2$ until EAD regime appeared consistently. After the induction of EADs, the endogenous $I_{Ca,L}$ was blocked with 20 μmol/L Nifedipine (with $H_2O_2$ still present) which markedly shortened APD and abolished EADs. The dynamic clamp was then turned on, adding the virtual $I_{Ca,L}$ computed from the UCLA rabbit ventricular AP cell model (Mahajan et al., 2008), whose properties which had been adjusted to simulate the previously analyzed effects of $H_2O_2$ on $I_{Ca,L}$ gating properties. Injection of this "$H_2O_2$-modified" virtual $I_{Ca,L}$ effectively restored the electrical properties of the myocyte membrane, resulting in AP prolongation and the reappearance of EADs. At the beginning of the experiment we measured cell capacitance for each cell and this parameter is imputed in the model to correctly scale the virtual $I_{Ca,L}$ to the size of the cell.

Reducing the pedestal current from 10% to 4% completely suppressed EADs occurrence (Figure 10) and also restored normal AP morphology shortening APD to 186 ± 2 ms (Figure 10). To notice is that this change in the parameter was done in the continuous presence of 0.6 mM $H_2O_2$.

The results from dynamic clamp experiments show that reducing the $I_{Ca,L}$ "window current" region by lowering the non-inactivating pedestal component of $I_{Ca,L}$ from 10% (the baseline pedestal in the presence of $H_2O_2$, Madhvani et al., 2011) to 4% (Figure 10), results in a 100% elimination of EADs.

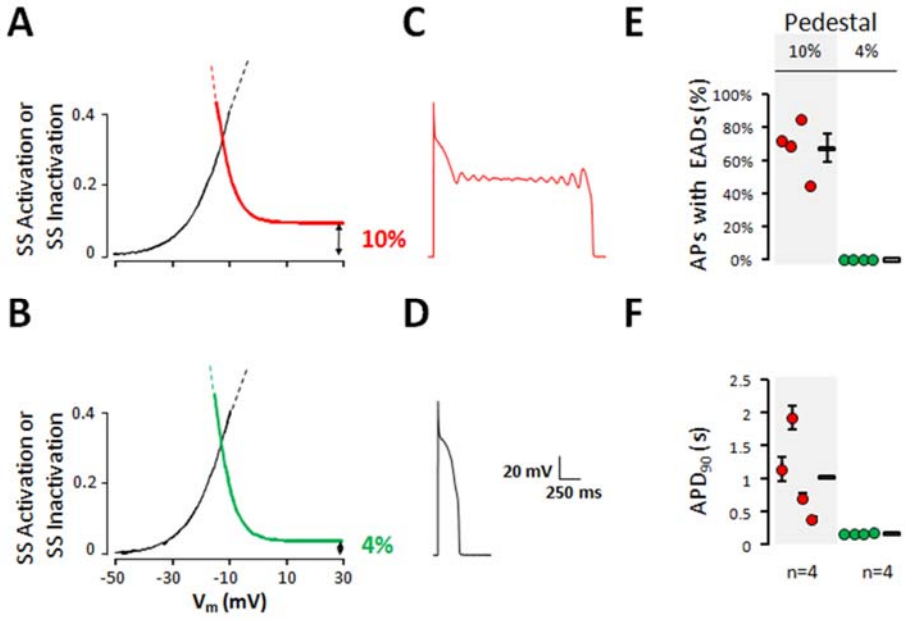


**Figure 10. A reduction in the non-inactivating (pedestal) $I_{Ca,L}$ potently suppresses EADs and restores APD.** A, B) Enlarged view of the steady-state activation and inactivation curves of $I_{Ca,L}$ shows changes made to the non-inactivating component (pedestal). Under dynamic clamp and in the presence of $H_2O_2$, we evaluated the effect of lowering the non-inactivating pedestal from 10% (A) to 4% of the peak current (B). C) Representative AP recorded in dynamic clamp under the conditions shown in (A). Note that lowering the pedestal current to 4% (B) eliminated EADs and restored a normal APD (E-F). E-F) The proportion of APs displaying EADs and $APD_{90}$ under two different pedestal amplitudes respectively. Individual experiments are shown as solid circle, the means for all experiments are plotted as open rectangles (n = 4, from 4 rabbits). Error bars indicate SEM.

This result strongly suggests that the $I_{Ca,L}$ pedestal current has an equivalent promise to the half-activation and half-inactivation potentials, previously identified by Madhavani and colleagues, as a novel anti-arrhythmic target to suppress EADs formation (Madhavani et al 2011). Note that all these promising therapeutic intervention, that potent suppress cardiac arrhythmias, are modifications of $I_{Ca,L}$ steady-state properties that result in the reduction of the "window current" region.

### 2.3.2. Different $Ca_V\beta$ subunit isoforms confer characteristic $I_{Ca,L}$ biophysical properties

Using the dynamic clamp we point out three highly effective targets to suppress EADs formation: the half-activation and half-inactivation potentials and the non-inactivating pedestal current. LTCCs are multiprotein complexes in which $Ca_V\beta$ subunits modulate the voltage dependence properties of the channel (Figure 8), therefore changing the height of the "window current" (Olcese et al., 1994; Neely et al., 1993). Thus, sice EADs are sensitive ont he biophysical properties of $I_{Ca,L}$, we explored whether modifying LTCC β subunit composition is a suitable therapeutic strategy to prevent EADs.

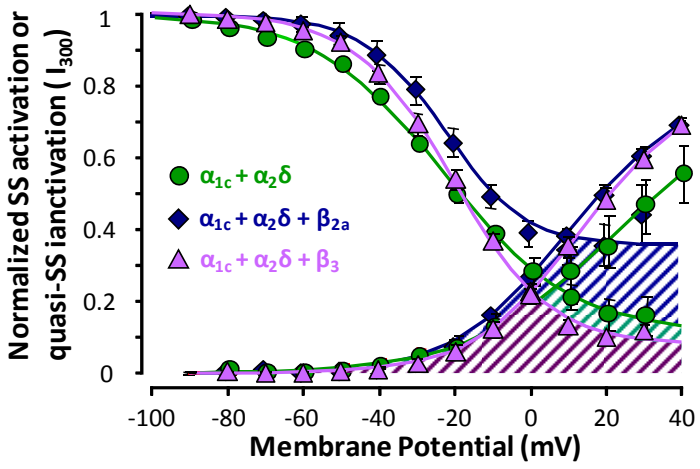


**Figure 11. Influence of Subunit Composition on the Biophysical Properties of LTCCs.** The experimental steady-state activation and quasi-steady-state inactivation curves from various L-type $Ca^{2+}$ channels compositions. The pore forming α1C subunit was expressed with the modulatory subunit $\alpha_2\delta$ (green circle) only or with $\beta_{2a}$ subunit (blue diamond) and $\beta_3$ (violet triangle). Different β subunit conferred specific activation and inactivation properties to the channel, resulting in a significant variation in the window current region. The coexpression of $\beta_{2a}$ subunit produces a left shift in the activation curve and a larger non-inactivating pedestal (as compare to $\alpha_{1C}/\alpha_2\delta$-1 channels). Thus $\beta_{2a}$ favors a larger window current region which we have shown to favor EADs formation.

Olcese and colleagues have previously demonstrated that different $Ca_v\beta$ modulatory subunits, when expressed with LTCC pore-forming subunit $\alpha_{1E}$ or $\alpha_{1C}$ the $Ca^{2+}$ channel profoundly modulate activation and inactivation properties of the channel (Neely et al., 1993; Olcese et al., 1994). Similar results were obtained in voltage clamp experiments

where we coexpressed the human pore forming subunit $\alpha_{1c}$ and the auxiliary $\alpha_2\delta$ subunits of LTCC with either $Ca_v\beta_{2a}$ or $Ca_v\beta_3$ subunit or without any $Ca_v\beta$ subunit in *Xenopus oocyte* system. Tail currents from 20 ms pulses were used to construct steady-state activation curves. Furthermore, considering that the average duration of a human cardiac AP is approximately 300 ms, we assessed the availability of channels (steady state inactivation curves) at this time point using a two-pulse protocol. Measuring the steady state activation and quasi steady state inactivation properties of each combination we demonstrated that $\alpha_{1c}/\alpha_2\delta/\beta_{2a}$ subunits exhibit higher non-inactivating pedestal current than $\alpha_{1c}/\alpha_2\delta/\beta_3$ and $\alpha_{1c}/\alpha_2\delta$. Furthermore, both $\beta_{2a}$ and $\beta_3$ subunits modulated steady state activation curve of LTCC shifting the curve to a more hyperpolarized potential ($\beta_{2a}$ $V_{1\backslash 2}$ act = 22.51 and $\beta_3$ $V_{1\backslash 2}$ act = 24.71) facilitating the opening of the channel at more negative potentials compared to LTCC without any β subunits ($V_{1\backslash 2}$ act = 34.64) as shown in Figure 11. Thus, the presence of β subunits increases the "window current" region by shifting the half-activation potential toward hyperpolarized potentials. Furthermore, $\beta_{2a}$ subunit subunit, which are abundantly expressed in ventricular myocytes (Hullin et al., 2003), give rise to LTCCs with voltage-dependent properties favoring EADs formation because it enhances the activation of $I_{Ca,L}$ , as well as increases the probability of $I_{Ca,L}$ reactivation.

### 2.3.3. Silencing of $Ca_V\beta_2$ in rabbit ventricular myocytes using shRNA

$\beta_2$ subunit displays properties that appears to favor $I_{Ca,L}$ reactivation that leads to EADs genesis. Considering this assumptions, we hypothesized that a reduction in $\beta_2$ subunit content in rabbit ventricular myocytes should generate $I_{Ca,L}$ with an overall voltage dependence unfavorable to EADs occurrence.

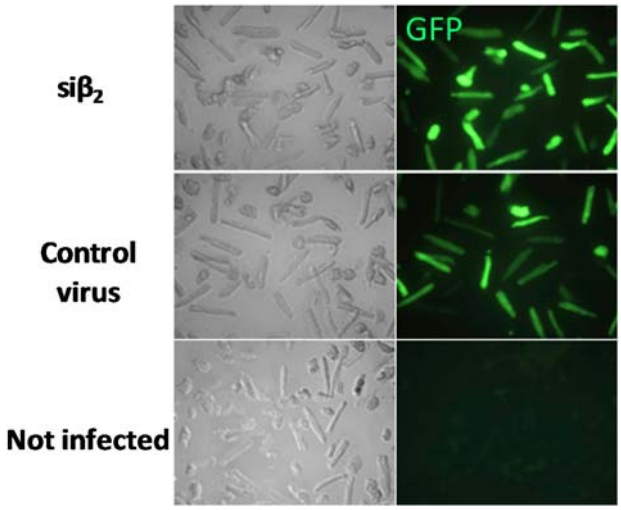


**Figure 12. Efficiently transduction of adenoviral construct.** Adult rabbit ventricular myocytes infected with adenoviral constructs (top, middle) or not infected (bottom) cultured for ~36 hours. The trasduction of the virus into target cells can be monitored by the GFP fluorescence of the reporting gene.

In order to reduce $\beta_2$ subunit expression in adult myocytes, we designed a short hairpin RNA (shRNA) against $Ca_v\beta_2$ that targets both the endogenous $Ca_v\beta_{2a}$ and $Ca_v\beta_{2b}$ subunits. An adenoviral vector that bicistronically encodes for the shRNA (short hairpin RNA) against $\beta_2$ and gene reporter, Green Fluorescent Protein (GFP) were engineered and transduced into myocytes ($si\beta_2$ cells). Our control vector consisted in an adenoviral construct that encoded only for the gene reporter GFP (control virus). We used adenoviruses, both $si\beta_2$ (silencing of $\beta_2$) and control virus to infect freshly dissociated rabbit ventricular myocytes. After 24-48 hours of incubation, the myocytes were examined under a fluorescence microscope verifying the virus tranduction using GFP reporter gene (Figure 12). To verify the extent of $\beta_2$silencing in myocytes infected with adenovirus, a quantification of the mRNA levels of subunits in rabbit ventricular myocytes were done using RT-PCR.

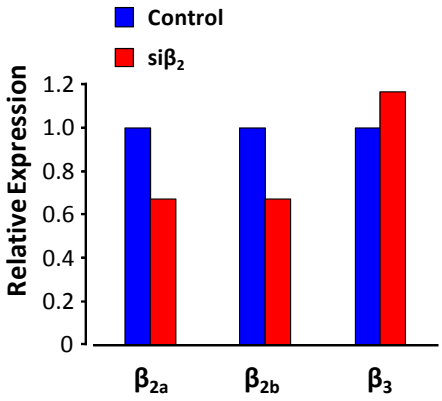


**Figure 13. $\beta_2$ silencing decreases the expression of $\beta_{2a}$ and $\beta_{2b}$ in rabbit ventricular myocytes.** Relative expression of $\beta_{2a}$, $\beta_{2b}$ and $\beta_3$ transcripts by RT-PCR in myocytes infected with control adenovirus (blue) or si$\beta_2$ (red). The relative expression were normalized by GADPH.

The levels of $\beta_{2a}$ and $\beta_{2b}$ subunit mRNA transcripts in myocytes infected with shRNA against $\beta_2$ (si$\beta_2$ myocytes) were both lower compared to those infected with control virus (Figure 13). Furthermore, we observed an increase in the expression of $\beta_3$ mRNA transcript in si$\beta_2$ myocytes compared to control myocytes (GFP only) that could be a compensatory mechanism that the myocytes expressed to allow for LTCCs to be expressed and trafficked to the cell membrane despite the silenced $\beta_{2a}$ and $\beta_{2b}$ subunits.

### 2.3.4. $Ca_V\beta_2$ silencing prevents EADs formation in rabbit ventricular myocytes

Since $\beta_2$ showed proarrhythmogenic properties, we asked whether the reduction in $\beta_2$ protein level obtained with shRNA, was associated with a reduction in the overall $I_{Ca,L}$ "window current" region that has been implicated in EADs genesis. We recorded cardiac APs in current clamp mode in ventricular myocytes cultured for 36-48 hours, in regular Tyrode's buffer solution with a pacing cycle length (PCL) of 6s. After 2 minutes we perfused Tyrode's solution containing 600 μM $H_2O_2$. APs recorded from control myocytes (GFP only) exhibited EADs (Figure 14, top panel), instead of si$\beta_2$ myocytes that did not show EADs in oxidative stress condition as shown in Figure 14, bottom panel. We plotted the percentage of APs showing EADs (% AP with EAD) in the two groups of cells. The % was 32.6 ± 6.1% in control and 0% in si$\beta_2$ myocytes infected.

Note that all siβ$_2$ myocytes that we have tested so far (n=8) did not display EADs (Figure 15 B).

Furthermore, the two groups of cells showed similar AP durations measured at 90% repolarization (APD$_{90}$) in Tyrode's solution: control 0.157 ± 0.02 s and in siβ$_2$ 0.151 ± 0.027s (Figure 15 A). On the contrary, the control myocytes exhibited longer APD$_{90}$ during exposure to 0.6 mM $H_2O_2$ with an average of 0.940 ± 0.5 s, while siβ$_2$ did not show a significant increase in the action potential duration (APD$_{90}$ 0.144 ± 0.024) compared to the AP recorded in regular Tyrode's (Figure 15 A). These results suggest that ventricular myocytes with lower expression of Cavβ$_2$ subunits are more resistant to EADs formation and APD as well. We next asked whether this absence of EADs in siβ$_2$ ventricular myocytes was related to a change in the $I_{Ca,L}$ "window current". We then characterized $I_{Ca,L}$ properties performing electrophysiological experiments in voltage-clamp configuration.

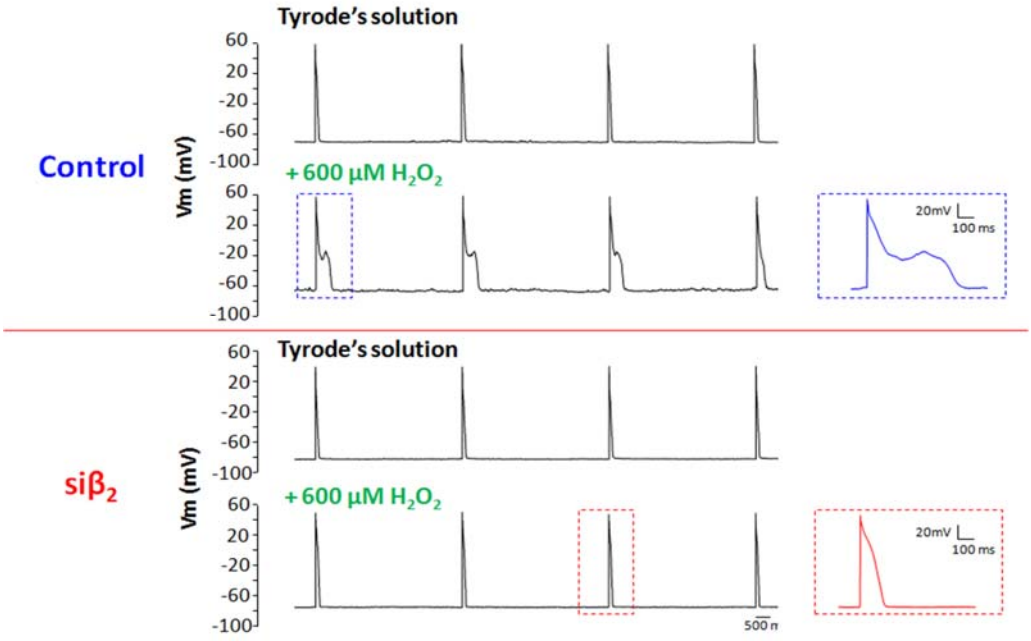


**Figure 14. Cavβ$_2$ silencing prevents EADs formation in ventricular myocytes.** Top) Train of APs recorded from control rabbit ventricular myocytes (infected with GFP only) stimulated with pacing cycle length of 5 s at 35–37°C in Tyrode's solution or in the presence of 600 µM $H_2O_2$. Bottom) As in Top, but recording from a myocyte infected with shRNA against β$_2$. Note that $H_2O_2$ did not induce EADs in β$_2$-suppressed myocytes.

During the experiments we perfused bath solution and 20 μM Nifedipine ($I_{Ca,L}$ inhibitor). By analytical subtraction, Nifedipine-sensitive currents were isolated from the total current of the cell (Figure 16).

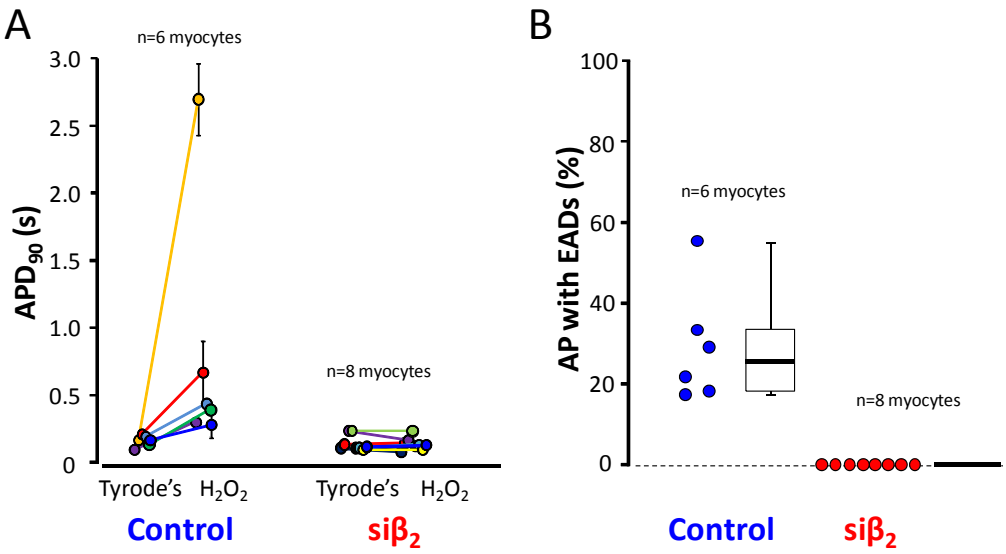


**Figure 15. $Ca_V\beta_2$ knock down protects cardiac myocytes from AP prolongation and oxidative-stress-induced EADs** A) The plot shows the distribution of action potential duration measured at 90% repolarization ($APD_{90}$) measurements for control (blue) and $\beta_2$ knock down myocytes (red) exposed to Tyrode's solution and after the exposure to 600 μM $H_2O_2$ . All values are mean ± SEM. B) Box plot showing the percentage of APs with EADs in control myocytes (blue) and $\beta_2$ knock down myocytes (red). Center line, median; box limits, 25th and 75th percentiles; n, number of experiments in the data set. Note that $\beta_2$ knock down protects the myocytes from $H_2O_2$-inducing EADs.

The $I_{Ca,L}$ amplitudes were then normalized by membrane capacitance of the cell measured before starting the experiment. (Figure 17 A). Averaging all the experiments performed at each membrane potential, we found that, for example +10 mV the current density was 6.61 ± 0.81 pA/pF for si$\beta_2$ and 6.67 ± 0.51 pA/pF for control indicating that reduction in $\beta_2$ subunits (si$\beta_2$) did not significantly alter $I_{Ca,L}$ density compared to control myocytes (Figure 17 A). By constructing steady-state activation and inactivation curves averaging all the experiments, we found that the silencing of $\beta_2$ (less $\beta_2$ content) produced a ~+4 mV shift of the steady-state half-activation potential ($V_{1/2}$ act) and ~-1 mV left shift in the steady-state inactivation curve ($V_{1/2}$ inact) (Figure 17 B). The reduction in $\beta_2$ content ($\beta_{2a}$ and $\beta_{2b}$) decreased the height of the $I_{Ca,L}$ "window current"

region by shifting $I_{Ca,L}$ steady-state activation curve to more depolarized potentials without significantly affect $I_{Ca,L}$ peak.

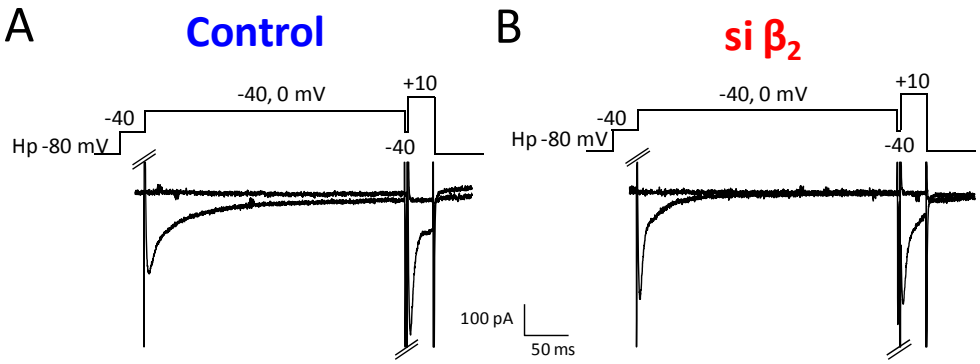


**Figure 16. Representative $I_{Ca,L}$ recording from infected myocytes.** A-B) Voltage clamp recording of nifedipine-sensitive $I_{Ca,L}$ current at -40 and 0 mV, in response to the protocol reported above. Representative current traces from myocytes infected with control (A) or si$\beta_2$ virus (B).

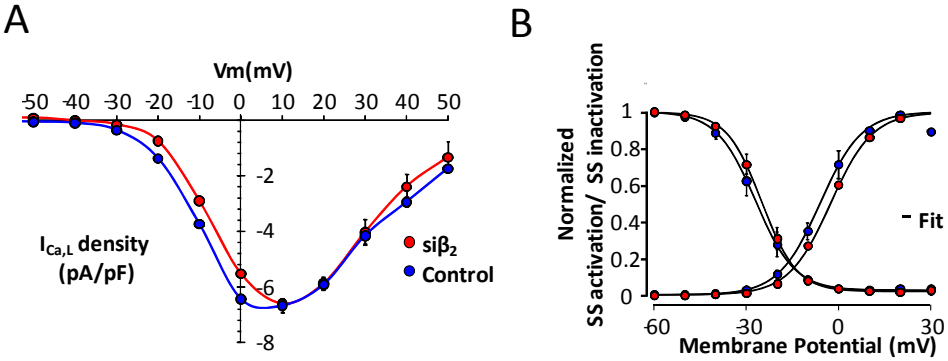


**Figure 17. Reduction in Cav$\beta_2$ subunits did not alter the peak current density of $I_{Ca,L}$ but modified the size of the ICa,L window current region.** A) Current–voltage (I–V) relationship for $I_{Ca,L}$ (normalized to the capacitance of the cells) in control (blue circles) and si$\beta_2$ (red circles) myocytes (n = 3). B) Mean of steady-state activation and inactivation curves for $I_{Ca,L}$ in control (blue circles) and $\beta_2$ knock down (red circles) myocytes (n = 3 each). Note in $\beta_2$ knock down myocytes the shift of steady-state curves to the right results in a decrease in $I_{Ca,L}$ "window current" region. All values are mean ± SEM.

To conclude, our results show that down-regulation of $\beta_2$ causes an overall reduction of the "window current" region shifting the steady state activation curve toward more

depolarized potential. This change in the $I_{Ca,L}$ voltage dependence properties successfully prevents oxidative stress-mediated EADs in ventricular myocytes. Our results are a first proof of concept of the finding that a tiny shift in the steady state activation curve resulted in a suppression of EADs.

## 2.4. Discussion

My PhD training at University of California-Los Angeles, focused on the mechanisms of cardiac arrhythmias. Specifically, I have investigated the role of voltage gated L-type calcium channel (LTCC) in the etiology of early afterdepolarizations (EADs).

EADs are membrane potential oscillations during the repolarizing phase of the ventricular action potential (AP) (phase 2 or 3) (Figure 6). These events are highly arrhytmogenic because they can generate a new AP that propagates to the surrounding tissue disrupting the normal sinus rhythm. It is widely accepted that EADs are important as cellular triggers to ventricular tachycardia (VT) and ventricular fibrillation (VF) (Figure 5). EADs are mainly due to either abnormally decreased outward currents, increased inward currents, or both, classically defined as reduced repolarization reserve. Even though different ionic currents are involved in the AP and can contribute to EAD formation, reactivation of $I_{Ca,L}$ plays a central role in providing a regenerative inward current required for EADs to propagate, thus causing triggered activity at the tissue level (January and Riddle, 1989; January et al., 1988). Understanding the mechanisms of EADs formation is critical to identify appropriate strategies to prevent EADs-related cardiac arrhythmias. Most EADs are initiated between -40 and 0 mV, corresponding to the range of membrane potentials where the steady-state activation and inactivation curves of $I_{Ca,L}$ overlap, often referred to as the "window current" region (Figure 6) (January and Riddle, 1989; Antoons et al., 2007;January & Riddle, 1989). In a previous study from our laboratory we used the dynamic clamp technique to explore systematically how biophysical properties of $I_{Ca,L}$ could be modified to suppress EADs without impairing excitation-contraction coupling (Madhvani et al., 2011). Isolated rabbit ventricular myocytes were first exposed to oxidative stress ($H_2O_2$) in order to generate a EADs regime, after which their endogenous $I_{Ca,L}$ (blocked with Nifedipine) was replaced by a virtual $I_{Ca,L}$ with tunable parameters, in dynamic clamp mode. This previous work demonstrated that EADs are highly sensitive to subtle changes in the half-activation or half-inactivation potentials of $I_{Ca,L}$, suggesting that a reduction of the $I_{Ca,L}$ "window current" may represent an effective maneuver to suppress EADs without blocking the early peak $I_{Ca,L}$ required to maintain normal excitation-contraction coupling. However other parameters also affect the $I_{Ca,L}$ "window current"; in this study, we took advantage of the dynamic clamp technique to systematically evaluate the

sensitivity of EAD to the non-inactivating (late component) of $I_{Ca,L}$, testing the hypothesis that EADs can be suppressed by selectively targeting this $I_{Ca,L}$ parameter.

**What is the role of the late component of L-type calcium current in EADs genesis?**

To test the susceptibility of EADs to the non-inactivating component of $I_{Ca,L}$, we selectively modified its amplitude in ventricular myocytes exhibiting $H_2O_2$-induced EADs using dynamic clamp approach. The reduction of non-inactivating component of $I_{Ca,L}$ pedestal current effectively suppresses EADs and restores APD to a normal value (Figure 10). An important novel contribution of the present study is the finding that the $I_{Ca,L}$ pedestal current has an equivalent promise to the half-activation and half-inactivation potentials, previously identified by Madhavani and colleagues as a novel anti-arrhythmic target to suppress EADs formation (Madhvani et al., 2011).

Thus, from our dynamic clamp studies, we predict that drugs or genetic interventions that leave peak $I_{Ca,L}$ and hence excitation-contraction coupling intact but selectively suppress one of these valuable targets (steady state activation, inactivation or pedestal current) will be effective at eliminate EADs.

We are currently directing our investigations on the voltage dependence properties of the channel LTCC in order to develop a genetic approach to prevent EADs-mediated arrhythmias. L-type calcium channel are multimeric complexes they are made up of a pore-forming $\alpha_{1C}$ subunit that co-assembles with modulatory subunits such as β and $\alpha_2\delta_1$ (Figure 7).

Since the early 90's, It is known that different β subunits modulate the biophysical properties of LTCC (Figure 8) (Perez-Reyes et al., 1992; Neely et al., 1993; Olcese et al., 1994).

In voltage clamp experiments we measured the steady state properties of $I_{Ca,L}$ in the presence of $\beta_{2a}$ and $\beta_3$ (Figure 11). We confirmed that $Ca_V\beta$ modified the steady state properties of LTCC. As shown in Figure 11, $\beta_{2a}$ subunit, which are abundantly expressed in ventricular myocytes (Hullin et al., 1992), give rise to LTCCs with voltage-dependent properties favoring EAD formation. In fact, $\beta_{2a}$ enhances the activation of $I_{Ca,L}$ and increases the probability of $I_{Ca,L}$ reactivation, in which both cases would lead to EAD formation following previous dynamic clamp results. Our findings are consistent with prior reports demonstrating the pro-EAD effects of the $\beta_{2a}$ subunits,

particularly due to phosphorylation by CaMKII (Koval et al., 2010). Interestingly, several groups have demonstrated that the $\beta_2$ subunits are the most abundant in the heart (Hullin et al., 2003; Hullin et al., 2007; Colecraft et al., 2002). Furthermore it has been shown a significant increase of $\beta_{2a}$ subunit expression in cardiomyocytes in mice model of heart failure (Hullin et al., 2007), a condition known to favor EADs. Other quantitative studies have suggested that in heart $\beta_{2b}$ expression is higher than $\beta_3$ and $\beta_{2a}$ (Hullin et al., 2003).

According to these findings and dynamic clamp data, we hypothesized that genetic interventions to tune the biophysical properties of $I_{Ca,L}$ by altering its subunit composition could be an effective non pharmacological strategy to suppress EADs in a highly specific manner.

Since there is a consensus that $\beta_2$ is highly expressed in the myocytes (Hullin et al., 2003; Colecraft et al., 2002) and because $\beta_{2a}$ shows pro arrhythmogenic characteristics, we delivered a shRNA into adult ventricular myocytes using an adenoviral construct (Figures 12 and 13). By silencing $\beta_2$ in cultured myocytes, we established that a reduction in the expression of $\beta_2$ affects the steady state activation properties of LTCC in a favorable way, shifting the activation curve to the right. This small change in the steady-state activation (~+4mV) potently prevents EADs formation in ventricular myocytes (Figures 15 and 17). This small change in the steady-state activation recapitulates the previous finding of Madhavani et al, in which they demonstrate that EADs are sensitive to small change in the LTCC in steady-state activation curve (~+4-5 mV). Interestingly, the effect on the steady-state activation property is without causing any changes in the current density of $I_{Ca,L}$ (Figure 17). This aspect is relevant from a therapeutic stand point because functional LTCCs are necessary for providing the major passageway for $Ca^{2+}$ entry and $Ca^{2+}$ signaling into the cell very critical for muscle contraction. Most importantly, our results show that lowering the levels of $\beta_2$ subunits completely abolish the EAD occurrence demonstrating that decreasing $\beta_2$ protects the cell from oxidative stress insult. Conversely, control myocytes from the same batches exhibit significant action potential prolongation and all cells develop EADs after $H_2O_2$ exposure.

These findings demonstrate that manipulation of the subunit composition can be an effective strategy for altering the steady-state properties of $I_{Ca,L}$. A major potential

advantage of using β subunits is their high selectivity for the LTCC pore-forming α1 subunit, minimizing side effects that common pharmacological therapy normally has. Thus, our results offer a proof of concept for a gene-therapy-based antiarrhythmic strategy that could effectively suppress EAD-and their arrhythmogenic concequences
We recognized that before considering the clinical utility of these findings, the results from this preliminary study need to be tested in perfused hearts and and animal models, possibly using a new generation of cardiac specific adeno-associated viral vectors (AAV 9) (Bish et al., 2008) in order to validate the efficacy of this interventions.

On a parallel path, using a more conventional pharmacological approach, we are screening compounds that can potentially affect one of the newly identified $I_{Ca,L}$ biophysical parameters to which EADs are particularly sensitive, in order to identify new antiarrhythmic agents. We know that conventional $Ca^{2+}$ channel blockers such as nifedipine, are highly effective at suppressing EADs mainly because they indiscriminately block $I_{Ca,L}$. However, by blocking peak $I_{Ca,L}$, these drugs also potently suppress excitation-contraction coupling, precluding clinical usefulness for EADs suppression. In this context an ideal $Ca^{2+}$ channel drug for suppressing EAD-mediated arrhythmias would leave peak $I_{Ca,L}$ intact to preserve normal excitation-contraction coupling, and for example, selectively blocks the late $I_{Ca,L}$ reactivated during repolarization when AP plateau enters the "window" voltage range. This is something possible if we consider that recently Ranolazine, a selective blocker of the late $Na^+$ current ($I_{Na}$) which leaves the peak $I_{Na}$ intact, has been approved and it is already in clinical for treatment in chronic angina patients (Belardinelli et al., 2006; Zerumsky and McBride, 2006).

While this study has greatly contributed to our understanding of EADs genesis and identified new strategies for their suppression, there are certain experimental limitations that deserve to be discussed. One important consideration is that this study was performed in rabbit ventricular myocytes, which differ in some respects from human ventricular myocytes. However, their L-type $Ca^{2+}$ current properties are generally similar (Grandi et al., 2010; Verkerk et al., 2011). To efficiently delivery adenoviral constructs in isolated adult myocytes, we have to maintain cells in culture for 24-48 hr.

We are aware to the fact that cultured myocytes are subject to changes in morphology and conductances compared to fresh dissociated myocytes (i.e. rounding of the edges of the ventricular myocytes and reduction in AP duration due to a decrease in the overall channel expressions). In fact, it will be important validate the results in an intact heart or in the animal model. Another limitation of this study is that in our dynamic clamp experiments the virtual programmable $I_{Ca,L}$ do not carry $Ca^{2+}$ ions. Therefore, the injected virtual $I_{Ca,L}$ do not trigger SR $Ca^{2+}$ release. Nevertheless, the depolarizing current has the shape and duration dictated by the $I_{Ca,L}$ model parameters and the membrane voltage. While this can be viewed as a limitation, it can also be considered an experimental advantage suggesting that EADs formation can have a purely electrical etiology that does not involve the biochemical consequences of $Ca^{2+}$ influx. Despite this limitation, we believe that this approach represents a powerful method to combine the screening for ion channel blockers and the identification of subtle and selective aspects of ion channel biophysics to guide drug discovery.

# Reference List


Al Khamici,H., L.J.Brown, K.R.Hossain, A.L.Hudson, A.A.Sinclair-Burton, J.P.M.Ng, E.L.Daniel, J.E.Hare, B.A.Cornell, P.M.G.Curmi, M.W.Davey, and S.M.Valenzuela. 2015. Members of the Chloride Intracellular Ion Channel Protein Family Demonstrate Glutaredoxin-Like Enzymatic Activity. *Plos One* 10.

Alseikhan,B.A., C.D.DeMaria, H.M.Colecraft, and D.T.Yue. 2002. Engineered calmodulins reveal the unexpected eminence of Ca2+ channel inactivation in controlling heart excitation. *Proc. Natl. Acad. Sci. U. S. A* 99:17185-17190.

Antoons,G., P.G.Volders, T.Stankovicova, V.Bito, M.Stengl, M.A.Vos, and K.R.Sipido. 2007. Window Ca2+ current and its modulation by Ca2+ release in hypertrophied cardiac myocytes from dogs with chronic atrioventricular block. *J. Physiol* 579:147-160.

Ashikaga,H., B.A.Coppola, B.Hopenfeld, E.S.Leifer, E.R.McVeigh, and J.H.Omens. 2007. Transmural dispersion of myofiber mechanics - Implications for electrical heterogeneity in vivo. *Journal of the American College of Cardiology* 49:909-916.

Averaimo,S., R.Abeti, N.Savalli, L.J.Brown, P.M.Curmi, S.N.Breit, and M.Mazzanti. 2013. Point mutations in the transmembrane region of the clic1 ion channel selectively modify its biophysical properties. *PLoS. One.* 8:e74523.

Averaimo,S., M.Gritti, E.Barini, L.Gasparini, and M.Mazzanti. 2014. CLIC1 functional expression is required for cAMP-induced neurite elongation in post-natal mouse retinal ganglion cells. *Journal of Neurochemistry* 131:444-456.

Averaimo,S., R.H.Milton, M.R.Duchen, and M.Mazzanti. 2010. Chloride intracellular channel 1 (CLIC1): Sensor and effector during oxidative stress. *FEBS Lett.* 584:2076-2084.

Baccelli,I. and A.Trumpp. 2012. The evolving concept of cancer and metastasis stem cells. *J. Cell Biol.* 198:281-293.

Bao,B., A.Azmi, S.Ali, F.Zaiem, and F.SArkar. 2014. Metformin may function as anti-cancer agent via targeting cancer stem cells: the potential biological significance of tumor-associated miRNAs in breast and pancreatic cancers. *Ann Transl Med.*

Bao,S., Q.Wu, R.E.McLendon, Y.Hao, Q.Shi, A.B.Hjelmeland, M.W.Dewhirst, D.D.Bigner, and J.N.Rich. 2006. Glioma stem cells promote radioresistance by preferential activation of the DNA damage response. *Nature* 444:756-760.

Becchetti,A. 2011. Ion channels and transporters in cancer. 1. Ion channels and cell proliferation in cancer. *American Journal of Physiology-Cell Physiology* 301:C255-C265.

Belardinelli,L., J.C.Shryock, and H.Fraser. 2006. Inhibition of the late sodium current as a potential cardioprotective principle: effects of the late sodium current inhibitor ranolazine. *Heart* 92 Suppl 4:iv6-iv14.

Berecki,G., H.M.Den Ruijter, A.O.Verkerk, C.A.Schumacher, A.Baartscheer, D.Bakker, B.J.Boukens, A.C.G.van Ginneken, J.W.T.Fiolet, T.Opthof, and R.Coronel. 2007. Dietary fish oil reduces the incidence of triggered arrhythmias in pig ventricular myocytes. *Heart Rhythm* 4:1452-1460.

Berecki,G., J.G.Zegers, A.O.Verkerk, Z.A.Bhuiyan, B.de Jonge, M.W.Veldkamp, R.Wilders, and A.C.G.van Ginneken. 2005. HERG channel (dys)function revealed by dynamic action potential clamp technique. *Biophysical Journal* 88:566-578.

Beresewicz,A. and M.Horackova. 1991. Alterations in electrical and contractile behavior of isolated cardiomyocytes by hydrogen peroxide: possible ionic mechanisms. *J. Mol. Cell Cardiol.* 23:899-918.

Bers,D.M. 2002. Cardiac excitation-contraction coupling. *Nature* 415:198-205.

Bers,D.M. and T.Guo. 2005. Calcium signaling in cardiac ventricular myocytes. *Communicative Cardiac Cell* 1047:86-98.

Bish,L.T., K.Morine, M.M.Sleeper, J.Sanmiguel, D.Wu, G.Gao, J.M.Wilson, and H.L.Sweeney. 2008. Adeno-associated virus (AAV) serotype 9 provides global cardiac gene transfer superior to AAV1, AAV6, AAV7, and AAV8 in the mouse and rat. *Hum. Gene Ther.* 19:1359-1368.

Bolen,S., L.Feldman, J.Vassy, L.Wilson, H.C.Yeh, S.Marinopoulos, C.Wiley, E.Selvin, R.Wilson, E.B.Bass, and F.L.Brancati. 2007. Systematic review: Comparative effectiveness and safety of oral medications for type 2 diabetes Mellitus. *Annals of Internal Medicine* 147:386-399.

Bonnet,D. and J.E.Dick. 1997. Human acute myeloid leukemia is organized as a hierarchy that originates from a primitive hematopoietic cell. *Nat. Med.* 3:730-737.

Boukens,B.J., V.M.Christoffels, R.Coronel, and A.F.Moorman. 2009. Developmental basis for electrophysiological heterogeneity in the ventricular and outflow tract myocardium as a substrate for life-threatening ventricular arrhythmias. *Circ. Res* 104:19-31.

Bowker,S.L., S.R.Majumdar, P.Veugelers, and J.A.Johnson. 2006. Increased cancer-related mortality for patients with type 2 diabetes who use sulforrylureas or insulin. *Diabetes Care* 29:254-258.

Brown,J.M., L.S.Terada, M.A.Grosso, G.J.Whitman, S.E.Velasco, A.Patt, A.H.Harken, and J.E.Repine. 1988a. Hydrogen peroxide mediates reperfusion injury in the isolated rat heart. *Mol. Cell Biochem.* 84:173-175.

Brown,J.M., L.S.Terada, M.A.Grosso, G.J.Whitmann, S.E.Velasco, A.Patt, A.H.Harken, and J.E.Repine. 1988b. Xanthine oxidase produces hydrogen peroxide which contributes to reperfusion injury of ischemic, isolated, perfused rat hearts. *J. Clin. Invest* 81:1297-1301.

Buraei,Z. and J.Yang. 2013. Structure and function of the beta subunit of voltage-gated Ca2+ channels. *Biochimica et Biophysica Acta-Biomembranes* 1828:1530-1540.

Calabrese,C., H.Poppleton, M.Kocak, T.L.Hogg, C.Fuller, B.Hamner, E.Y.Oh, M.W.Gaber, D.Finklestein, M.Allen, A.Frank, I.T.Bayazitov, S.S.Zakharenko, A.Gajjar, A.Davidoff, and R.J.Gilbertson. 2007. A perivascular niche for brain tumor stem cells. *Cancer Cell* 11:69-82.

Catterall,W.A. 2011. Voltage-gated calcium channels. *Cold Spring Harb. Perspect. Biol.* 3:a003947.

Catterall,W.A. and A.P.Few. 2008. Calcium channel regulation and presynaptic plasticity. *Neuron* 59:882-901.

Chamberlain,M.C. 2010. Emerging clinical principles on the use of bevacizumab for the treatment of malignant gliomas. *Cancer* 116:3988-3999.

Chang,Y.H., C.C.Wu, K.P.Chang, J.S.Yu, Y.C.Chang, and P.C.Liao. 2009. Cell secretome analysis using hollow fiber culture system leads to the discovery of CLIC1 protein as a novel plasma marker for nasopharyngeal carcinoma. *J. Proteome. Res.* 8:5465-5474.

Charles,N. and E.C.Holland. 2010. The perivascular niche microenvironment in brain tumor progression. *Cell Cycle* 9:3012-3021.

Chen,C.D., C.S.Wang, Y.H.Huang, K.Y.Chien, Y.Liang, W.J.Chen, and K.H.Lin. 2007. Overexpression of CLIC1 in human gastric carcinoma and its clinicopathological significance. *Proteomics.* 7:155-167.

Chen,G.F., S.H.Xu, K.Renko, and M.Derwahl. 2012a. Metformin Inhibits Growth of Thyroid Carcinoma Cells, Suppresses Self-Renewal of Derived Cancer Stem Cells, and Potentiates the Effect of Chemotherapeutic Agents. *Journal of Clinical Endocrinology & Metabolism* 97:E510-E520.

Chen,J., R.M.McKay, and L.F.Parada. 2012b. Malignant glioma: lessons from genomics, mouse models, and stem cells. *Cell* 149:36-47.

Chen,Y.H., M.H.Li, Y.Zhang, L.L.He, Y.Yamada, A.Fitzmaurice, Y.Shen, H.Zhang, L.Tong, and J.Yang. 2004. Structural basis of the alpha1-beta subunit interaction of voltage-gated Ca2+ channels. *Nature* 429:675-680.

Cheng,Y., J.Zhao, W.Qiao, and K.Chen. 2014. Recent advances in diagnosis and treatment of gliomas using chlorotoxin-based bioconjugates. *Am. J. Nucl. Med. Mol. Imaging* 4:385-405.

Cohen,A. and H.Colman. 2015. Glioma biology and molecular markers.

Colecraft,H.M., B.Alseikhan, S.X.Takahashi, D.Chaudhuri, S.Mittman, V.Yegnasubramanian, R.S.Alvania, D.C.Johns, E.Marban, and D.T.Yue. 2002. Novel functional properties of Ca(2+) channel beta subunits revealed by their expression in adult rat heart cells. *J. Physiol* 541:435-452.

Cranefield,P.F. 1977. Action potentials, afterpotentials, and arrhythmias. *Circ. Res.* 41:415-423.

Cranefield,P. and R.S.Aronson. 1974. Initiation of Sustained Rhythmic Activity by Single Propagated Action Potentials in Canine Cardiac Purkinje-Fibers Exposed to Sodium-Free Solution Or to Ouabain. *Circulation Research* 34:477-481.

Cranefield,P., A.L.Wit, and B.F.Hoffman. 1972. Conduction of Cardiac Impulse .3. Characteristics of Very Slow Conduction. *Journal of General Physiology* 59:227-&.

Cross,M., M.Fernandes, H.Dirr, and S.Fanucchi. 2015. Glutamate 85 and glutamate 228 contribute to the pH-response of the soluble form of chloride intracellular channel 1. *Molecular and Cellular Biochemistry* 398:83-93.

Cuddapah,V.A., S.Robel, S.Watkins, and H.Sontheimer. 2014. A neurocentric perspective on glioma invasion. *Nature Reviews Neuroscience* 15:455-465.

Cufi,S., B.Corominas-Faja, A.Vazquez-Martin, C.Oliveras-Ferraros, J.Dorca, J.Bosch-Barrera, B.Martin-Castillo, and J.A.Menendez. 2012. Metformin-induced preferential killing of breast cancer initiating CD44(+)CD24(-/low) cells is sufficient to overcome primary resistance to trastuzumab in HER2+human breast cancer xenografts. *Oncotarget* 3:395-398.

Curtis,B.M. and W.A.Catterall. 1984. Purification of the Calcium-Antagonist Receptor of the Voltage-Sensitive Calcium-Channel from Skeletal-Muscle Transverse Tubules. *Biochemistry* 23:2113-2118.

Damiano,B.P. and M.R.Rosen. 1984. Effects of pacing on triggered activity induced by early afterdepolarizations. *Circulation* 69:1013-1025.

Davies,A., I.Kadurin, A.Alvarez-Laviada, L.Douglas, M.Nieto-Rostro, C.S.Bauer, W.S.Pratt, and A.C.Dolphin. 2010. The alpha(2)delta subunits of voltage-gated calcium channels form GPI-anchored proteins, a posttranslational modification essential for function. *Proceedings of the National Academy of Sciences of the United States of America* 107:1654-1659.

Denysenko,T., L.Gennero, M.A.Roos, A.Melcarne, C.Juenemann, G.Faccani, I.Morra, G.Cavallo, S.Reguzzi, G.Pescarmona, and A.Ponzetto. 2010. Glioblastoma cancer stem cells: heterogeneity, microenvironment and related therapeutic strategies. *Cell Biochem. Funct.* 28:343-351.

Detaille,D., B.Guigas, X.Leverve, N.Wiernsperger, and P.Devos. 2002. Obligatory role of membrane events in the regulatory effect of metformin on the respiratory chain function. *Biochemical Pharmacology* 63:1259-1272.

Dolphin,A.C. 2012. Calcium channel auxiliary alpha2delta and beta subunits: trafficking and one step beyond. *Nat. Rev. Neurosci.* 13:542-555.

Dorval,A.D., D.J.Christini, and J.A.White. 2001. Real-Time linux dynamic clamp: a fast and flexible way to construct virtual ion channels in living cells. *Ann. Biomed. Eng* 29:897-907.

Dzhura,I. and A.Neely. 2003. Differential modulation of cardiac Ca2+ channel gating by beta-subunits. *Biophys. J.* 85:274-289.

Evans,J.M.M., L.A.Donnelly, A.M.Emslie-Smith, D.R.Alessi, and A.D.Morris. 2005. Metformin and reduced risk of cancer in diabetic patients. *British Medical Journal* 330:1304-1305.

Flavell,S.W. and M.E.Greenberg. 2008. Signaling mechanisms linking neuronal activity to gene expression and plasticity of the nervous system. *Annual Review of Neuroscience* 31:563-590.

Fraser,S.P. and L.A.Pardo. 2008. Ion channels: functional expression and therapeutic potential in cancer. Colloquium on Ion Channels and Cancer. *EMBO Rep.* 9:512-515.

Furnari,F.B., T.Fenton, R.M.Bachoo, A.Mukasa, J.M.Stommel, A.Stegh, W.C.Hahn, K.L.Ligon, D.N.Louis, C.Brennan, L.Chin, R.A.DePinho, and W.K.Cavenee. 2007. Malignant astrocytic glioma: genetics, biology, and paths to treatment. *Genes Dev.* 21:2683-2710.

Galli,R., E.Binda, U.Orfanelli, B.Cipelletti, A.Gritti, V.S.De, R.Fiocco, C.Foroni, F.Dimeco, and A.Vescovi. 2004. Isolation and characterization of tumorigenic, stem-like neural precursors from human glioblastoma. *Cancer Res.* 64:7011-7021.

Gilbertson,R.J. and J.N.Rich. 2007. Making a tumour's bed: glioblastoma stem cells and the vascular niche. *Nat. Rev. Cancer* 7:733-736.

Goodchild,S.C., M.W.Howell, N.M.Cordina, D.R.Littler, S.N.Breit, P.M.Curmi, and L.J.Brown. 2009. Oxidation promotes insertion of the CLIC1 chloride intracellular channel into the membrane. *Eur. Biophys. J.* 39:129-138.

Graham,G.G., J.Punt, M.Arora, R.O.Day, M.P.Doogue, J.K.Duong, T.J.Furlong, J.R.Greenfield, L.C.Greenup, C.M.Kirkpatrick, J.E.Ray, P.Timmins, and K.M.Williams. 2011. Clinical Pharmacokinetics of Metformin. *Clinical Pharmacokinetics* 50:81-98.

Grandi,E., F.S.Pasqualini, and D.M.Bers. 2010. A novel computational model of the human ventricular action potential and Ca transient. *Journal of Molecular and Cellular Cardiology* 48:112-121.

Gritti,M., R.Wurth, M.Angelini, F.Barbieri, M.Peretti, E.Pizzi, A.Pattarozzi, E.Carra, R.Sirito, A.Daga, P.M.G.Curmi, M.Mazzanti, and T.Florio. 2014. Metformin repositioning as antitumoral agent: selective antiproliferative effects in human glioblastoma stem cells, via inhibition of CLIC1-mediated ion current. *Oncotarget* 5:11252-11268.

Habela,C.W., N.J.Ernest, A.F.Swindall, and H.Sontheimer. 2009. Chloride accumulation drives volume dynamics underlying cell proliferation and migration. *J. Neurophysiol.* 101:750-757.

Habela,C.W., M.L.Olsen, and H.Sontheimer. 2008. ClC3 is a critical regulator of the cell cycle in normal and malignant glial cells. *J. Neurosci.* 28:9205-9217.

Halling,D.B., P.racena-Parks, and S.L.Hamilton. 2006. Regulation of voltage-gated Ca2+ channels by calmodulin. *Sci. STKE.* 2006:er1.

Hamill,O.P., A.Marty, E.Neher, B.Sakmann, and F.J.Sigworth. 1981. Improved patch-clamp techniques for high-resolution current recording from cells and cell-free membrane patches. *Pflugers Arch.* 391:85-100.

Hanahan,D. and R.A.Weinberg. 2000. The hallmarks of cancer. *Cell* 100:57-70.

Hardie,D.G., F.A.Ross, and S.A.Hawley. 2012. AMP-activated protein kinase: a target for drugs both ancient and modern. *Chem. Biol.* 19:1222-1236.

Harrop,S.J., M.Z.DeMaere, W.D.Fairlie, T.Reztsova, S.M.Valenzuela, M.Mazzanti, R.Tonini, M.R.Qiu, L.Jankova, K.Warton, A.R.Bauskin, W.M.Wu, S.Pankhurst, T.J.Campbell, S.N.Breit, and P.M.Curmi. 2001. Crystal structure of a soluble form of the intracellular chloride ion channel CLIC1 (NCC27) at 1.4-A resolution. *J. Biol. Chem.* 276:44993-45000.

Havens,C.G., A.Ho, N.Yoshioka, and S.F.Dowdy. 2006. Regulation of late G1/S phase transition and APC Cdh1 by reactive oxygen species. *Mol. Cell Biol.* 26:4701-4711.

Hirsch,H.A., D.Iliopoulos, P.N.Tsichlis, and K.Struhl. 2009. Metformin Selectively Targets Cancer Stem Cells, and Acts Together with Chemotherapy to Block Tumor Growth and Prolong Remission. *Cancer Research* 69:7507-7511.

Hoekstra,M., C.L.Mummery, A.A.M.Wilde, C.R.Bezzina, and A.O.Verkerk. 2012. Induced pluripotent stem cell derived cardiomyocytes as models for cardiac arrhythrnias. *Frontiers in Physiology* 3.

Hosey,M.M., A.J.Chien, and T.S.Puri. 1996. Structure and regulation of L-type calcium channels - A current assessment of the properties and roles of channel subunits. *Trends in Cardiovascular Medicine* 6:265-273.

Hullin,R., I.F.Khan, S.Wirtz, P.Mohacsi, G.Varadi, A.Schwartz, and S.Herzig. 2003. Cardiac L-type calcium channel beta-subunits expressed in human heart have differential effects on single channel characteristics. *J. Biol. Chem.* 278:21623-21630.

Hullin,R., J.Matthes, V.S.von, I.Bodi, M.Rubio, K.D'Souza, K.Friedrich, I, D.Rottlander, U.C.Hoppe, P.Mohacsi, E.Schmitteckert, R.Gilsbach, M.Bunemann, L.Hein, A.Schwartz, and S.Herzig. 2007. Increased expression of the auxiliary beta(2)-subunit of ventricular L-type Ca(2)+ channels leads to single-channel activity characteristic of heart failure. *PLoS. One.* 2:e292.

Hullin,R., D.Singer-Lahat, M.Freichel, M.Biel, N.Dascal, F.Hofmann, and V.Flockerzi. 1992. Calcium channel beta subunit heterogeneity: functional expression of cloned cDNA from heart, aorta and brain. *EMBO J.* 11:885-890.

Huse,J.T. and E.C.Holland. 2010. Targeting brain cancer: advances in the molecular pathology of malignant glioma and medulloblastoma. *Nat. Rev. Cancer* 10:319-331.

Inzucchi,S.E. 2002. Oral antihyperglycemic therapy for type 2 diabetes - Scientific review. *Jama-Journal of the American Medical Association* 287:360-372.

Isakovic,A., L.Harhaji, D.Stevanovic, Z.Markovic, M.Sumarac-Dumanovic, V.STarcevic, D.Micic, and V.Trajkovic. 2007. Dual antiglioma action of metformin: cell cycle arrest and mitochondria-dependent apoptosis. *Cellular and Molecular Life Sciences* 64:1290-1302.

January,C.T. and J.M.Riddle. 1989. Early afterdepolarizations: mechanism of induction and block. A role for L-type Ca2+ current. *Circ. Res.* 64:977-990.

January,C.T., J.M.Riddle, and J.J.Salata. 1988. A model for early afterdepolarizations: induction with the Ca2+ channel agonist Bay K 8644. *Circ. Res.* 62:563-571.

Jiralerspong,S., S.L.Palla, S.H.Giordano, F.Meric-Bernstam, C.Liedtke, C.M.Barnett, L.M.Hsu, M.C.Hung, G.N.Hortobagyi, and A.M.Gonzalez-Angulo. 2009. Metformin and Pathologic Complete Responses to Neoadjuvant Chemotherapy in Diabetic Patients With Breast Cancer. *Journal of Clinical Oncology* 27:3297-3302.

John,R.M., U.B.Tedrow, B.A.Koplan, C.M.Albert, L.M.Epstein, M.O.Sweeney, A.L.Miller, G.F.Michaud, and W.G.Stevenson. 2012. Ventricular arrhythmias and sudden cardiac death. *Lancet* 380:1520-1529.

Jones,T.S. and E.C.Holland. 2010. Molecular Pathogenesis of Malignant Glial Tumors. *Toxicol. Pathol.*

Kourelis,T.V. and R.D.Siegel. 2012. Metformin and cancer: new applications for an old drug. *Medical Oncology* 29:1314-1327.

Koval,O.M., X.Q.Guan, Y.J.Wu, M.L.Joiner, Z.Gao, B.Y.Chen, I.M.Grumbach, E.D.Luczak, R.J.Colbran, L.S.Song, T.J.Hund, P.J.Mohler, and M.E.Anderson. 2010. Ca-V 1.2 beta-subunit coordinates CaMKII-triggered cardiomyocyte death and afterdepolarizations. *Proceedings of the National Academy of Sciences of the United States of America* 107:4996-5000.

Kusne,Y., E.L.Goldberg, S.S.Parker, S.M.Hapak, I.Y.Maskaykina, W.M.Chew, K.H.Limesand, H.L.Brooks, T.J.Price, N.Sanai, J.Nikolich-Zugich, and S.Ghosh. 2014. Contrasting effects of chronic, systemic treatment with mTOR inhibitors rapamycin and metformin on adult neural progenitors in mice. *Age* 36:199-212.

Labuzek,K., D.Suchy, B.Gabryel, A.Bielecka, S.Liber, and B.Okopien. 2010. Quantification of metformin by the HPLC method in brain regions, cerebrospinal fluid and plasma of rats treated with lipopolysaccharide. *Pharmacological Reports* 62:956-965.

Landry,D., S.Sullivan, M.Nicolaides, C.Redhead, A.Edelman, M.Field, Q.al-Awqati, and J.Edwards. 1993. Molecular cloning and characterization of p64, a chloride channel protein from kidney microsomes. *J. Biol. Chem.* 268:14948-14955.

Lang,F., M.Foller, K.S.Lang, P.A.Lang, M.Ritter, E.Gulbins, A.Vereninov, and S.M.Huber. 2005. Ion channels in cell proliferation and apoptotic cell death. *Journal of Membrane Biology* 205:147-157.

Lee,H.Y., D.Wei, and M.R.Loeken. 2014. Lack of metformin effect on mouse embryo AMPK activity: implications for metformin treatment during pregnancy. *Diabetes-Metabolism Research and Reviews* 30:23-30.

Lefranc,F., J.Brotchi, and R.Kiss. 2005. Possible future issues in the treatment of glioblastomas: special emphasis on cell migration and the resistance of migrating glioblastoma cells to apoptosis. *J. Clin. Oncol.* 23:2411-2422.

Lin,R.J., J.Bettencourt, I.J.Wha, D.J.Christini, and R.J.Butera. 2010. Real-time experiment interface for biological control applications. *Conf. Proc. IEEE Eng Med. Biol. Soc.* 2010:4160-4163.

Littler,D.R., S.J.Harrop, W.D.Fairlie, L.J.Brown, G.J.Pankhurst, S.Pankhurst, M.Z.DeMaere, T.J.Campbell, A.R.Bauskin, R.Tonini, M.Mazzanti, S.N.Breit, and P.M.Curmi. 2004. The intracellular chloride ion channel protein CLIC1 undergoes a redox-controlled structural transition. *J. Biol. Chem.* 279:9298-9305.

Littler,D.R., S.J.Harrop, S.C.Goodchild, J.M.Phang, A.V.Mynott, L.Jiang, S.M.Valenzuela, M.Mazzanti, L.J.Brown, S.N.Breit, and P.M.Curmi. 2010. The enigma of the CLIC proteins: Ion channels, redox proteins, enzymes, scaffolding proteins? *FEBS Lett.* 584:2093-2101.

Liu,T. and B.O'Rourke. 2013. Regulation of the Na+/Ca2+ exchanger by pyridine nucleotide redox potential in ventricular myocytes. *J. Biol. Chem.* 288:31984-31992.

Liu,Y. and D.D.Gutterman. 2002. Oxidative stress and potassium channel function. *Clin. Exp. Pharmacol. Physiol* 29:305-311.

Luo,C.H. and Y.Rudy. 1991. A model of the ventricular cardiac action potential. Depolarization, repolarization, and their interaction. *Circ. Res.* 68:1501-1526.

Luo,C.H. and Y.Rudy. 1994. A dynamic model of the cardiac ventricular action potential. I. Simulations of ionic currents and concentration changes. *Circ. Res.* 74:1071-1096.

Madhvani,R.V., Y.Xie, A.Pantazis, A.Garfinkel, Z.Qu, J.N.Weiss, and R.Olcese. 2011. Shaping a new Ca(2) conductance to suppress early afterdepolarizations in cardiac myocytes. *J. Physiol* 589:6081-6092.

Mahajan,A., Y.Shiferaw, D.Sato, A.Baher, R.Olcese, L.H.Xie, M.J.Yang, P.S.Chen, J.G.Restrepo, A.Karma, A.Garfinkel, Z.Qu, and J.N.Weiss. 2008b. A rabbit ventricular action potential model replicating cardiac dynamics at rapid heart rates. *Biophys. J.* 94:392-410.

Maher,E.A., F.B.Furnari, R.M.Bachoo, D.H.Rowitch, D.N.Louis, W.K.Cavenee, and R.A.DePinho. 2001. Malignant glioma: genetics and biology of a grave matter. *Genes Dev.* 15:1311-1333.

Mao,J., L.Chen, B.Xu, L.Wang, H.Li, J.Guo, W.Li, S.Nie, T.J.Jacob, and L.Wang. 2008. Suppression of ClC-3 channel expression reduces migration of nasopharyngeal carcinoma cells. *Biochem. Pharmacol.* 75:1706-1716.

Marban,E., S.W.Robinson, and W.G.Wier. 1986. Mechanisms of arrhythmogenic delayed and early afterdepolarizations in ferret ventricular muscle. *J. Clin. Invest* 78:1185-1192.

Martin-Castillo,B., A.Vazquez-Martin, C.Oliveras-Ferraros, and J.A.Menendez. 2010. Metformin and cancer Doses, mechanisms and the dandelion and hormetic phenomena. *Cell Cycle* 9:1057-1064.

McFerrin,M.B. and H.Sontheimer. 2006. A role for ion channels in glioma cell invasion. *Neuron Glia Biol.* 2:39-49.

Meissner,M., P.Weissgerber, J.E.Londono, J.Prenen, S.Link, S.Ruppenthal, J.D.Molkentin, P.Lipp, B.Nilius, M.Freichel, and V.Flockerzi. 2011. Moderate calcium channel dysfunction in adult mice with inducible cardiomyocyte-specific excision of the cacnb2 gene. *J. Biol. Chem.* 286:15875-15882.

Menon,S.G. and P.C.Goswami. 2007. A redox cycle within the cell cycle: ring in the old with the new. *Oncogene* 26:1101-1109.

Menon,S.G., E.H.Sarsour, D.R.Spitz, R.Higashikubo, M.Sturm, H.N.Zhang, and P.C.Goswami. 2003. Redox regulation of the G(1) to S phase transition in the mouse embryo fibroblast cell cycle. *Cancer Research* 63:2109-2117.

Mikami,A., K.Imoto, T.Tanabe, T.Niidome, Y.Mori, H.Takeshima, S.Narumiya, and S.Numa. 1989. Primary structure and functional expression of the cardiac dihydropyridine-sensitive calcium channel. *Nature* 340:230-233.

Milton,R.H., R.Abeti, S.Averaimo, S.DeBiasi, L.Vitellaro, L.Jiang, P.M.Curmi, S.N.Breit, M.R.Duchen, and M.Mazzanti. 2008a. CLIC1 function is required for beta-amyloid-induced generation of reactive oxygen species by microglia. *J. Neurosci.* 28:11488-11499.

Napolitano,C. and C.Antzelevitch. 2011. Phenotypical Manifestations of Mutations in the Genes Encoding Subunits of the Cardiac Voltage-Dependent L-Type Calcium Channel. *Circulation Research* 108:607-618.

Neely,A., X.Wei, R.Olcese, L.Birnbaumer, and E.Stefani. 1993. Potentiation by the beta subunit of the ratio of the ionic current to the charge movement in the cardiac calcium channel. *Science* 262:575-578.

Ning,X., J.Shu, Y.Du, Q.Ben, and Z.Li. 2013a. Therapeutic strategies targeting cancer stem cells. *Cancer Biol. Ther.* 14:295-303.

Olcese,R., N.Qin, T.Schneider, A.Neely, X.Y.Wei, E.Stefani, and L.Birnbaumer. 1994. The Amino-Terminus of A Calcium-Channel Beta-Subunit Sets Rates of Channel Inactivation Independently of the Subunits Effect on Activation. *Neuron* 13:1433-1438.

Olsen,M.L., S.Schade, S.A.Lyons, M.D.Amaral, and H.Sontheimer. 2003. Expression of voltage-gated chloride channels in human glioma cells. *Journal of Neuroscience* 23:5572-5582.

Ono,K. and T.Iijima. 2010. Cardiac T-type Ca2+ channels in the heart. *Journal of Molecular and Cellular Cardiology* 48:65-70.

Opatowsky,Y., C.C.Chen, K.P.Campbell, and J.A.Hirsch. 2004. Structural analysis of the voltage-dependent calcium channel beta subunit functional core and its complex with the alpha 1 interaction domain. *Neuron* 42:387-399.

Orkand, R.K and R.Niedergerke. 1964. Heart action potential dependence on external calcium and sodium ions. *Science* 146:1176-1177.

Ortensi,B., D.Osti, S.Pellegatta, F.Pisati, P.Brescia, L.Fornasari, D.Levi, P.Gaetani, P.Colombo, A.Ferri, S.Nicolis, G.Finocchiaro, and G.Pelicci. 2012. Rai is a new regulator of neural progenitor migration and glioblastoma invasion. *Stem Cells* 30:817-832.

Pani,G., T.Galeotti, and P.Chiarugi. 2010. Metastasis: cancer cell's escape from oxidative stress. *Cancer Metastasis Rev.* 29:351-378.

Pantazis,A., N.Savalli, D.Sigg, A.Neely, and R.Olcese. 2014. Functional heterogeneity of the four voltage sensors of a human L-type calcium channel. *Proceedings of the National Academy of Sciences of the United States of America* 111:18381-18386.

Paradisi,S., A.Matteucci, C.Fabrizi, M.A.Denti, R.Abeti, S.N.Breit, F.Malchiodi-Albedi, and M.Mazzanti. 2008. Blockade of chloride intracellular ion channel 1 stimulates Abeta phagocytosis. *J. Neurosci. Res.* 86:2488-2498.

Perez-Reyes,E., A.Castellano, H.S.Kim, P.Bertrand, E.Baggstrom, A.E.Lacerda, X.Y.Wei, and L.Birnbaumer. 1992. Cloning and expression of a cardiac/brain beta subunit of the L-type calcium channel. *J. Biol. Chem.* 267:1792-1797.

Pernicova,I. and M.Korbonits. 2014. Metformin-mode of action and clinical implications for diabetes and cancer. *Nature Reviews Endocrinology* 10:143-156.

Peterson,B.Z., C.D.DeMaria, J.P.Adelman, and D.T.Yue. 1999. Calmodulin is the Ca2+ sensor for Ca2+ -dependent inactivation of L-type calcium channels. *Neuron* 22:549-558.

Petrova,D.T., A.R.Asif, V.W.Armstrong, I.Dimova, S.Toshev, N.Yaramov, M.Oellerich, and D.Toncheva. 2008. Expression of chloride intracellular channel protein 1 (CLIC1) and tumor protein D52 (TPD52) as potential biomarkers for colorectal cancer. *Clin. Biochem.* 41:1224-1236.

Pollak,M. 2012. The insulin and insulin-like growth factor receptor family in neoplasia: an update. *Nature Reviews Cancer* 12:159-169.

Ponten,J. and E.H.Macintyre. 1968. Long term culture of normal and neoplastic human glia. *Acta Pathol. Microbiol. Scand.* 74:465-486.

Pragnell,M., W.M.De, Y.Mori, T.Tanabe, T.P.Snutch, and K.P.Campbell. 1994. Calcium channel beta-subunit binds to a conserved motif in the I-II cytoplasmic linker of the alpha 1-subunit. *Nature* 368:67-70.

Prevarskaya,N., R.Skryma, and Y.Shuba. 2010. Ion channels and the hallmarks of cancer. *Trends Mol. Med.* 16:107-121.

Qiu,M.R., L.Jiang, K.I.Matthaei, S.M.Schoenwaelder, T.Kuffner, P.Mangin, J.E.Joseph, J.Low, D.Connor, S.M.Valenzuela, P.M.Curmi, L.J.Brown, M.Mahaut-Smith, S.P.Jackson, and S.N.Breit. 2010. Generation and characterization of mice with null mutation of the chloride intracellular channel 1 gene. *Genesis.* 48:127-136.

Qu,Z. and D.Chung. 2012. Mechanisms and determinants of ultralong action potential duration and slow rate-dependence in cardiac myocytes. *PLoS. One.* 7:e43587.

Qu,Z. and J.N.Weiss. 2015. Mechanisms of Ventricular Arrhythmias: From Molecular Fluctuations to Electrical Turbulence.

Qu,Z., L.H.Xie, R.Olcese, H.S.Karagueuzian, P.S.Chen, A.Garfinkel, and J.N.Weiss. 2013. Early afterdepolarizations in cardiac myocytes: beyond reduced repolarization reserve. *Cardiovasc. Res.* 99:6-15.

Ravens,U. and E.Cerbai. 2008. Role of potassium currents in cardiac arrhythmias. *Europace* 10:1133-1137.

Reya,T., S.J.Morrison, M.F.Clarke, and I.L.Weissman. 2001. Stem cells, cancer, and cancer stem cells. *Nature* 414:105-111.

Reynolds,B.A. and S.Weiss. 1992. Generation of neurons and astrocytes from isolated cells of the adult mammalian central nervous system. *Science* 255:1707-1710.

Rose,W.C., C.W.Balke, W.G.Wier, and E.Marban. 1992. Macroscopic and unitary properties of physiological ion flux through L-type Ca2+ channels in guinea-pig heart cells. *J. Physiol* 456:267-284.

Ruth,P., A.Rohrkasten, M.Biel, E.Bosse, S.Regulla, H.E.Meyer, V.Flockerzi, and F.Hofmann. 1989. Primary Structure of the Beta-Subunit of the Dhp-Sensitive Calcium-Channel from Skeletal-Muscle. *Science* 245:1115-1118.

Sanai,N., A.varez-Buylla, and M.S.Berger. 2005. Neural stem cells and the origin of gliomas. *N. Engl. J. Med.* 353:811-822.

Sato,A., J.Sunayama, M.Okada, E.Watanabe, S.Seino, K.Shibuya, K.Suzuki, Y.Narita, S.Shibui, T.Kayama, and C.Kitanaka. 2012. Glioma-Initiating Cell Elimination by Metformin Activation of FOXO3 via AMPK. *Stem Cells Translational Medicine* 1:811-824.

Sato,D., L.H.Xie, A.A.Sovari, D.X.Tran, N.Morita, F.Xie, H.Karagueuzian, A.Garfinkel, J.N.Weiss, and Z.Qu. 2009. Synchronization of chaotic early afterdepolarizations in the genesis of cardiac arrhythmias. *Proc. Natl. Acad. Sci. U. S. A* 106:2983-2988.

Setti,M., N.Savalli, D.Osti, C.Richichi, M.Angelini, P.Brescia, L.Fornasari, M.S.Carro, M.Mazzanti, and G.Pelicci. 2013. Functional Role of CLIC1 Ion Channel in Glioblastoma-Derived Stem/Progenitor Cells. *Jnci-Journal of the National Cancer Institute* 105:1644-1655.

Sharp,A.A., M.B.O'Neil, L.F.Abbott, and E.Marder. 1993. The dynamic clamp: artificial conductances in biological neurons. *Trends Neurosci.* 16:389-394.

Shaw,R.M. and H.M.Colecraft. 2013. L-type calcium channel targeting and local signalling in cardiac myocytes. *Cardiovasc. Res.* 98:177-186.

Shiferaw,Y., M.A.Watanabe, A.Garfinkel, J.N.Weiss, and A.Karma. 2003. Model of intracellular calcium cycling in ventricular myocytes. *Biophys. J.* 85:3666-3686.

Shorofsky,S.R. and C.T.January. 1992. L- and T-type Ca2+ channels in canine cardiac Purkinje cells. Single-channel demonstration of L-type Ca2+ window current. *Circ. Res.* 70:456-464.

Shu,Y., S.A.Sheardown, C.Brown, R.P.Owen, S.Z.Zhang, R.A.Castro, A.G.Ianculescu, L.Yue, J.C.Lo, E.G.Burchard, C.M.Brett, and K.M.Giacomini. 2007. Effect of genetic variation in the organic cation transporter 1 (OCT1) on metformin action. *Journal of Clinical Investigation* 117:1422-1431.

Simms,B.A. and G.W.Zamponi. 2014. Neuronal Voltage-Gated Calcium Channels: Structure, Function, and Dysfunction. *Neuron* 82:24-45.

Singer,D., M.Biel, I.Lotan, V.Flockerzi, F.Hofmann, and N.Dascal. 1991. The roles of the subunits in the function of the calcium channel. *Science* 253:1553-1557.

Singh,H. 2010. Two decades with dimorphic Chloride Intracellular Channels (CLICs). *FEBS Lett.* 584:2112-2121.

Singh,H. and R.H.Ashley. 2006. Redox regulation of CLIC1 by cysteine residues associated with the putative channel pore. *Biophys. J.* 90:1628-1638.

Singh,H., M.A.Cousin, and R.H.Ashley. 2007. Functional reconstitution of mammalian 'chloride intracellular channels' CLIC1, CLIC4 and CLIC5 reveals differential regulation by cytoskeletal actin. *FEBS J.* 274:6306-6316.

Singh,S.K., C.Hawkins, I.D.Clarke, J.A.Squire, J.Bayani, T.Hide, R.M.Henkelman, M.D.Cusimano, and P.B.Dirks. 2004. Identification of human brain tumour initiating cells. *Nature* 432:396-401.

Slezak,J., N.Tribulova, J.Pristacova, B.Uhrik, T.Thomas, N.Khaper, N.Kaul, and P.K.Singal. 1995. Hydrogen peroxide changes in ischemic and reperfused heart. Cytochemistry and biochemical and X-ray microanalysis. *Am. J. Pathol.* 147:772-781.

Sontheimer,H. 2008. An unexpected role for ion channels in brain tumor metastasis. *Exp. Biol. Med. (Maywood. )* 233:779-791.

Stiles,C.D. and D.H.Rowitch. 2008. Glioma stem cells: a midterm exam. *Neuron* 58:832-846.

Takahashi,S.X., J.Miriyala, L.H.Tay, D.T.Yue, and H.M.Colecraft. 2005. A CaVbeta SH3/guanylate kinase domain interaction regulates multiple properties of voltage-gated Ca2+ channels. *J. Gen. Physiol* 126:365-377.

Tan,R.C. and R.W.Joyner. 1990. Electrotonic influences on action potentials from isolated ventricular cells. *Circ. Res.* 67:1071-1081.

Tanabe,T., H.Takeshima, A.Mikami, V.Flockerzi, H.Takahashi, K.Kangawa, M.Kojima, H.Matsuo, T.Hirose, and S.Numa. 1987. Primary Structure of the Receptor for Calcium-Channel Blockers from Skeletal-Muscle. *Nature* 328:313-318.

Tang,H.Y., L.A.Beer, T.Chang-Wong, R.Hammond, P.Gimotty, G.Coukos, and D.W.Speicher. 2012. A Xenograft Mouse Model Coupled with In-depth Plasma Proteome Analysis Facilitates Identification of Novel Serum Biomarkers for Human Ovarian Cancer. *Journal of Proteome Research* 11:678-691.

Tonini,R., A.Ferroni, S.M.Valenzuela, K.Warton, T.J.Campbell, S.N.Breit, and M.Mazzanti. 2000. Functional characterization of the NCC27 nuclear protein in stable transfected CHO-K1 cells. *FASEB J.* 14:1171-1178.

Tsien,R.W., D.Lipscombe, D.V.Madison, K.R.Bley, and A.P.Fox. 1988. Multiple Types of Neuronal Calcium Channels and Their Selective Modulation. *Trends in Neurosciences* 11:431-438.

Tucker,G.T., C.Casey, P.J.Phillips, H.Connor, J.D.Ward, and H.F.Woods. 1981. Metformin kinetics in healthy subjects and in patients with diabetes mellitus. *Br. J. Clin. Pharmacol.* 12:235-246.

Tulk,B.M., S.Kapadia, and J.C.Edwards. 2002. CLIC1 inserts from the aqueous phase into phospholipid membranes, where it functions as an anion channel. *Am. J. Physiol Cell Physiol* 282:C1103-C1112.

Tulk,B.M., P.H.Schlesinger, S.A.Kapadia, and J.C.Edwards. 2000. CLIC-1 functions as a chloride channel when expressed and purified from bacteria. *J. Biol. Chem.* 275:26986-26993.

Tung,J.J. and J.Kitajewski. 2010. Chloride intracellular channel 1 functions in endothelial cell growth and migration. *J. Angiogenes. Res.* 2:23.

Ulmasov,B., J.Bruno, P.G.Woost, and J.C.Edwards. 2007. Tissue and subcellular distribution of CLIC1. *BMC. Cell Biol.* 8:8.

Valenzuela,S.M., D.K.Martin, S.B.Por, J.M.Robbins, K.Warton, M.R.Bootcov, P.R.Schofield, T.J.Campbell, and S.N.Breit. 1997. Molecular cloning and expression of a chloride ion channel of cell nuclei. *J. Biol. Chem.* 272:12575-12582.

Valenzuela,S.M., M.Mazzanti, R.Tonini, M.R.Qiu, K.Warton, E.A.Musgrove, T.J.Campbell, and S.N.Breit. 2000. The nuclear chloride ion channel NCC27 is involved in regulation of the cell cycle. *J. Physiol* 529 Pt 3:541-552.

Van,P.F., K.A.Clark, F.C.Chatelain, and D.L.Minor, Jr. 2004. Structure of a complex between a voltage-gated calcium channel beta-subunit and an alpha-subunit domain. *Nature* 429:671-675.

Varadi,G., P.Lory, D.Schultz, M.Varadi, and A.Schwartz. 1991. Acceleration of Activation and Inactivation by the Beta Subunit of the Skeletal-Muscle Calcium-Channel. *Nature* 352:159-162.

Verkerk,A.O., A.Baartscheer, G.de, Jr., R.Wilders, and R.Coronel. 2011. Etiology-dependency of ionic remodeling in cardiomyopathic rabbits. *Int. J. Cardiol.* 148:154-160.

Vescovi,A.L., R.Galli, and B.A.Reynolds. 2006. Brain tumour stem cells. *Nat. Rev. Cancer* 6:425-436.

Wagner,S., N.Dybkova, E.C.L.Rasenack, C.Jacobshagen, L.Fabritz, P.Kirchhof, S.K.G.Maier, T.Zhang, G.Hasenfuss, J.H.Brown, D.M.Bers, and L.S.Maier. 2006. Ca2+/calmodulin-dependent protein kinase II regulates cardiac Na+ channels. *Journal of Clinical Investigation* 116:3127-3138.

Wagner,S., H.M.Ruff, S.L.Weber, S.Bellmann, T.Sowa, T.Schulte, M.E.Anderson, E.Grandi, D.M.Bers, J.Backs, L.Belardinelli, and L.S.Maier. 2011. Reactive oxygen species-activated Ca/calmodulin kinase IIdelta is required for late I(Na) augmentation leading to cellular Na and Ca overload. *Circ. Res.* 108:555-565.

Wakamori,M., G.Mikala, and Y.Mori. 1999. Auxiliary subunits operate as a molecular switch in determining gating behaviour of the unitary N-type Ca2+ channel current in Xenopus oocytes. *J. Physiol* 517 ( Pt 3):659-672.

Wang,G.L., X.R.Wang, M.J.Lin, H.He, X.J.Lan, and Y.Y.Guan. 2002. Deficiency in ClC-3 chloride channels prevents rat aortic smooth muscle cell proliferation. *Circulation Research* 91:E28-E32.

Wang,J.W., S.Y.Peng, J.T.Li, Y.Wang, Z.P.Zhang, Y.Cheng, D.Q.Cheng, W.H.Weng, X.S.Wu, X.Z.Fei, Z.W.Quan, J.Y.Li, S.G.Li, and Y.B.Liu. 2009. Identification of metastasis-associated proteins involved in gallbladder carcinoma metastasis by proteomic analysis and functional exploration of chloride intracellular channel 1. *Cancer Lett.* 281:71-81.

Wang,L., S.He, Y.Tu, P.Ji, J.Zong, J.Zhang, F.Feng, J.Zhao, Y.Zhang, and G.Gao. 2012. Elevated expression of chloride intracellular channel 1 is correlated with poor prognosis in human gliomas. *J. Exp. Clin. Cancer Res.* 31:44.

Warton,K., R.Tonini, W.D.Fairlie, J.M.Matthews, S.M.Valenzuela, M.R.Qiu, W.M.Wu, S.Pankhurst, A.R.Bauskin, S.J.Harrop, T.J.Campbell, P.M.Curmi, S.N.Breit, and M.Mazzanti. 2002. Recombinant CLIC1 (NCC27) assembles in lipid bilayers via a pH-dependent two-state process to form chloride ion channels with identical characteristics to those observed in Chinese hamster ovary cells expressing CLIC1. *J. Biol. Chem.* 277:26003-26011.

Weber,C.R., V.Piacentino, III, K.S.Ginsburg, S.R.Houser, and D.M.Bers. 2002. Na(+)-Ca(2+) exchange current and submembrane [Ca(2+)] during the cardiac action potential. *Circ. Res.* 90:182-189.

Wei,X.Y., J.Li, H.Y.Xie, H.X.Wang, J.G.Wang, X.Y.Zhang, R.Z.Zhuang, D.Lu, Q.Ling, L.Zhou, X.Xu, and S.S.Zheng. 2015. Chloride intracellular channel 1 participates in migration and invasion of hepatocellular carcinoma by targeting maspin. *Journal of Gastroenterology and Hepatology* 30:208-216.

Weiss,J.N., P.S.Chen, Z.L.Qu, H.S.Karagueuzian, and A.Garfinkel. 2000. Ventricular fibrillation - How do we stop the waves from breaking? *Circulation Research* 87:1103-1107.

Weiss,J.N., A.Garfinkel, H.S.Karagueuzian, P.S.Chen, and Z.Qu. 2010. Early afterdepolarizations and cardiac arrhythmias. *Heart Rhythm.* 7:1891-1899.

Weissgerber,P., B.Held, W.Bloch, L.Kaestner, K.R.Chien, B.K.Fleischmann, P.Lipp, V.Flockerzi, and M.Freichel. 2006. Reduced cardiac L-type Ca2+ current in Ca(V)beta2-/- embryos impairs cardiac development and contraction with secondary defects in vascular maturation. *Circ. Res.* 99:749-757.

Wibo,M., G.Bravo, and T.Godfraind. 1991. Postnatal maturation of excitation-contraction coupling in rat ventricle in relation to the subcellular localization and surface density of 1,4-dihydropyridine and ryanodine receptors. *Circ. Res.* 68:662-673.

Wilders,R. 2006. Dynamic clamp: a powerful tool in cardiac electrophysiology. *J. Physiol* 576:349-359.

Wulfkuhle,J.D., D.C.Sgroi, H.Krutzsch, K.McLean, K.McGarvey, M.Knowlton, S.Chen, H.J.Shu, A.Sahin, R.Kurek, D.Wallwiener, M.J.Merino, E.F.Petricoin, Y.M.Zhao, and P.S.Steeg. 2002. Proteomics of human breast ductal carcinoma in situ. *Cancer Research* 62:6740-6749.

Wurth,R., F.Barbieri, and T.Florio. 2014. New Molecules and Old Drugs as Emerging Approaches to Selectively Target Human Glioblastoma Cancer Stem Cells. *Biomed Research International*.

Wurth,R., A.Pattarozzi, M.Gatti, A.Bajetto, A.Corsaro, A.Parodi, R.Sirito, M.Massollo, C.Marini, G.Zona, D.Fenoglio, G.Sambuceti, G.Filaci, A.Daga, F.Barbieri, and T.Florio. 2013. Metformin selectively affects human glioblastoma tumor-initiating cell viability A role for metformin-induced inhibition of Akt. *Cell Cycle* 12:145-156.

Xie,L.H., F.Chen, H.S.Karagueuzian, and J.N.Weiss. 2009. Oxidative-stress-induced afterdepolarizations and calmodulin kinase II signaling. *Circ. Res.* 104:79-86.

Yang,S.N. and P.O.Berggren. 2006. The role of voltage-gated calcium channels in pancreatic beta-cell physiology and pathophysiology. *Endocrine Reviews* 27:621-676.

Zerumsky,K. and B.F.McBride. 2006. Ranolazine in the management of chronic stable angina. *Am. J. Health Syst. Pharm.* 63:2331-2338.